POWER REACTOR TECHNOLOGY

A Quarterly Technical Progress Review

Prepared for DIVISION OF TECHNICAL INFORMATION, USAEC, by
W. H. ZINN and J. R. DIETRICH, GENERAL NUCLEAR ENGINEERING CORPORATION

December 1962

● VOLUME 6

● NUMBER 1

TECHNICAL PROGRESS REVIEWS

To meet the needs of industry for concise summaries of current atomic developments, the Atomic Energy Commission is publishing this series, Technical Progress Reviews. Issued quarterly, each of the reviews digests and evaluates the latest findings in a specific area of nuclear technology and science.

The four journals published in this series are:

Nuclear Safety, Wm. B. Cottrell, W. H. Jordan, and associates, Oak Ridge National Laboratory

Power Reactor Technology, W. H. Zinn and J. R. Dietrich, General Nuclear Engineering Corporation

Reactor Materials, R. W. Dayton, E. M. Simons, and associates, Battelle Memorial Institute

Reactor Fuel Processing, Stephen Lawroski and associates, Chemical Engineering Division, Argonne National Laboratory

Each journal may be purchased ($2.00 per year for subscription and individual issues $0.55) from the Superintendent of Documents, U. S. Government Printing Office, Washington 25, D. C. See back cover for remittance instructions and foreign postage requirements.

Availability of Reports Cited in This Review

Unclassified AEC reports are available for inspection at AEC depository libraries and are sold by the Office of Technical Services, Department of Commerce, Washington 25, D. C. Some of the reports cited are not available owing to their preliminary nature; however, the information contained in them will eventually be made available in formal progress or topical reports.

Unclassified reports issued by other Government agencies or private organizations should be requested from the originator.

Unclassified British and Canadian reports may be inspected at AEC depository libraries. British reports are sold by the British Information Service, 45 Rockefeller Plaza, New York, N. Y.; Canadian reports (AECL series) are sold by the Scientific Document Distribution Office, Atomic Energy of Canada, Ltd., Chalk River, Ontario, Canada.

Classified U. S. and foreign reports identified in this journal as Classified may be purchased by properly cleared Access Permit Holders from the Division of Technical Information Extension, U. S. Atomic Energy Commission, P. O. Box 1001, Oak Ridge, Tenn. Such reports may be inspected at classified AEC depository libraries.

POWER REACTOR TECHNOLOGY

A REVIEW OF RECENT DEVELOPMENTS

Prepared for DIVISION OF TECHNICAL INFORMATION, USAEC,
by W. H. ZINN and J. R. DIETRICH,
GENERAL NUCLEAR ENGINEERING CORPORATION

● DEC. 1962
● VOLUME 6
● NUMBER 1

Foreword

This quarterly review of reactor development has been prepared at the request of the Division of Technical Information of the U. S. Atomic Energy Commission. Its purpose is to assist interested organizations in the task of keeping abreast of new results in reactor technology for civilian application.

Power Reactor Technology contains reviews of selected recently published reports that are judged noteworthy, in the fields of power-reactor research and development, power-reactor applications, design practice, and operating experience. It is not meant to be a comprehensive abstract of all material published during the quarter, nor is it meant to be a treatise on any part of the subject. However, related articles are often treated together to yield reviews having some breadth of scope, and from time to time background material is added to place recent developments in perspective.

The intention is to cover the various areas of reactor development from the general viewpoint of the reactor designer rather than from the more detailed points of view of specialists in the individual areas. To whatever extent the coverage of *Power Reactor Technology* may occasionally overlap the fields of the other Technical Progress Reviews, the overlaps will be motivated by this objective of viewing current progress through the eyes of the reactor designer.

A degree of critical appraisal and some interpretation of results are often necessary to define the significance of reported work. Any such appraisals or interpretations represent only the opinions of the reviewers and the editor of *Power Reactor Technology*, who are General Nuclear Engineering Corporation personnel. Readers are urged to consult the original references in order to obtain all the background of the work reported and to obtain the interpretation of the results given by the original authors.

W. H. ZINN, President
J. R. DIETRICH, Vice President and Editor
General Nuclear Engineering Corporation

Issued quarterly by the U. S. Atomic Energy Commission. Use of funds for printing this publication approved by the Director of the Bureau of the Budget on November 1, 1960.

Contents

Section

I

Power Reactor Technology

Economics: Cost Evaluation Guide

A five-part handbook, "Guide to Nuclear Power Cost Evaluation," has been published by the Division of Technical Information,[1] U. S. Atomic Energy Commission (AEC). The handbook was prepared by Kaiser Engineers Division of Henry J. Kaiser Co. under the direction of and in technical cooperation with AEC's Division of Reactor Development.

The guide, which was prepared primarily for AEC use, is intended to be a multipurpose tool in the preparation of and comparative evaluation of nuclear-power-plant cost estimates. It will also be useful for assuring the presentation of estimated costs according to a uniform classification of cost accounts. Since it is expected to be useful outside the Commission, it has been published for general use; however, users are cautioned that it does not necessarily represent the official position of the AEC on all subjects.

The Guide should prove useful in the preparation of cost estimates for most proposed nuclear central-station plants. The authors explain that its use in such an estimation should be a two-step process:

1. Review of data in the Guide
2. Application of the user's engineering judgment to the results in step 1

Since the Guide covers only five reactor concepts, the proportionate emphasis applied to steps 1 and 2 will vary with the reactor type under consideration. These reactor concepts are:

1. Pressurized-Water Reactor
2. Boiling-Water Reactor
3. Organic-Moderated and -Cooled Reactor
4. Sodium-Cooled Graphite-Moderated Reactor
5. Fast-Breeder Reactor

Plants covered are in the range 70 to 360 Mw(e). The cost material is compiled from AEC reports, government regulations, and commercial publications issued between 1955 and 1961. The majority of the publications cited are dated 1957 to 1959. It is stated that revisions of the Guide are contemplated to include other reactor concepts and to take advantage of new cost data as they become available.

To help the designer prepare a comprehensive cost estimate, the Guide provides a detailed checklist of all items reasonably expected to be needed for a nuclear central station. If this list is conscientiously filled in, item by item, one can be rather confident that all necessary items of cost for designing, building, and operating the plant have been considered.

Most items listed are necessarily subject to interpretation. To reduce the amount of judgment required, a detailed explanation is included with the checklist for clarifying what the authors include in each account. However, the specific design being evaluated must still be the determining factor in locating an item within the checklist. For example, concrete at a particular location in the design may serve as both shield and structure; therefore there is no need to prorate the value between the shielding and structural accounts.

As an aid to the checklist, the authors have drawn flow diagrams of each of the major reactor plant systems required by the five reactor concepts under consideration. Again the major value of these diagrams is as a reminder of the general considerations required in estimating plant costs. The diagrams are not intended as design criteria.

For applications in which it is not feasible to obtain more accurate costs for specific plant components, approximations for some major items are included in the Guide. These include specific suggestions for site criteria, catalog-

like compilations of major components such as turbines and condensers, graphical representations for costs of buildings and pressure vessels, cost-capacity data for certain other major equipment items, cost data for fuel cycles, and estimating factors for engineering costs, capital requirements, and contingencies. It is not possible here to attempt to evaluate the degree of accuracy of these data. It might be suggested that the Guide would be more helpful if estimated ranges of variation were given in more cases and if the date of estimate were specified for the specific cost information.

There are many ways in which a guide of this sort may be useful to the designer of nuclear plants. Inevitably the Guide will have limitations, and the authors point them out. If their words of caution are observed and if the publication is regarded literally as a "guide," the benefits from its publication should be substantial and the opportunities for its misuse should be minimized.

Reference

1. Kaiser Engineers Division, Henry J. Kaiser Co., Guide to Nuclear Power Cost Evaluation, Volumes 1–5, USAEC Report TID-7025 as follows: Vol. 1, Reference Data and Standards; Vol. 2, Land, Improvements, Buildings and Structures; Vol. 3, Equipment Costs; Vol. 4, Fuel Cycle Costs; and Vol. 5, Production Costs.

Section

II

Power Reactor Technology

Reactor Physics

Critical and Exponential Experiments

A series of critical mass experiments[1,2] using plutonium nitrate solutions was initiated at the Hanford Critical Mass Laboratory during June of 1961. The critical assembly for this series of experiments is a 14-in.-diameter stainless-steel sphere with a 0.044-in. wall thickness. The control and safety rods are hollow tubes, mounted coaxially, which enter the vessel from above along the vertical axis. The control rod is a 1-in.-diameter stainless-steel tube, and the safety rod is a 1.5-in.-diameter cadmium tube with stainless-steel cladding.

References 1 and 2 contain the results of critical mass experiments through the first quarter of this year. Plutonium concentrations that ranged from 30 to 238 g/liter had acid molarities that varied from 1.1 M to 5.3 M. Multiplication and critical measurements were performed with the bare vessel and with the vessel reflected by one or more of the following: 0.072 in. of stainless steel, 0.5 in. of paraffin, 1 in. of paraffin, 4 in. of concrete, 10 in. of concrete, and 0.030 in. of cadmium backed with 4 in. of concrete or 1 in. of paraffin. The critical volumes for cases in which the vessel was subcritical when full were determined by extrapolation of the multiplication curve. Reflector savings were evaluated by correcting the critical volume for the effect of the vessel wall and then comparing equivalent spherical radii. For cases in which the vessel was critical when partially filled, the equivalent spherical radii were estimated on the basis of equal surface-to-volume ratios for equivalent systems.

Experimental extrapolation distances for the Handbook of Nuclear Safety[3] were obtained by comparing calculated material bucklings with geometric bucklings of critical systems. These extrapolation distances were then used to construct tables of critical and safe (i.e., k_{eff} = 0.95) dimensions of spheres, cylinders, and slabs.

Reference 4 contains the results of an effort to improve the calculational scheme for the material bucklings of plutonium-H_2O systems and to obtain some estimate of the degree of conservatism contained in the Handbook values. The calculational scheme makes use of the transport approximation in multigroup calculations of the material bucklings of infinite systems. These bucklings, together with average nuclear constants generated from solutions to the multigroup wave equation, were used in a two-group one-dimensional diffusion type calculation of the extrapolation distances for bare and water-reflected spheres, cylinders, and slabs. The use of the transport approximation in the multigroup calculation and the boundary conditions employed in the two-group calculation are discussed. Comparisons between calculation and experiment are given for bare and water-reflected spheres and for water-reflected cylinders containing plutonium nitrate solutions of varying concentrations; additional variables include the Pu^{240} and nitrate concentrations. Calculated bucklings and extrapolation distances for nitrate-free systems with two concentrations of Pu^{240} are given for use in nuclear-safety calculations. Curves based on the latter calculations for homogeneous mixtures of $Pu_2^{239}O_3$ and water are given to show critical and safe (k_{eff} = 0.95) masses for bare and water-reflected spheres and critical and safe diameters and thicknesses of infinite cylinders and slabs, respectively, as functions of concentration. Values from the Handbook and results of DSN calculations for plutonium metal and water solutions are compared with the curves.

Reference 5 describes the present status of an IBM code developed to calculate lattice parameters for heavy-water systems and makes a comparison between calculated and experimental bucklings. This code calculates lattice parameters (i.e., η, ϵ, p, f, L^2, τ, k, and B^2) for solid rods, hexagonal clusters, or concentric tubes of uranium metal or uranium oxide. In addition, the effects of temperature changes and void formation in the water may be evaluated. Provisions are made for admixtures of light water, up to a few percent, in the D_2O moderator. The method of application of the code to lattices of tubular and rod-cluster elements is discussed in detail. Calculated and measured bucklings are compared for single-rod assemblies, tubular assemblies, and metal and oxide clusters. The sources of experimental data consist of the following: Chalk River (Canada), Saclay (France), Stockholm (Sweden), North American Aviation, Inc., and Savannah River. Deviations between experimental and calculated results are discussed in terms of both random deviations in the measurements and systematic variations in the measurements and calculations.

Reference 6 contains the results of two independent sets of measurements leading to an evaluation of the infinite-medium thermal-neutron multiplication factor, k_∞, for hydrogen-moderated uranium enriched to 2 wt.% U^{235}. The first set of measurements was carried out at the Physical Constants Testing Reactor (PCTR) at Hanford Atomic Products Operation, and the second at the Oak Ridge National Laboratory Critical Facility (ORNL). The same fuel was used in both laboratories (blocks containing a homogeneous mixture of 92.1 wt.% UF_4 and 7.9 wt.% paraffin).

An experimental determination of k_∞ in the PCTR is based (1) on the principle that no perturbation of an infinite critical homogeneous medium will result when any volume of the medium is replaced by a vacuum and (2) on certain assumptions concerning the neutron spectrum. The procedure employed at ORNL was more conventional in that it was based on measurements of steady-state critical dimensions and the reactivity resulting from small buckling perturbations to a critical system. The values of k_∞ deduced from the data obtained at the PCTR and ORNL facilities are 1.216 ± 0.013 and 1.197 ± 0.015, respectively. Additional results of the ORNL analyses include values for the neutron age to thermal energy, critical buckling, bare extrapolation distance, and fast-fission factor.

Experiments[7] were performed in the PCTR to determine the limiting concentration (i.e., that for which k_∞ is unity) of plutonium nitrate and 93% enriched UO_2F_2 solutions. The test assembly, which consisted of a large annular buffer tank, the core tank, and two end buffer tanks, was inserted into the central cavity of the PCTR. The reactivities of several core tanks containing solutions of different concentrations were compared with a void tank containing helium. The adequacy of the buffer region was established by the close agreement of the extrapolated results obtained with both a "thermal" and a "fast" flux entering the buffer region. The plutonium nitrate data were corrected for the Pu^{240}, Pu^{241}, and nitrate content of the solutions to give an extrapolated result of 8.1 ± 0.03 g/liter as the limiting concentration of a Pu^{239}-H_2O solution. The limiting concentration for the UO_2F_2 solution was 12.05 ± 0.03 g of U^{235} per liter; this may be compared to an Oak Ridge value of 12.1 g/liter.

The results of an experiment to determine the fuel temperature coefficient of k_∞ for plutonium-aluminum fuel are reported in Ref. 8. The central cavity of the PCTR was loaded with a three-by-three array of 6.5-in.-square graphite lattice cells. Each cell contained a 19-rod cluster of 1.8 wt.% low-exposure plutonium-aluminum rods, each $\frac{1}{2}$ in. in diameter. The proper two-group spectrum (in the three-by-three lattice) and neutron multiplication factor were obtained by fuel adjustments in the driver region and by copper poisoning of the plutonium-aluminum cells, respectively. The change in reactivity of the PCTR was measured as the temperature of the central cell in the plutonium-aluminum lattice varied from room temperature to approximately 400°C. Measurements were made with 1.88 wt.% low-exposure plutonium-aluminum, 2.07 wt.% high-exposure plutonium-aluminum, and dummy aluminum rods in the test cell.

Reactor Physics Constants

Some recent compilations and new measurements of basic nuclear constants have been reported which are of importance in reactor analysis. Reference 9 lists sources of cross-

section data for 33 of the more common elements and isotopes used in reactor design. This compilation was made in connection with data source tapes for the C-FINE computer program, used in the generation of multigroup constants. Also included in the reference is a brief résumé of the methods and auxiliary computer programs used to fill in gaps in the available data and to ensure a smooth connection of data generated by different methods.

The Reactor Physics Constants Center at Argonne National Laboratory has issued the second in a series of newsletters[10] covering zero-temperature resonance-integral data for Th^{232}, U^{238}, Au^{197}, and In^{115}. The intermediate resonance (IR) approximation of Goldstein and Cohen[11] is used in tabulating the resonance integrals for 54 resolved resonances of U^{238} and for 49 resolved resonances of Th^{232} at several values of the moderator scattering cross section. A tabulation of the resolved resonance integrals for Au^{197} and In^{115}, evaluated on the same basis, is also presented. The theory underlying the IR approximation, which is a combination of the usual narrow resonance (NR) and wide resonance (WR or NRIA) approximations, is given in Ref. 11.

The effective cross section of Pu^{240} has been measured[12] both in a thermal-neutron spectrum and in the pile spectrum of the DIMPLE Reactor, using a sample containing 91.5% Pu^{240}. From these two measurements, a cross section of 290 ± 9 barns and a resonance integral of 8200 ± 1100 barns for a neutron velocity of 2200 m/sec have been derived. This cross section is in good agreement with the previous value of 286 ± 7 barns (BNL-325, 2nd Ed. and Suppl.). The large error range for the resonance integral is due primarily to uncertainty in the resonance self-shielding. However, by utilizing the known resonance parameters of the 1.05-ev resonance and by fitting a least-squares straight line to the experimental data for several Pu^{240} concentrations, the authors obtained the following equation for the effective resonance integral of Pu^{240} mixed with a scattering medium:

$$I_a' = 8270 - \frac{1.22 \times 10^8}{\sigma_p}$$

where σ_p is the potential scattering cross section (barns) per Pu^{240} atom. This equation is valid (within $\pm 6\%$) over the range of concentrations investigated (i.e., to an effective resonance integral as low as about 89% of the infinitely dilute value).

The cross-section values of Pa^{231} in the range from 0.01 ev to 2 kev, measured with the fast chopper at the Materials Testing Reactor (MTR), are tabulated in Ref. 13. This isotope is important in thorium fuel cycles since it is an intermediate in the production chain leading to U^{232}, which, in turn, increases the difficulty of fuel handling because of the energetic gamma radiation emitted by its daughter isotopes. The thermal (2200 m/sec) cross section obtained by a linear least-squares fit in the low-energy region was evaluated at 211 ± 2.2 barns. Reference 14 presents further analyses of the experimental data, including a Breit-Wigner single-level fit and the derived resonance parameters of 24 resolved resonance peaks. These parameters imply a resonance absorption integral (> 0.1 ev) of 1650 ± 55 barns, of which 1395 barns is attributable to the resolved resonances. Approximately 65% of the resonance integral is contributed by the large resonance at 0.396 ev.

In the interest of providing the necessary cross sections to improve the calculated nuclear characteristics of polyethylene-moderated assemblies, Ref. 15 presents experimentally derived transport cross sections of a chemically similar material, paraffin. These values were derived from measurements of the relaxation length of thermal neutrons in paraffin in the temperature range 60 to 130°C. Good agreement was obtained between the experimentally derived transport cross sections and those calculated by applying the scattering cross sections pertinent to paraffin[16] in a prescription analogous to the familiar Radkowsky formula for water. Since the difference in total scattering cross sections of paraffin and polyethylene is small, implying that the chemical binding energy of hydrogen in the two materials is similar, the authors conclude that the Radkowsky formula with polyethylene scattering cross sections will predict accurately the temperature-dependent transport cross section of polyethylene.

In support of the Spectral Shift Control Reactor concept (SSCR), the age to indium resonance in H_2O-D_2O mixtures containing ThO_2 rods has been measured at a moderator-to-clad-ThO_2 volume ratio of 1.0. Reference 17 reports these values as follows:

D_2O concentration, %	Age, cm^2
0	49.7 ± 2.5
49.77	67.4 ± 3.5
69.19	80.0 ± 1.2
79.19	97.6 ± 3.4
90.0	119.8 ± 4.8

The age was determined by using a beam from the thermal column of the Lynchburg Pool Reactor (LPR) to induce fission in an enriched disk of U^{235} and by experimentally measuring the activation in cadmium-covered indium foils at varying distances from the source. The results of measurements made parallel and perpendicular to the ThO_2 rods were the same within the experimental uncertainty, which implies that no significant anisotropy existed. Since the scattering properties of the clad ThO_2 resemble those of many fuel elements ordinarily used in core design, these measurements may be considered as typical of fuel lattices moderated by D_2O-H_2O mixtures.

Neutron Thermalization Experiments

With the development of reactor design to encompass systems that are more heavily loaded with fuel and with the increasing importance of reactivity lifetime predictions in systems containing substantial quantities of the plutonium isotopes, the need for a fundamental understanding of neutron thermalization in the energy range below 1 ev has become increasingly important. Since a proper theoretical treatment of neutron thermalization in this energy range must include not only the effects of moderator mass and scattering amplitude but also effects dependent on the state of chemical binding of the moderator and the moderator temperature, the problem is a complex one, and rapid progress toward its solution is greatly facilitated by good experimental information. In the last few years, an increasing amount of experimental work has been devoted to this problem, and an experimental basis for understanding neutron thermalization below 1 ev is being developed. Some of the present experimental programs are concerned with the systematic measurement of the differential-energy-change cross section $\partial^2\sigma/(\partial E\, \partial \Omega)$ for the common moderators at various moderator temperatures and with measurements of the infinite-medium and spatially dependent neutron spectra in pure moderators as well as in moderators poisoned with varying amounts of $1/v$ and resonance absorbers. Recent results of these types are described briefly in the following reviews.

Scattering-Law Experiments

Systematic programs initiated by Egelstaff of Harwell and Brugger of Phillips Petroleum to measure the slow-neutron differential-energy-change cross sections and angle-dependent inelastic scattering cross sections of the important moderators are currently in operation at the NRU Reactor, Chalk River,[18,19] and the MTR at the National Reactor Testing Station in Idaho.[20,21]

If a beam of monoenergetic neutrons is directed at a sample of scattering material, the paths of the scattered neutrons will lie in some distribution in the angle Ω relative to the incident beam, and the energies of the scattered neutrons will lie in some distribution in the energy variable, E. If one picks a specific energy E_1 and a specific angle Ω_1, a cross section can be identified $\sigma(E_1, \Omega_1)$ for the scatterer which expresses the probability that an incident neutron will be scattered into that angle with an energy E. Evidently, if $\sigma(E, \Omega)$ is known for a given material, over the range of possible incident neutron velocities, the basic information is available for computing the transport and the energy distribution of neutrons in the material. The same information can also be expressed in a different way by giving the partial derivative of the scattering cross section, σ, with respect to E and Ω: $\partial^2\sigma/(\partial E\, \partial\Omega)$.

In the programs at Chalk River and at the MTR, the conceptual experiments postulated above have been reduced to practice. A beam of neutrons extracted from the reactor is passed through a number of choppers, and a series of neutron bursts of well-defined energy E_0 is obtained. These neutrons are directed to the sample, and approximately 10% are scattered into multiple detectors arranged in a vertical plane around the sample. The scattering angle Ω as well as the time of flight, and consequently the final energy E, are recorded on large multiparameter recorders. These data are corrected for background and detector efficiency, and the standard deviation is computed for each energy interval and detector. In the

NRU experiments two methods for normalizing the data are used. In the first method the corrected counts are summed over all energies and angles, and the result, $K(1)$, is divided by the total scattering cross section σ_t for the material. Subsequently the corrected counts in each energy interval in each detector are multiplied by $\sigma_t/K(1)$. This method is inaccurate if the measured material does not have a sufficiently smooth angular distribution. The second method is based on measurement of the transmitted beam through the sample. The normalization factor is $K(2) = 1/(N_s N \Delta\phi)$, where N_s is the number of atoms per square centimeter of beam as determined from transmission measurements and the incident energy cross section of the material, N is the number of neutrons through the sample as determined by separate measurements with a vanadium sample, and $\Delta\phi$ is the solid angle subtended by each detector. These measurements have been made at room temperature for graphite, light water, heavy water, beryllium oxide, and uranium dioxide. Additional measurements[18] have been made at elevated temperatures for graphite (300 and 600°C), light water (150°C), heavy water (150°C), and uranium dioxide (450°C). Although different in details, the MTR instrument and the data-handling programs provide similar information. Results published include the organic-moderating terphenyls as a function of temperature,[22] methane as a function of temperature,[23] and propane.[24]

It has been found convenient, for several reasons, to express the results in terms of a "scattering law," $S(\alpha,\beta)$. This function includes all the characteristics of the scattering distribution which are dependent on the properties of the scattering material, and, for a given material, at a given temperature, it is a function of only the relative momentum transfer (α) and the relative energy transfer (β) in the collision. Specifically, $S(\alpha,\beta)$ is related to the experimentally determined quantity $\partial^2\sigma/(\partial E\ \partial\Omega)$ by:

$$S(\alpha,\beta) = \frac{4\pi}{\sigma_b}\sqrt{\frac{E_0}{E}}\ kT\ \exp\left(\frac{\beta}{2}\right)\frac{\partial^2\sigma}{\partial E\ \partial\Omega}$$

where σ_b is the bound cross section of the principal scatterer. The expressions for alpha and beta are

$$\alpha = \frac{m[E_0 + E - 2(E_0 E)^{1/2}\ \cos\ \Omega]}{MkT} \qquad (1)$$

$$\beta = \frac{E - E_0}{kT} \qquad (2)$$

where E_0 = the incident neutron energy, ev
E = neutron energy after scattering, ev
kT = sample temperature, ev
m = neutron mass, amu
M = mass of principal scatterer, amu
Ω = angle of detector with respect to direction of incident beam

The general survey of scattering from H_2O, D_2O, and graphite has, to a large extent, been completed. The data have been reduced, and the results for H_2O and D_2O are compiled[25,26] in the form of measured cross sections and standard deviations listed in order of increasing energy and temperature for each angular detector position. Each set of cross sections for a given incident energy and temperature is followed by scattering-law tables listing alpha, beta, $S(\alpha,\beta)$, and the standard deviation. A fairly complete graphic compilation of inelastic-scattering-law data is given by Brugger.[27]

The advantages of the presentation of the measured scattering data $\partial^2\sigma/(\partial E\ \partial\Omega)$ in the form of a scattering law are: (1) a large number of data can be presented in a compact form, (2) systematic experimental errors are more easily detected using this formulation, and (3) $\partial^2\sigma/(\partial E\ \partial\Omega)$ can be generated at angles and energies other than those measured in the determination of $S(\alpha,\beta)$. The scattering-law formulation assumes additional importance in computer programs for the calculation of reactor spectra where the storage of sufficient information at a few initial neutron energies makes possible the generation of partial differential cross sections for many initial neutron energies and angles.

In the inversion of differential scattering cross-section data into the scattering-law formulation, data at different initial energies and scattering angles are intermixed so that the scattering law is experimentally overdetermined in certain regions. Since the general theory of the scattering law shows that $S(\alpha,\beta)$ is an even function, there should not be splitting of $S(\alpha,\beta)$ into $+\beta$ and $-\beta$ branches for a given beta. However, because such systematic errors as incorrectly measured flight distances, time-of-flight measurement errors, incorrect background, wrong sample temperature, or large multiple-scattering effects can cause the $S(\alpha,\beta)$

curve to split, the data are checked for internal consistency. In the experimental case each value of beta represents a definite time of flight, and the variation in alpha represents the angular variation in the occurrence of that flight time.

Illustrations of the Scattering Law

The calculated scattering law using the Krieger-Nelkin theory[28] for a perfect monatomic gas is given in Fig. II-1. For a perfect monatomic gas there is no explicit dependence of the scattering law on temperature or the mass of the gas molecule. The particular utility of the dimensionless parameters alpha and beta in this situation is seen in that data obtained under a variety of conditions are related to the same point on the scattering law.

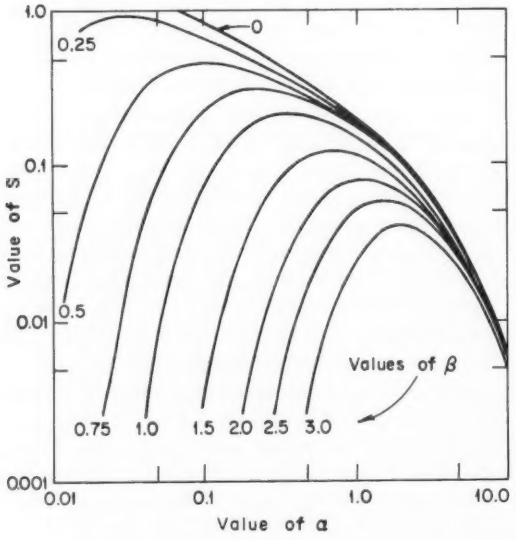

Fig. II-1 Scattering law for a perfect gas.[19]

Figure II-2 shows the measured scattering law for graphite at room temperature. The effect of structure can be seen at low values of beta, in the 0.2 and 0.4 range, where the spacing of adjacent curves is quite close. The closing up or overlapping of adjacent curves indicates that scattering is more likely in that range of beta, and hence the presence of energy levels is shown. Reference 19 states that the fluctuations in Fig. II-2 agree fairly well with known data on crystalline planes in graphite. The upward trend in the curves in the range alpha = 0.5 to 1.0 is consistent with the large structure factors for this range of alpha.[19] The curves in Fig. II-2 appear to be "cut off" at the ends; this is due to the limiting effects of simultaneous momentum and energy conservation. Only part of the scattering law is accessible to convenient neutron experiments; although alpha and beta are independent variables in the scattering law, they are related in the dynamics of the scattering process. However, by judicious choice of incident neutron velocities, a large part of the scattering law can be obtained in a few runs.

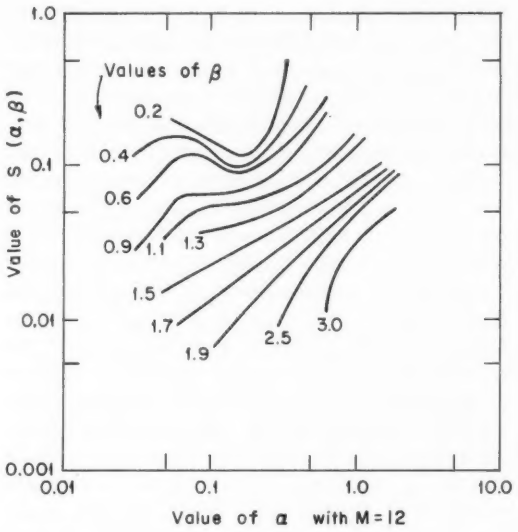

Fig. II-2 Best lines through measured scattering law for room-temperature graphite[19] ($\beta = 0.2$ to $\beta = 3.0$).

Figure II-3 illustrates the measured scattering law for light water. The curves are similar to those of the perfect gas (Fig. II-1) (note change of alpha scale) because the water scattering is entirely incoherent; therefore structure effects are not noted. The neutron energies and sample temperature used were not in the range to excite energy levels such as those due to the O–H bond. Although the curves are similar to those of a gas, their shapes do not correspond exactly to those which would characterize a gas having a well-defined mass. The insert in Fig. II-3 shows the measured scattering law for light water at beta = 2 when alpha is computed (Eq. 1) with $M = 4$ instead of with $M = 1$ as in the main part of the figure. The insert curve is compared with the corresponding perfect-gas curve. It is seen that

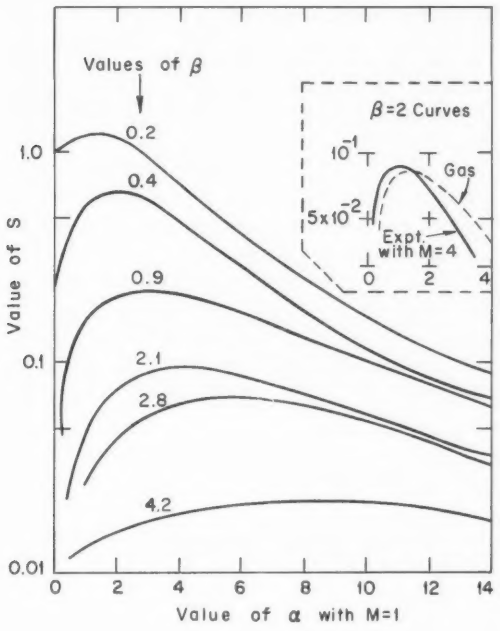

Fig. II-3 Best lines[19] through measured scattering law for room-temperature H_2O.

there is approximate agreement between the curves. Separate comparisons of this type at each value of beta would yield an equivalent gas mass for each value of beta.

The most nearly complete theoretical interpretation of inelastic scattering has been applied to methane;[29] it has been concluded that a detailed account of the shape of the scattering law requires quantum mechanically discrete rotational levels at small scattering angles and consideration of interference between hydrogen atoms to account for the observed structure in the scattering-law curves.

Interpretation of Scattering-Law Data

The scattering law $S(\alpha,\beta)$ is composed of a "self-term" S_s, which arises from neutron scattering from a single nucleus, and an interference term S_d, which represents the interference wavelets scattered from several atoms. The interference term S_d is generally small* and, in practice, is calculated and subtracted from $S(\alpha,\beta)$ when values of S_s are desired. The self-term S_s is the double Fourier transform of the self-correlation functions of Van Hove[30] which represent the motion of an individual atom in the system as a gaussian distribution of atomic position plus correction terms. One objective of the analysis of the scattering law is to show that the contributions of these correction terms to the scattering are negligible. If the correction terms are negligible, direct comparisons can be made of the experimental scattering law to calculated values of S obtained by using the perfect-gas model, the Debye model,[31] Vineyard's[32] diffusion models, and Nelkin's[33] water model.

The correction terms to the gaussian distribution can be evaluated experimentally. The double-time differential of the time-dependent width of the gaussian distribution is the velocity correlation function for an atom in the system. Since the Fourier transform of the velocity correlation function can be determined from the experimental results as

$$p(\beta) = \beta^2 \left[\frac{S_s(\alpha,\beta)}{\alpha}\right] \quad \alpha \to 0$$

the self-part of the scattering can be determined for all values of alpha and beta. By subtraction the correction terms can then be found.

Application of Neutron Scattering Law to Spectrum Calculations

The scattering law $S(\alpha,\beta)$ is simply related to the scattering kernel $\sigma(\beta,E_0)$ required for spectrum calculations:

$$\sigma(\beta,E_0) = \frac{\sigma_b}{4\alpha_0} e^{-\beta/2} \int S(\alpha,\beta)\, d\alpha$$

where the limits of α are given by

$$\alpha^{1/2} = \left(\frac{\beta m}{M} + \alpha_0\right)^{1/2} \pm \alpha_0^{1/2}$$

and m is the neutron mass in amu and α_0 is $E_0 m/MkT$. The other symbols retain their previous definition.

In the present methods of calculation of the reactor spectrum which assume isotropic scattering, the scattering kernel must be calculated for each value of beta from the measured scattering laws. However, when analytical methods are extended to include the effects of non-

*For many strongly coherent crystalline materials, notably graphite and beryllium, the S_d term is not expected to be small, and the use of the "incoherent approximation" is open to considerable question.

isotropic angular distributions, the scattering law may be used directly.

Another approach to calculating the neutron spectrum is to use the measured scattering data in Corngold's asymptotic solution of the neutron spectrum in an infinite homogeneous absorbing medium. The coefficients of the Corngold series are given in terms of the beta moments of the scattering law. When only the self-part of the scattering is considered, these moments are expressed directly in terms of $p(\beta)$, and therefore it is possible to calculate the spectrum directly from experiment with a considerable reduction in labor and improvement in accuracy.

Spectrum Measurements

A combined experimental and theoretical program[35] with primary emphasis on describing the neutron interaction with bound moderator atoms is being carried on at General Atomic under sponsorship of the AEC. In the infinite-media experiments, pulses of fast neutrons provided by the Linac accelerator are thermalized in a cubical volume of the sample material, and a neutron beam is extracted from the sample. This beam is analyzed by time-of-flight techniques, and the shape of the thermal spectrum is determined. Spectra were measured in pure water and in water poisoned with varying

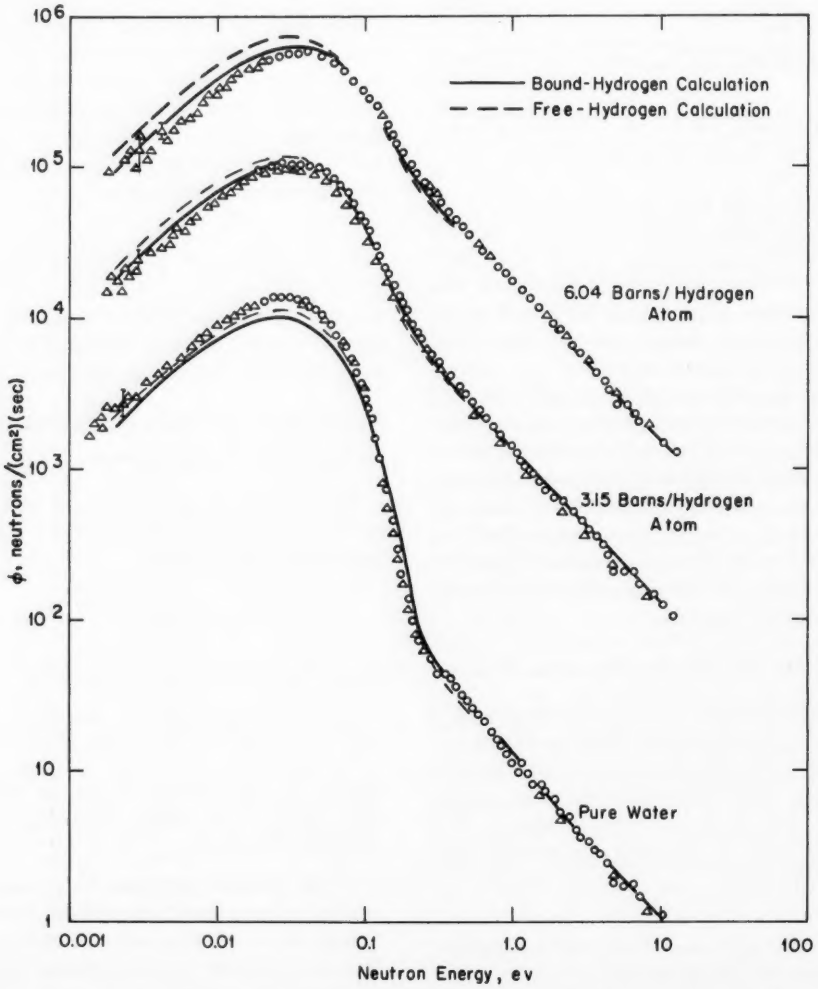

Fig. II-4 Neutron spectra in pure water and water poisoned with boric acid.[35]

amounts of boron and other distinctive absorbing materials such as cadmium, samarium, erbium, and gadolinium. Pulse-spectrum measurements were also made in pure polyethylene, graphite, beryllium oxide, zirconium hydride, and in these materials when poisoned with boron. In addition, spatially dependent spectra were measured within and near the edges of boron-poisoned water slabs.

As part of the program, a series of comparisons has been made between measured and calculated spectra in infinite pure-water media and in water poisoned with various absorbers. Figure II-4 shows these measurements of the neutron spectrum in pure water and in water poisoned with boric acid. The calculations shown were made using the free-hydrogen model and Nelkin's[33] bound-hydrogen model for energies below 1 ev. An explicit asymptotic expansion using the formalism of Corngold[34] was derived for the neutron flux above 1 ev for the cases containing $1/v$ absorption. All spectra are near the characteristic Maxwellian shape below the thermal peak. It is seen that the measurements on systems containing a $1/v$ absorber agree better with the predictions of the bound-hydrogen model than with those of the free-hydrogen model. These measurements were sufficiently precise to discriminate between the two models, the discrepancy between the models being greater than the experimental errors by factors of 2 or 3. The spectrum measurements in pure water did not make a sensitive discrimination between the calcula-

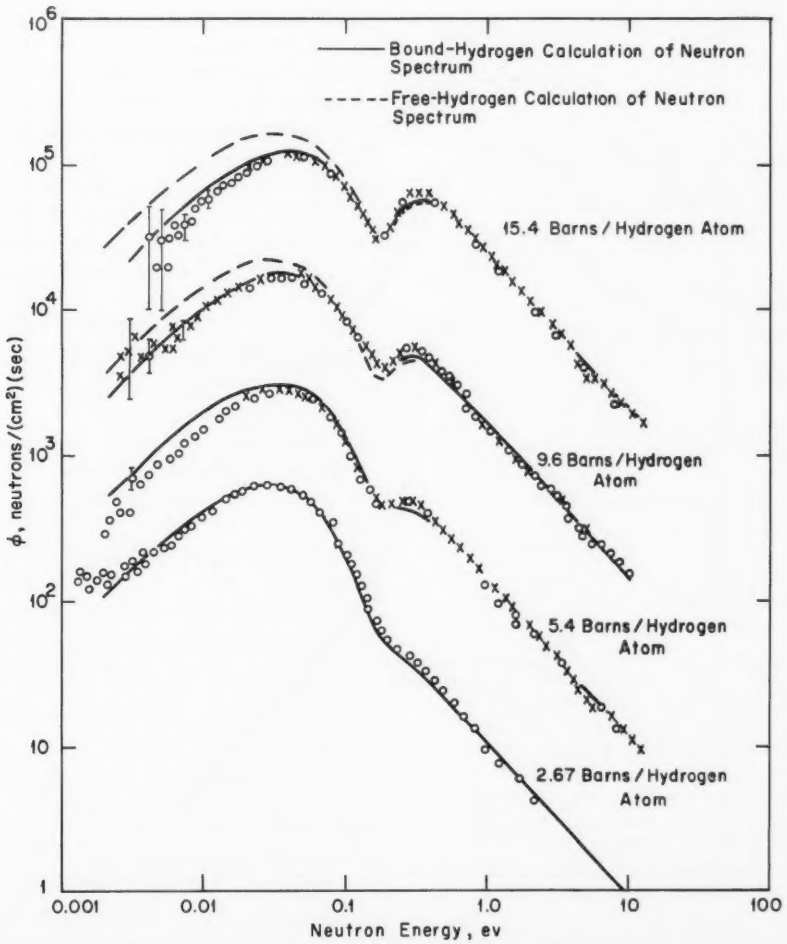

Fig. II-5 Neutron spectra in water poisoned with cadmium sulfate.[35]

tional models because the large neutron-leakage probability for pure water made the establishment of an infinite-medium spectrum impossible.

Measured spectra in water solutions of cadmium sulfate are compared with calculated spectra in Fig. II-5. At all concentrations measured, the bound-hydrogen model gave reasonable agreement with the measured spectra, whereas the poorer agreement of the free-hydrogen prediction is readily apparent. The best agreement of the Nelkin bound-hydrogen model was obtained at the largest cadmium concentration, which indicated an overestimation of down-scattering in the Nelkin water kernel. It is thought that a small modification in the energy-transfer kernel for water would improve the overall agreement.

Similar studies on water poisoned with samarium chloride indicated the same general deficiency of the free-hydrogen model and, in addition, relatively poor agreement between the measured spectra and those calculated by the bound-hydrogen model. Possible reasons for the greater discrepancy are (1) that a true infinite-medium spectrum may not have been attained and (2) that uncertainties in the cross section of samarium may have been reflected in the calculations.

Good agreement between measured spectra and bound-hydrogen calculations was obtained in the case of water poisoned with erbium chloride.

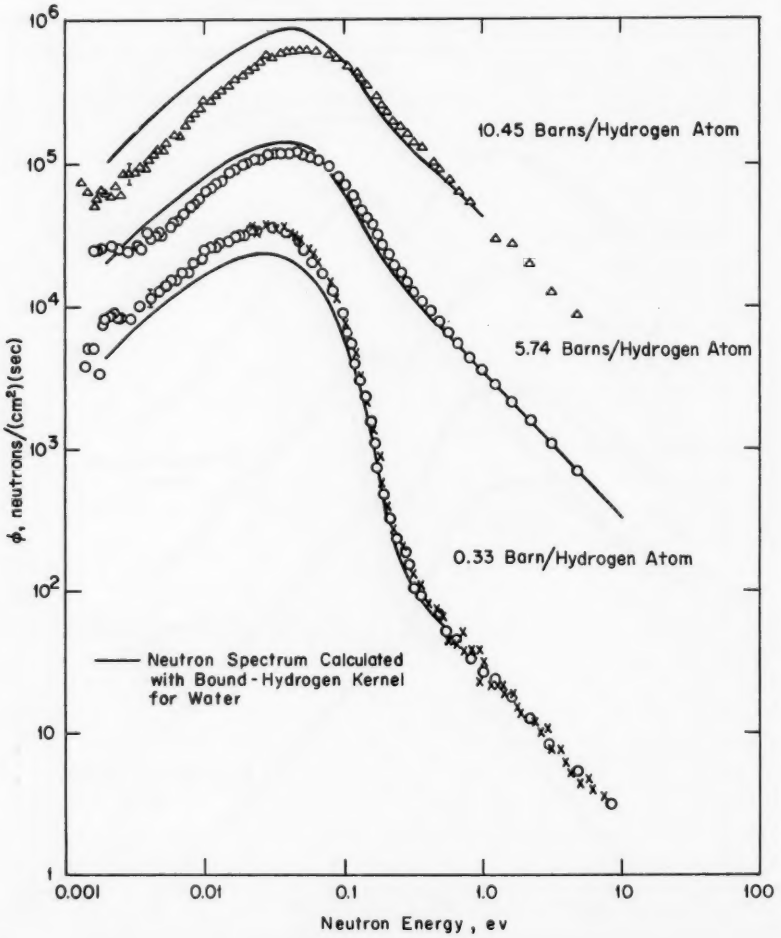

Fig. II-6 Neutron spectra in pure and borated polyethylene.[35]

Of special significance was the capability of the Nelkin bound-hydrogen model to calculate the spectrum in the neighborhood of the erbium resonances at 0.5 ev, which implies that this model should also give good results in calculations involving the 0.3-ev plutonium resonance.

The thermal-neutron spectrum in polyethylene is of interest because polyethylene is frequently used in critical mockups. Figure II-6 compares polyethylene spectra measured at General Atomic[35] with calculations using Nelkin's water kernel. It is seen that the calculation yields a softer spectrum than the measured spectrum because of the strong binding of the hydrogen atoms in the polyethylene molecule.

Spatially Dependent Spectra

Conventional reentrant tube techniques as well as a novel method of neutron-beam extraction were used at General Atomic to measure spatially dependent flux spectra in "infinite" thermalizing slabs of water. The new technique involves penetrating the slab with a hole, along the thickness dimension, and placing an ideally incoherent nonabsorbing scatter (approximated by zirconium or lead) within the hole at the point of measurement. Thus all neutrons incident on the scatterer are scattered with equal probability into the time-of-flight detection system collimated to view only the scatterer.

The spectrum measurements were made in slabs of pure and $1/v$ poisoned water ranging from 2 to 8 in. thick. Calculations were made, in the case of the 4-in. slab poisoned with boric acid to 6 barns/hydrogen atom, by diffusion theory with a bound-hydrogen kernel and a fictitious $D(E)B_g^2$ to account for leakage and also by SLOP-1 (Ref. 36) and by a one-dimensional transport-theory code, THERMOS. Agreement to within 10% with measurement was found for each of the calculational methods at the peak of the spatial neutron distribution. When these techniques were applied to the calculation of the scalar and angular neutron spectra at a position $2\frac{1}{2}$ in. inside the edge of the 4-in. slab, some differences with experiment were found for the scalar fluxes, and, in addition, the angular or leakage spectrum was found to be very poorly represented by the predictions of THERMOS, the discrepancy being as much as 50%.

For spectrum measurements made at the center of the 4-in. pure-water slab, there was significant disagreement with the results of diffusion theory, SLOP-1, and THERMOS. The analytical difficulties in pure water result from the lack of coincidence of the thermal- and fast-flux distribution; therefore two distributions prevail in the presence of strong diffusion effects.

More favorable agreement between theory and experiment was found for measurements on a 2-in. poisoned-water slab than for those on thicker slabs. The improvement is attributed to the finer mesh spacings possible in the thinner slab calculations. It is felt that the present codes are not adequate for calculations on thick slabs and that integral transport-theory approaches will have to be tried in place of the present differential transport-theory methods since the latter cannot be extended to finer spatial resolution without exceeding the limitations of the present computers.

References

1. E. D. Clayton et al., Critical Mass Experiments with Plutonium-Nitrate Solutions, in Physics Research Quarterly Report, October, November, December 1961, USAEC Report HW-72586, pp. 54–65, Hanford Atomic Products Operation, Jan. 31, 1962.
2. R. C. Lloyd, E. D. Clayton, and W. A. Reardon, Critical Mass Experiments with Plutonium-Nitrate Solutions, in Physics Research Quarterly Report, January–March 1962, USAEC Report HW-73116, pp. 101–107, Hanford Atomic Products Operation, Apr. 16, 1962.
3. H. K. Clark, Handbook of Nuclear Safety, USAEC Report DP-532, p. 150, Savannah River Laboratory, January 1961.
4. H. K. Clark, Bucklings of Pu-H_2O Systems, USAEC Report DP-701, p. 28, Savannah River Laboratory, May 1962.
5. F. E. Driggers and J. C. English, Calculation of Heavy Water Lattice Parameters, USAEC Report DP-661, p. 44, Savannah River Laboratory, November 1961.
6. J. T. Mihalczo and V. I. Neeley, The Infinite Neutron Multiplication Constant of Homogeneous Hydrogen Moderated 2.0 Wt.% U^{235} Enriched Uranium, *Nucl. Sci. Eng.*, 13(1): 6–11 (May 1962).
7. R. H. Masterson, V. I. Neeley, and T. J. Powell, Limiting Critical Concentrations for a Plutonium Nitrate Solution and for a Uranium-235 Solution, in Physics Research Quarterly Report, January–March 1962, USAEC Report HW-73116, pp. 108–120, Hanford Atomic Products Operation, Apr. 16, 1962.
8. R. I. Smith, The Fuel Temperature Coefficient of k_∞ for Plutonium-Aluminum Fuel, in Physics

Research Quarterly Report, January–March 1962, USAEC Report HW-73116, pp. 71–81, Hanford Atomic Products Operation, Apr. 16, 1962.

9. J. R. Cooper, R. E. Sullivan, and W. B. Henderson, Reactor Neutron Cross Sections in Fine Energy Detail, USAEC Report APEX-704, General Electric Co., Flight Propulsion Laboratory Dept., November 1961.
10. A. E. McArthy, C. N. Kelber, and L. J. Templin, Neutron Resonance Integral and Age Data, USAEC Report TID-14652, Argonne National Laboratory, Nov. 20, 1961.
11. R. Goldstein and E. R. Cohen, Theory of Resonance Absorption of Neutrons, *Nucl. Sci. Eng.*, 13(2): 132 (June 1962).
12. R. B. Tattersall, Thermal Cross-Section and Resonance Absorption Integral of Pu-240, British Report AEEW-R-115, March 1962.
13. F. B. Simpson and W. H. Burgus, Tabulation of the Pa-231 Total Neutron Cross Sections, USAEC Report IDO-16698, Phillips Petroleum Co., January 1962.
14. F. B. Simpson, W. H. Burgus, J. E. Evans, and H. W. Kirby, Total Neutron Cross Section of Pa^{231}, *Nucl. Sci. Eng.*, 12(2): 243 (February 1962).
15. L. J. Esch, Temperature Dependence of the Neutron Transport Cross Section in Paraffin and Polyethylene, USAEC Report KAPL-2204, Knolls Atomic Power Laboratory, Feb. 1, 1962.
16. L. J. Rainwater, W. W. Havens, Jr., J. R. Dunning, and C. S. Wu, Slow Neutron Velocity Quartz, *Phys. Rev.*, 73: 733 (1948).
17. D. M. Roberts and W. G. Pettus, Spectral Shift Control Reactor Basic Physics Program. Age Measurements in ThO_2-D_2O-H_2O Lattices, USAEC Report BAW-1234, Babcock & Wilcox Co., December 1961.
18. P. A. Egelstaff, The Scattering of Thermal Neutrons by Moderators, British Report AERE-R-4041, April 1962.
19. P. A. Egelstaff, Progress of the Scattering Law Experiment, British Report AERE-R-4019, April 1962.
20. R. M. Brugger and J. E. Evans, MTR Phased Chopper Velocity Selector, *Nuclear Instr. and Methods*, 12: 75 (1961).
21. R. M. Brugger and J. E. Evans, Slow-Neutron Inelastic Scattering Measurements at the Materials Testing Reactor, Paper IS/31 presented at IAEA Symposium on Inelastic Scattering of Neutrons in Solids and Liquids, Vienna, 1960.
22. R. M. Brugger, Scattering of Slow Neutrons by Solid and Liquid Terphenyls, *Phys. Rev.*, 126(1): 29 (April 1962).
23. P. D. Randolph, R. M. Brugger, K. A. Strong, and R. E. Schmunk, Inelastic Scattering of Slow Neutrons from Methane, *Phys. Rev.*, 124(2): 460 (October 1961).
24. K. A. Strong, G. D. Marshall, R. M. Brugger, and P. D. Randolph, Scattering of Slow Neutrons from Propane Gas, *Phys. Rev.*, 125(3): 933 (February 1962).
25. H. Greenspan and I. G. Baksys, Differential Scattering Cross Sections for Slow Neutrons in H_2O, USAEC Report TID-15721, Argonne National Laboratory, March 1962.
26. H. Greenspan and I. G. Baksys, Differential Scattering Cross Sections for Slow Neutrons in D_2O, USAEC Report TID-15990, Argonne National Laboratory, April 1962.
27. R. M. Brugger, Compilation of Reduced Slow Neutron Partial Differential Scattering Cross Sections, USAEC Report IDO-16699(Rev.), Phillips Petroleum Co., July 2, 1962.
28. T. J. Krieger and M. S. Nelkin, *Phys. Rev.*, 106: 290 (1957).
29. G. W. Griffing, Scattering of Slow Neutrons by Gaseous Methane, Paper SM-30/44 presented at Symposium on Inelastic Scattering of Neutrons in Solids and Liquids, Chalk River, Sept. 10–14, 1962.
30. L. Van Hove, Correlations in Space and Time and Born Approximation Scattering in Systems of Interacting Particles, *Phys. Rev.*, 95: 259 (1954).
31. R. C. F. McLatchie, C. Heard, P. A. Egelstaff, and P. Schofield, Examples of the Thermal Neutron Scattering Law, British Report AERE-R-3847, July 1961.
32. G. Vineyard, Scattering of Slow Neutrons by Water, *Phys. Rev.*, 110(5): 999 (June 1958).
33. M. Nelkin, Scattering of Slow Neutrons by Water, *Phys. Rev.*, 119(2): 741 (July 1960).
34. N. Corngold, Thermalization of Neutrons in Infinite Homogeneous Systems, *Ann. Phys. (N. Y.)*, 6: 368 (1959).
35. J. R. Beyster, W. M. Lopez, Y. D. Naliboff, D. E. Parks, G. D. Trimble, J. C. Young, and R. B. Walton, Integral Neutron Thermalization Annual Summary Report, October 1, 1960 Through September 30, 1961, USAEC Report GA-2544, General Atomic Div., General Dynamics Corp., Sept. 30, 1961.
36. H. Bohl, E. Gelbard, P. Buerger, and G. Culpepper, SLOP-1, A Thermal Multigroup Program for the IBM-704, USAEC Report WAPD-TM-188, Westinghouse Electric Corp., Bettis Atomic Power Laboratory, October 1960.

Section

III

Power Reactor Technology

Heat Transfer

The Fifth National Heat Transfer Conference and Exhibit was held in Houston, Tex., on Aug. 5–8, 1962. The meeting was sponsored jointly by the Heat Transfer Divisions of the American Society of Mechanical Engineers and the American Institute of Chemical Engineers. The conference papers are available individually, but they have not been collected as a complete volume. Many of them will be published in the journals of the two sponsoring organizations. The following review covers a number of the papers which are of interest in the nuclear engineering field; where applicable other references are used to broaden the coverage of the particular subject.

Subcooled Nucleate Boiling in Forced Convection

Heat-transfer measurements on a long, small-diameter tube are described in Ref. 1. The test section was a 0.226-in.-ID by 10 ft 2 in.-long Inconel tube which gave an L/D of 540. The tube was heated by direct electrical conduction. Pure water (from condensed steam) was pumped through the test section with an inlet subcooling of 0 to 130°F, at pressures of 15 to 65 psia, at mass velocities up to 900,000 lb/(hr)(sq ft), and at Reynolds numbers from 7000 to 40,000.

Some interesting qualitative relations may be observed when one parameter is varied while the others are held constant. When the mass velocity and the pressure are held constant, the heat-transfer coefficient increases as the subcooling decreases. With constant pressure and subcooling, the heat-transfer coefficient increases as the mass velocity increases.

The point of burnout was assumed to be reached when the wall temperature of the test section became unstable and fluctuated over a wide range. Burnout was reached with heat fluxes generally in the vicinity of 5000 to 15,000 Btu/(hr)(sq ft). In reply to an oral question as to the reason for the very low burnout fluxes, the author stated that the temperature oscillations were brought on by a choking effect in the long test section.

Perhaps the most interesting result of the program is the heat-transfer correlation that was developed for the subcooled nucleate-boiling range:[1]

$$(\mathrm{Nu})_a = 0.0011\,(\mathrm{Re})_a^{1.32} \times (\mathrm{Pr})_a^{0.4} \times \left(\frac{\mu_a}{\mu_s}\right)^{0.14} \times \left(\frac{D}{L}\right)^{0.055}$$

where Nu = Nusselt number
Re = Reynolds number
Pr = Prandtl number
μ = dynamic viscosity
D = diameter
L = length
a = arithmetic mean
s = surface

This correlation appears to be very useful at low heat-flux values, up to 15,000 Btu/(hr)(sq ft). Extrapolation of the correlation to high heat fluxes probably is not warranted. This test is a good example of burnout caused by hydrodynamic instability in subcooled flow.

Reference 2 contains a qualitative review and a quantitative study of the increase in pressure drop due to nucleate boiling in flowing subcooled water. The stainless-steel test section used for the experimental work was 30 in. long and 0.416 in. in inside diameter, giving

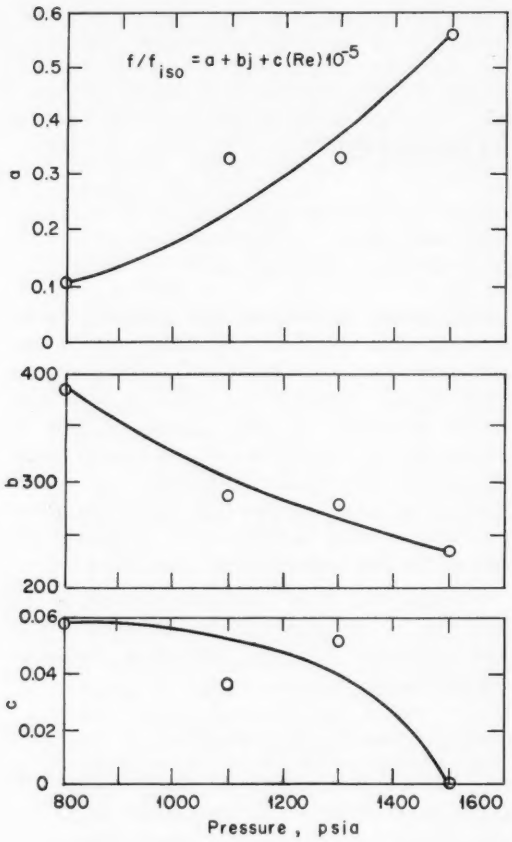

Fig. III-1 Pressure-dependent constants for empirical equation.[2]

an L/D of 72. The tube section was designed to simulate a PM-1 reactor fuel element, and it was heated by direct electrical conduction from a d-c power supply. Static pressure taps were located at 20% increments along the length of the test section.

The following pressure-drop equation (in ratio form) is proposed in the paper:[2]

$$f/f_{iso} = a + b(j) + c(\mathrm{Re})$$

where a, b, c = pressure-dependent constants
f_{iso} = single-phase isothermal pressure drop in a smooth tube
f = local subcooled nucleate-boiling pressure drop
j = local Stanton number × (Prandtl number)$^{2/3}$
Re = Reynolds number

Figure III-1* gives the values of a, b, and c as functions of pressure, from 800 to 1600 psia, as determined by the experimental work.

The theoretical approach to the problem embraces the assumption that local surface boiling affects the pressure drop in a manner similar to surface roughness. The experimental heat-transfer measurements were made in order to determine the relation between j and f in local boiling. It is interesting to note qualitatively that j increases as the subcooling decreases, in agreement with the information from Ref. 1. Reference 2 also includes a review of bubble dynamics in nucleate boiling which covers the nucleation of a bubble, its growth, and its collapse.

Boiling Burnout in Rod Bundles

Most of the previous experimental work on forced-convection burnout has been performed with fluid flow through circular or rectangular tubes. The question of burnout in rod bundles is equally, or more, important in reactor technology. References 3 and 4 contain experimental information on this question; the first reference treats water at 2000 psia, whereas the second reference is concerned with water at 30 psia.

Reference 3 states that: "Tests are reported which show that pressure drop and DNB correlations developed with rectangular channels are applicable for flow parallel to rod bundles. These tests were conducted using d-c resistance heating with vertical upflow of water through a heated nine-rod prototype of the PWR blanket rod bundle at 2000 psia with inlet temperatures of 400 to 625°F, mass velocities from 0.7 to 2.0×10^6 lb/(hr)(sq ft), at heat fluxes up to 1.4×10^6 Btu/(hr)(sq ft). The heated test section comprised nine rods 0.413 in. OD × 13 in. long on a 0.468-in. square pitch having a uniformly heated length of 9¼ in."

Reference 4 states that: "The effect of nonuniform heating, nonuniform spacing, and the presence of restrictions on burnout and the behavior of two-phase flow in a rod type reactor fuel geometry has been investigated. Tests were conducted using electrically heated rods and

*Figures III-1 to III-6 are reprinted here by permission from the American Society of Mechanical Engineers.

water at 30 psia. The results show that neither local power peaking of 17 per cent, nor displacement of a rod from its normal position by 0.132 in., nor restriction of the flow by a plate type spacer had any adverse effect on burnout. On the contrary, the presence of the spacer improved the burnout characteristics."

The two burnout points reported in Ref. 3 represent actual burnout of the test section since the test section was not instrumented with thermocouples to detect departure from nucleate boiling (DNB). Many other runs were made at values below burnout, which obviously established a "lower limit" for burnout. Figure III-2 shows a comparison[3] of the burnout heat flux for the rod bundle with the burnout heat flux for rectangular channels (Ref. 5). As noted in Fig. III-2, the two points of rod-bundle burnout agree well with the rectangular channel points. The rod-bundle nonburnout points (identified in the figure as "parallel-flow-rod scanning points") plot just below the burnout points. In response to an oral question, one of the authors[3] replied that their experience indicated burnout to be reached with about 5% higher heat flux than DNB.

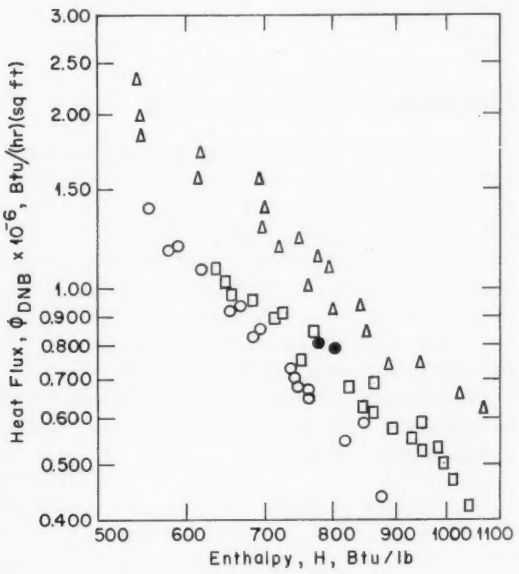

Fig. III-2 Burnout heat flux in rod bundles and rectangular channels.[3] ○, parallel-flow-rod scanning point. ●, parallel-flow-rod burnout point. △, 0.097-in. by 1-in. by 6-in.-long rectangular-channel DNB point. □, 0.097-in. by 1-in. by 12-in.-long rectangular-channel DNB point.

The test section of Ref. 3 was instrumented to measure the static pressure at numerous points. The axial pressure gradient was measured along the wall of the flow liner and also from end to end for several rods. The radial pressure gradient was measured at each end between the rods and flow liner. Radial pressure gradients did exist, and they were functions of operating and design conditions. The degree of flow redistribution as a result of the gradients is estimated and discussed.[3] The axial pressure-drop measurements, with and without local boiling, compared very well with calculated values based on Ref. 6.

The report states in conclusion that: "In the range of variables covered, the rectangular channel correlations... for pressure drop and DNB were found to be applicable for rod bundles. The detection of radial pressure gradients, which increased when boiling began, implied that flow redistribution occurred. However, this redistribution had negligible effect on the burnout and axial pressure drop results."

The heated rods discussed in Ref. 4 are 0.25 in. in diameter, arranged in a square four-rod configuration. In one case the rods are spaced at 0.625 in. and are fitted in a 1.25-in.-square flow channel. In a more compact grouping, the same rods are spaced at 0.50 in. and are fitted in a 1.00-in.-square flow channel. A typical rod has a heated length of 8.5 in. The flow channels, which are made of pyrex glass, allow visual and photographic observation. In the burnout tests natural circulation was used through the loop. With the electric power held constant at some predetermined point, the water flow rate was gradually reduced by adjusting an inlet valve. Burnout was determined visually by the operator as the point at which one or more of the rods reached red heat. By immediately shutting off the power, manually, when this point was reached, the operator could prevent damage of the test section.

Burnout generally occurred at the top end of the rod, where the steam quality was highest. With the wide-spaced test section, burnout was investigated over the following range of conditions:

Pressure	30 psia
Subcooling at inlet	4 to 12°F
Inlet velocity	0.08 to 2.41 ft/sec
Exit quality	0.02 to 0.30

The results are shown in Fig. III-3 as a function of inlet velocity. They have been compared[4] with Eq. 15 of Ref. 7, which was derived from experimental results on an annular test section:

$$(q/A)_{bo} = (400{,}000 + 4800\ \Delta t_{sub}) \times v_0^{1/3}$$

where $(q/A)_{bo}$ is the burnout heat flux, Btu/(hr)(sq ft); Δt_{sub} is the inlet subcooling, °F; and v_0 is the inlet velocity, ft/sec. This equation is plotted in Fig. III-3 for zero subcooling and for 10°F subcooling. The experimental points generally fall a little above the curve for 10°F subcooling. In consideration of the differences between the two test sections, the agreement was judged to be quite good.[4] According to the following equations, the experimental points also correlate well (±20%) with exit quality:

$$(q/A)_{bo} = 121{,}000/X^{0.42}, \text{ when } X < 0.082$$

$$(q/A)_{bo} = 190{,}000/X^{0.24}, \text{ when } X > 0.082$$

where X is the exit quality.

The test points in Fig. III-3 include data for two special situations: (1) the situation where one of the rods was operated at a power density 17% higher than the average, and (2) the situation where the hot rod was moved radially 0.132 in. toward the corner of the flow liner. Neither of these two variations caused any discernible effect upon the burnout heat flux. The burnout values for the close-spaced test section were in reasonable agreement with the values shown for the wide-spaced test section.

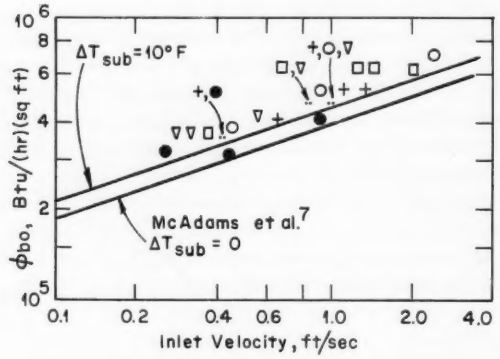

Fig. III-3 Burnout heat flux as a function of inlet velocity for the 1.25- by 1.25-in. channel.[4] +, ●, normal rods. ○, one hot rod. ∇, □, hot rod displaced.

Two types of restrictions were placed at the axial midpoint of the test section to observe what effect this might have on the burnout. Interestingly, there was no harmful effect, and in some cases the burnout heat flux was higher. In some cases burnout was reached in the lower part of the test section, which indicated that the restriction was suppressing burnout at the upper part, where burnout had normally occurred without the spacer.

High-speed movies were taken of the test section during some of the tests to study the flow behavior. Reference 4 states that "most of the shots were under conditions of low inlet subcooling, approximately 10°F. Under these conditions bubbles collapse slowly, and the volume occupied by steam voids may be relatively large. The steam voids can be 'seen' only because of light refraction at interfaces between vapor and liquid. . . . Quite a bit can be learned about the qualitative character of the flow, however. It is swirling, surging, eddying. In the geometries which were investigated, no steam-channeling tendency is apparent."

Both the high-speed movies and the pressure-drop results indicate that, even in the subcooled zone, there may be a significant void fraction in the channel before bulk boiling occurs.

Burnout Correlation

A generalized prediction of burnout heat flux for flowing, subcooled, wetting liquids is treated in Ref. 8. The reference formulates the burnout heat flux as the sum of two terms. The author notes that additive types of correlations have been proposed by other investigators in the field of boiling heat transfer, but these correlations were different in detail and scope. In the additive approach of Ref. 8, there is a boiling contribution and a convective contribution to the heat flux at the burnout point, each independently formulated:

$$\phi_{total} = \underbrace{\phi_{sat}\left(\frac{\phi_{sub}}{\phi_{sat}}\right)}_{\text{boiling term}} + \underbrace{h_{nb}\,(t_w - t_b)_{bo}}_{\text{convection term}}$$

where

$$\phi_{sat} = KL_v\rho_v\left(\frac{\sigma g_c\, a\, \Delta\rho}{\rho_v^2}\right)^{1/4}$$

is for pool boiling;

$$\frac{\phi_{sub}}{\phi_{sat}} = 1 + \left(\frac{\rho_l}{\rho_v}\right)^{0.923} \left(\frac{c_p \, \Delta t_{sub}}{25 L_v}\right)$$

is a correction for subcooling; and

$$h_{nb} = K' \left(\frac{k}{D}\right) \times \mathrm{Re}^m \times \mathrm{Pr}^n$$

is a relation of the Colburn type.

In these four equations, the meanings of the symbols are as follows:

ϕ_{total} = total heat flux at burnout
ϕ_{sat} = heat flux at burnout, in saturated fluid
ϕ_{sub} = heat flux at burnout, in subcooled fluid
h_{nb} = heat-transfer coefficient, no boiling
t_w = wall temperature at burnout point
t_b = bulk temperature of fluid at burnout point
K = 0.12 to 0.17, adjustable constant
L_v = latent heat of vaporization of fluid
ρ_v = density of vapor
ρ_l = density of liquid
$\Delta\rho = \rho_l - \rho_v$
g = acceleration conversion constant
a = local acceleration
σ = surface tension
c_p = specific heat of liquid
Δt_{sub} = subcooling
K' = 0.018 to 0.027, adjustable constant
k = thermal conductivity
D = hydraulic diameter
Re = Reynolds number
Pr = Prandtl number
m = normally 0.8, adjustable constant
n = normally 0.333, adjustable constant

The formulation was used to compute analytical values of the burnout heat flux, and these values were compared with 1263 experimental points. These points represented all the available experimental burnout data for flowing, wetting liquids in the absence of significant net vapor generation. In addition to water, the data include six fluids in axial, swirl, and cross flow, in tubular, annular, rectangular, and rod geometries. The flow conditions were within the following broad limits:

Velocity	0.05 to 174 ft/sec
Pressure	4.2 to 3000 psia
Subcooling	0 to 506°F
Acceleration	1 to 57,000 g
ϕ_{total}	100,000 to 37,400,000 Btu/(hr)(sq ft)

After deleting some of the experimental points that were determined to be unrepresentative, 815 selected points were compared with the computed values. Of these, it is stated[8] that 95% of the predictions agree with the experimental values within a maximum deviation of 40%. The reference contains a discussion of the significance of, and the methods of handling, the adjustable constants K and K', and describes the sources of data used for the various liquids treated. The paper cites some 90 references that constitute a useful bibliography on burnout and related subjects.

Pool Boiling

The heat-transfer characteristics of boiling organic fluids is of increasing interest in organic reactor technology. An experimental investigation of this subject is given in Ref. 9. The objectives of the investigations were "(1) Determination of the boiling heat transfer characteristics of organic coolants and the development of correlations to aid in feasibility analyses of organic-cooled and moderated reactors utilizing nucleate boiling, (2) determination of the minimum critical heat flux for the coolants under consideration for organic reactors, and (3) determination of the effect of additives on boiling heat transfer and critical heat flux."[9] The experimental pool-boiling apparatus was operated in the pressure range 13.5 to 488.5 psia. The heating surface was a 0.375-in.-OD horizontal tube. Measurements were made for nucleate boiling of benzene, diphenyl, and benzene-diphenyl mixtures. The data on critical heat flux at DNB for the pure fluids correlated reasonably well with some of the equations in the literature. For both pure fluids at 13.5 psia, ϕ_{DNB} was approximately 85,000 Btu/(hr)(sq ft). For benzene, ϕ_{DNB} increased as a function of pressure up to 300 psia, reaching a maximum of about 160,000 Btu/(hr)(sq ft), and began to decrease at higher pressures. The ϕ_{DNB} of diphenyl also increased as pressure increased. The highest pressure investigated was 115 psia. Mixtures of diphenyl and benzene were also investigated. For a mixture of 5% benzene and 95% diphenyl, operating at 13.5 psia, ϕ_{DNB} is approximately 155,000 Btu/(hr)(sq ft), 180% of the pure fluid values. Similar increases in ϕ_{DNB}, when small amounts of volatile components are added, have been noted by other investigators; however, no generalized correlations have been advanced.

Reference 10 reports experiments on pool-boiling burnout in saturated water subject to rapid pressure decreases. The burnout heat flux in saturated water was first determined as a function of the steady-state pressure at pressures from atmospheric to about 75 psig. The burnout heat flux was found to increase by more than a factor of 2.5 over this range. The heating surface was a 0.001-in.-thick by 0.75-in.-wide stainless-steel ribbon, oriented horizontally. For a typical transient test, the pool of degassed, deionized water in a closed pressure vessel was heated to the desired temperature by steam coils, and the condition of steady saturation pressure was established. The power to the steel ribbon was adjusted to give a heat flux slightly below the ϕ_{DNB} corresponding to that saturation pressure. A quick-opening valve was then released which allowed the pressure to drop at a rate of 5 to 10 psi/sec, and the pressure was recorded during the transient until the heated ribbon actually burned out. It was found that, for a given heat flux, burnout occurred at lower pressures in the transient tests than in the steady-state tests. Alternatively, it may be considered that some time interval is required for the burnout process to occur after the pressure has fallen to the steady-state burnout value. By analysis of the experimental data, the time span from DNB to actual burnout was determined to be of the order of 1 sec. The authors conclude that[10] "It appears that the violent convective currents caused by bulk nucleation within the body of the liquid after pressure release tend to delay burnout past the point predicted by steady-state considerations."

The distribution of boiling sites on a smooth flat surface in pool boiling is discussed in Ref. 11. The author explains that many experimenters have observed what is described in the literature as patchwise boiling, the apparent tendency of nucleation sites to cluster on the heat-transfer surface. The purpose of the study was to analyze the available data for the spatial distributions of boiling nucleation sites in order to determine whether they follow familiar statistical laws. The data did, in fact, fit a Poisson distribution quite well. By this approach it is possible to determine also the distribution of nearest-neighbor distances between boiling sites. This statistical evidence tends to refute the idea of patchwise boiling as a distinct phenomenon and simultaneously throws doubt on the validity of proposed theories to explain patchwise boiling. However, a reasonable confidence level in the statistical conclusion is yet to be established.

An analytical analysis is presented in Ref. 12 of two hydrodynamic transitions in nucleate pool boiling. When the heat flux is low, individual bubbles are formed which float upward separately. As the heat flux is increased, the bubbles come into closer proximity, and, at a sufficiently high heat flux, they actually form a vertical vapor column. This transition results in a change in the vapor-removal process from an intermittent process to a continuous one. The existence of the two regions is supported by photographs taken by various investigators. The transition occurs well below the burnout point or second transition. The heat flux at which the transition from bubbles to columns occurs depends upon the number of active boiling sites and therefore depends upon the surface condition. The second transition or burnout point is apparently due to the lateral interaction of the vapor columns and the inflowing liquid. As the surface heat flux is increased, a vapor generation rate is reached at which the spacing between columns becomes small. This leads to high relative velocities between the upflowing vapor and the downflowing water and to instability. This type of instability is known in the literature as Taylor-Helmholtz hydrodynamic instability. When it occurs, the transition to film boiling has begun, and the burnout region has been reached. Since the transition is determined by this type of instability consideration, the burnout heat flux is essentially independent of local surface conditions. Two equations derived in Ref. 12 predict, respectively, the heat flux for the first transition and the heat flux for burnout. The equations give reasonable agreement with experimental results.

Additional analytical work on the critical conditions in nucleate boiling is given in Ref. 13. An equation is derived for the burnout condition in an ideal system, and its application to various practical systems, including pool-boiling and forced-convection systems, is discussed.

Sodium Pool Boiling

New experimental work is reported in Ref. 14 on pool boiling in sodium. The boiling took

place in a 6-in.-long by 6-in.-diameter horizontal cylindrical boiler, partially filled with liquid sodium. The heating surface was a 3-in.-long by 0.375-in.-diameter rod, located axially in the boiler.

The vapor flowed upward from the vapor space of the boiler into an air-cooled condenser, and the condensed liquid returned to the bottom of the boiler (by gravity flow). At a given heat load, the system pressure was controlled by changing the air flow rate over the condenser surface. External electric heaters were placed on all parts of the apparatus to minimize external heat losses and to preheat the system prior to filling with sodium.

The rod heaters were specially constructed for the project to obtain the high heat fluxes associated with boiling sodium. Nine thermocouples were located in the boiler to measure the sodium pool temperature. The operational procedures were thoroughly checked and reviewed to assure a negligible amount of subcooling. In the range tested the burnout heat flux decreased with decreasing pressure. The burnout tests were conducted with a fixed heat rate, and the saturation pressure was slowly reduced until the temperature of the cladding on the heater rod began to fluctuate because of the formation and collapse of vapor patches. In two instances the heater was burned out shortly after the fluctuations began.

The results of the experimental investigation are discussed in the reference and are compared with previous information; the agreement is reasonably good.

The nucleate-boiling heat-transfer results are correlated by the equation:

$$q/A = 180\ (\Delta t_{sat})^{2.35}$$

over the range of q/A from 100,000 to 1,000,000 Btu/(hr)(sq ft).

For pool-boiling burnout the following equation is given:

$$q/A = 0.144\lambda\rho_v \left(\frac{\rho_l - \rho_v}{\rho_v}\right)^{1/2} \left(\frac{gg_c\sigma}{\rho_l}\right)^{1/4} \mathrm{Pr}^{-0.245}$$

where q/A = burnout heat flux, Btu/(hr)(sq ft)
Δt_{sat} = wall temperature − saturation temperature, °F
Pr = Prandtl number
ρ_l = liquid density, lb/cu ft
ρ_v = vapor density, lb/cu ft
λ = heat of vaporization, Btu/lb
σ = surface tension, lb(force)/ft
g = local acceleration, ft/hr^2
g_c = conversion factor, lb(mass)/lb (force) × ft/hr^2

This equation was developed not only to correlate the test points but as a general correlation that also fits the results of pool boiling for water and several organic liquids. It yields a value of 1,900,000 Btu/(hr)(sq ft) for the burnout heat flux of saturated sodium at 1 atm.

All the experimental data in Ref. 14 were obtained at pool temperatures between 1200 and 1500°F. The corresponding saturation pressures range from 1 to 8 psia.

Swirl Flow

"Swirl flow" is the descriptive term for fluid flow through a smooth tube containing a twisted tape. The presence of the twisted tape introduces the following changes:

1. The flow path is longer.
2. The free area is decreased.
3. The fluid experiences an angular acceleration.

A considerable amount of swirl-flow information has accrued from several organizations. Most of the information is on air, water, and ethylene glycol. Reference 15 gives a compilation of the data available through January 1962. The data cover both nonboiling and boiling regimes and include pressure-drop, heat-transfer, and burnout information.

For nonboiling cases the heat-transfer characteristics are plotted in terms of the Nusselt-number ratio (swirl flow/axial flow) as a function of Reynolds number. The following equation is a good correlation of the water-heating data:

$$\frac{(\mathrm{Nu})_s}{(\mathrm{Nu})_a} = 2.43\ (\mathrm{Gr}/\mathrm{Re}^2)^{0.042}$$

where $(\mathrm{Nu})_s$ = Nusselt number in swirl flow
$(\mathrm{Nu})_a$ = Nusselt number in axial flow
Gr = Grashof number
Re = Reynolds number

and all values are based on inside pipe diameter.

A more generalized correlation that is applicable to all the swirl-flow heating data is also given in the reference. The Nusselt-number ratios are smaller for cooling than for heating, but the ratio is greater than unity. The reduction in ratio may be due to the tendency of the cooled higher-density fluid to remain on the tube wall under the influence of the acceleration forces.

A general correlation is presented for swirl-flow friction factors.[15] The pressure drops are always larger than the corresponding axial-flow values owing to the higher velocity, longer flow path, greater frictional surface, and increased shear stress due to acceleration.

In studies of swirl flow with boiling, the liquid-film superheat, Δt_{sat} (wall temperature–saturation temperature), has been measured with water, and the results are comparable with axial-flow values when the swirl flow has a low centrifugal intensity. At a high centrifugal intensity, the results are scattered; the values of Δt_{sat} lie in a band that includes values from about one-half to two times the Δt_{sat} values predicted by axial-flow correlations.

The burnout heat fluxes are higher with swirl flow than with axial flow. The reference shows data which indicate that the burnout heat flux in swirl flow may be as much as a factor of 2.5 times that in axial flow at the same value of pumping power. In general, the burnout heat flux increases with the amount of swirl; the largest increases cited[15] corresponded to values of $(a_t/g)_w$ of about 6×10^4, although substantial increases in burnout heat flux were observed at values of $(a_t/g)_w$ about a factor of 10 lower. The ratio $(a_t/g)_w$, which indicates the centrifugal acceleration in nondimensional terms, is given by:

$$(a_t/g)_w = (K/D_i)(V_a/y)^2$$

where D_i = inside diameter of circular flow passage
V_a = axial component of flow velocity
y = twist ratio = number of tube diameters per 180° twist of the internal spiral ribbon
K = a constant; its value is 1.845 if D_i is in inches and V_a is in ft/sec.

The reference concludes that "a considerable amount of somewhat disconnected swirl-flow data exists. A uniform comparison of these data clearly shows that heat-transfer rates in both the nonboiling and boiling regimes may be considerably augmented with no increase in pumping power by swirling the coolant."[15]

Gas-Solid Mixtures

Gas-solid mixtures have had some consideration as reactor coolants. Typical mixtures are helium loaded with solid particles with solid-to-gas mass ratios as high as 100. The particle size may range from submicron to 200 μ in diameter. The basic advantage of the mixture as a reactor coolant is the increase in heat capacity over that of the gas alone.

Experimental work on this subject, which began several years ago, is described in Refs. 16 and 17. In Ref. 16 nitrogen and helium were used as the gases and graphite particles as the solids. The graphite particles were nonuniform in size. The results indicated increases in the overall heat-transfer coefficient by as much as a factor of 6.

Reference 18 reports measurements of heat-transfer coefficients for various gases with nonmetallic particles. A simple conduction model was used to compare these results with predicted values.

Measurements of heat-transfer coefficients for air loaded with approximately spherical particles of lead and glass are reported in Ref. 19. To cover a wide range of specific heats and densities, lead and glass were chosen as the loading materials. The particles were used in two discrete sizes: 30 and 200 μ. The solid-to-gas ratio was in the "lightly loaded" range, from 0 to 3, and Reynolds numbers of 15,000 and 30,000 were investigated. The test section was a 0.710-in.-ID uniformly heated vertical tube which had a heated length of 35.55 in. The local Nusselt number in Fig. III-4, at a point 46.4 diameters down the heated tube, is given as a function of the solid-to-gas mass ratio. The Nusselt number decreases for small additions of solid, and in several cases it reaches its lowest value when the mass ratio is in the range 1.0 to 2.0. Figure III-5 shows the local Nusselt number as a function of the axial distance down the tube for several mixtures of the 30-μ lead particles in air. The results of the glass particles agree well with those of the lead particles.

The reference[19] states that the major difficulty encountered during the air-solids ex-

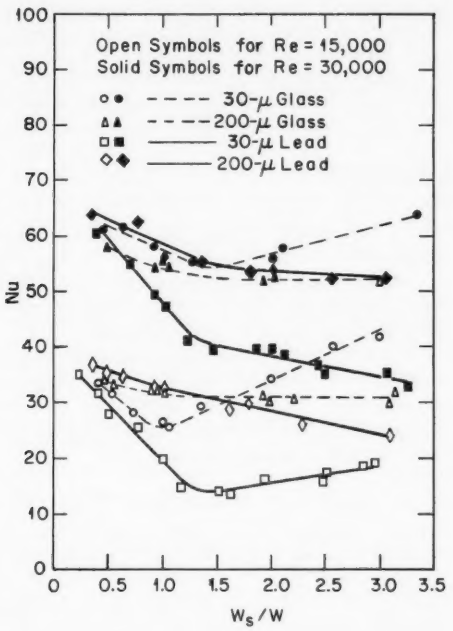

Fig. III-4 Nusselt number as a function of solid-to-gas mass ratio at 46.4 tube diameters from inlet.[19] W_S is the mass flow rate of solids, and W is the mass flow rate of air.

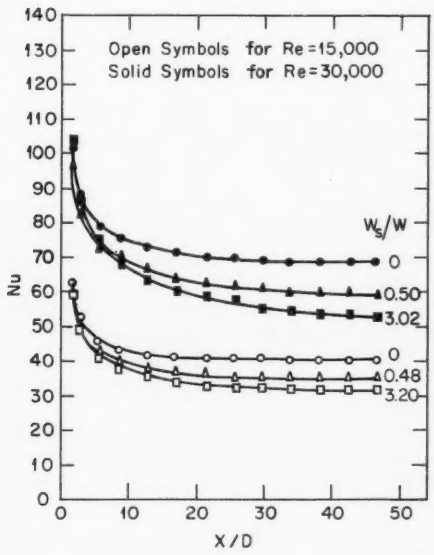

Fig. III-5 Local Nusselt number as a function of axial distance for mixtures of air and 30-μ lead particles.[19] X is the axial distance from point at which heating begins, and D is the tube diameter.

periments was in maintaining a steady solid flow rate. Several runs were discarded because this rate changed before all the thermocouple readings were recorded.

Analysis of Multipass Cores

In the design of a pressurized-water reactor, the heat-removal capability is at a maximum when the outlet water temperature from all parts of the core is uniform. The following are advantages in having the exit water at a uniform temperature:

1. The bulk water temperature from the reactor is equal to the maximum temperature allowed in the hot channel.

2. For a given power capability, less water flow is required since the bulk temperature rise is the same as the maximum temperature rise.

There are two ideal ways to attain this uniformity: (1) provide a uniform radial power distribution or (2) provide continuously adjustable orifices to each small subdivision of the core. However, neither approach may be practical in a power reactor.

In a typical reactor the ratio of the enthalpy rise ($\triangle H$ of hot channel/$\triangle H$ of average channel) may be 2.0 or more if no preferential coolant orificing is used. Normally the designer will use fixed orifices to reduce the enthalpy ratio to the range of about 1.3 to 1.5. Further reductions in the ratio can be achieved by using a multipass system with mixing between passes.

Reference 20 is a study of multipass configurations for core 2 for the Shippingport plant. The analysis was made to estimate the advantages in heat-removal capability which might be gained by multipass core configurations. The report states that the effectiveness of the multipass system is dependent upon two fundamental core parameters: (1) the gross core power distribution and (2) the interpass mixing factor. If there is no mixing between the passes from one hot channel to the next hot channel, then there is no thermal advantage in multipass flow. The report states[20] that the experimentally determined values for the hot channel-to-hot channel mixing ability in the interpass usually ranges from 0.8 to 1.0.

Figure III-6 illustrates the thermal improvement that is available as a function of the number of core passes. The improvement is characterized by the term "multipass core effectiveness," F_n. This term is a measure of the heat-removal capacity of a multipass core relative to a one-pass core, using the hot-channel coolant enthalpy rise for comparative purposes, with the two cores operating at the same power output and the same flow input. Mathematically,

$$F_n = \frac{(H_{hc})_{exit}^{1 \text{ pass core}} - H_{inlet}^{core}}{(H_{hc})_{exit}^{n \text{ pass core}} - H_{inlet}^{core}}$$

where H_{hc} is the exit coolant enthalpy of the hot channel in Btu/lb and H_{inlet} is the inlet coolant enthalpy of the core in Btu/lb. Two curves are shown: (1) for an enthalpy ratio of 2.0 and (2) for an enthalpy ratio of 1.5. As might be expected the curves rise very rapidly and then become asymptotic after several passes. A substantial improvement is available for the second pass and for the third pass, but after that the improvement becomes small.

The multipass core is behaving similar to a multipass heat exchanger, where there is complete mixing between each pass. Plotted in Fig. III-6 is the performance of a heat exchanger; this portion of the figure was taken from Fig. 12 in Ref. 21. The figure shows the similarity between a multipass reactor core and a multipass heat exchanger.

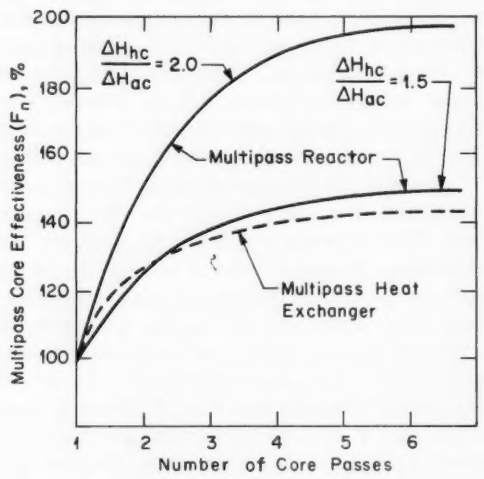

Fig. III-6 Thermal improvement as a function of core passes with complete mixing between passes.[20, 21] ΔH_{hc} is the hot-channel enthalpy rise, Btu/lb, and ΔH_{ac} is the average channel enthalpy rise, Btu/lb.

References

1. S. T. Hsu and P. W. Ing, Experiments of Forced Convection Subcooled Nucleate Boiling Heat Transfer, Paper ASME No. 62-HT-38 presented at Fifth National Heat Transfer Conference and Exhibit, Houston, Tex., Aug. 5–8, 1962.
2. J. J. Jicha and S. Frank, An Experimental Local Boiling Heat Transfer and Pressure Drop Study of a Round Tube, Paper ASME No. 62-HT-48 presented at Fifth National Heat Transfer Conference and Exhibit, Houston, Tex., Aug. 5–8, 1962.
3. S. J. Green, G. W. Maurer, and A. Weiss, Burnout and Pressure Drop Studies for Forced Convection Flow of Water Parallel to Rod Bundles, Paper ASME No. 62-HT-43 presented at Fifth National Heat Transfer Conference and Exhibit, Houston, Tex., Aug. 5–8, 1962.
4. E. Janssen, Multirod Burnout at Low Pressure, Paper ASME No. 62-HT-26 presented at Fifth National Heat Transfer Conference and Exhibit, Houston, Tex., Aug. 5–8, 1962.
5. R. A. DeBortoli, S. J. Green, B. W. LeTourneau, M. Troy, and A. Weiss, Forced-Convection Heat Transfer Burnout Studies for Water in Rectangular Channels and Round Tubes at Pressures Above 500 psia, USAEC Report WAPD-188, Westinghouse Electric Corp., Bettis Atomic Power Lab., October 1958.
6. N. C. Sher and S. J. Green, Boiling Pressure Drop in Thin Rectangular Channels, *Nucl. Eng., Part VI, Chem. Eng. Progr. Symp. Ser.*, 55(23): (1959).
7. W. H. McAdams, W. E. Kennel, C. S. Minden, Rudolph Carl, P. M. Picornell, and J. E. Dew, Heat Transfer at High Rates to Water with Surface Boiling, *Ind. Eng. Chem.*, 41: (September 1949).
8. W. R. Gambill, Generalized Prediction of Burnout Heat Fluxes for Flowing, Subcooled, Wetting Liquids, Paper AIChE No. 17 presented at Fifth National Heat Transfer Conference and Exhibit, Houston, Tex., Aug. 5–8, 1962.
9. D. A. Huber and J. C. Hoene, Pool Boiling of Benzene, Diphenyl and Benzene-Diphenyl Mixtures Under Pressure, Paper ASME No. 62-HT-30 presented at Fifth National Heat Transfer Conference and Exhibit, Houston, Tex., Aug. 5–8, 1962.
10. J. R. Howell and K. J. Bell, An Experimental Investigation of the Effect of Pressure Transients on Pool Boiling Burnout, Paper AIChE No. 18 presented at Fifth National Heat Transfer Con-

ference and Exhibit, Houston, Tex., Aug. 5–8, 1962.

11. R. F. Gaertner, Distribution of Active Sites in the Nucleate Boiling of Liquids, Paper AIChE No. 5 presented at Fifth National Heat Transfer Conference and Exhibit, Houston, Tex., Aug. 5–8, 1962.
12. R. Moissis and P. Berenson, On the Hydrodynamic Transitions in Nucleate Boiling, Paper ASME No. 62-HT-8 presented at Fifth National Heat Transfer Conference and Exhibit, Houston, Tex., Aug. 5–8, 1962.
13. Y. P. Chang, Some Possible Critical Conditions in Nucleate Boiling, Paper ASME No. 62-HT-37 presented at Fifth National Heat Transfer Conference and Exhibit, Houston, Tex., Aug. 5–8, 1962.
14. R. C. Noyes, An Experimental Study of Sodium Pool Boiling Heat Transfer, Paper ASME No. 62-HT-24 presented at Fifth National Heat Transfer Conference and Exhibit, Houston, Tex., Aug. 5–8, 1962.
15. W. R. Gambill and R. D. Bundy, An Evaluation of the Present Status of Swirl-Flow Heat Transfer, Paper ASME No. 62-HT-42 presented at Fifth National Heat Transfer Conference and Exhibit, Houston, Tex., Aug. 5–8, 1962.
16. Babcock & Wilcox Co., Gas-Suspension Coolant Project, Final Report, USAEC Report BAW-1159, Aug. 15, 1959.
17. C. A. Depew, Heat Transfer to Pneumatically Conveyed Glass Particles of Fixed Size, Paper ASME No. 62-HT-14 presented at Fifth National Heat Transfer Conference and Exhibit, Houston, Tex., Aug. 5–8, 1962.
18. N. K. Harakes and K. O. Beatty, Jr., Surface Heat Transfer to Moving Beds of Non-Metallic Particles, Paper AIChE No. 10, presented at Fifth National Heat Transfer Conference and Exhibit, Houston, Tex., Aug. 5–8, 1962.
19. C. L. Tien and V. Quan, Local Heat Transfer Characteristics of Air-Glass and Air-Lead Mixtures in Turbulent Pipe Flow, Paper ASME No. 62-HT-15 presented at Fifth National Heat Transfer Conference and Exhibit, Houston, Tex., Aug. 5–8, 1962.
20. F. R. Vaughan, The Effect of Multi-Pass Hydraulic Core Configurations in PWR Core Two, Paper ASME No. 62-HT-45 presented at Fifth National Heat Transfer Conference and Exhibit, Houston, Tex., Aug. 5–8, 1962.
21. W. M. Kays and A. L. London, *Compact Heat Exchangers*, National Press, Palo Alto, Calif., 1955.

Section

IV

Power Reactor Technology

Fuel Elements: Fabrication by Powder Compaction

Previous issues of *Power Reactor Technology* have discussed, briefly, the powder-compaction methods that are under development for the fabrication of UO_2 fuel elements. Basically these approaches consist of packing loose UO_2 powder into the metal fuel-element jackets by vibratory compaction, swaging, or extrusion or combinations of these methods. The mechanically compacted UO_2 body is not sintered before the element goes into service, but ordinary in-pile sintering will occur in service throughout all the oxide volume except that portion near the cool jacket interface. The principal incentives for the development of the packed-powder methods of fabrication, as distinguished from the conventional sintered-pellet methods, are usually considered to be (1) their promise for fabrication-cost reductions, (2) their greater adaptability to remote fabrication techniques, and (3) their greater adaptability (particularly in the case of the vibratory compaction) to the fabrication of fuel elements of complex shapes. Quite evidently there is no reason to assume that the operating characteristics of powder-compacted elements will be the same as those of sintered-pellet elements. Consequently the development of fabrication techniques must go hand in hand with in-pile performance evaluations. This review summarizes briefly the information contained in a number of recent reports concerning fabrication developments. Information on the performance of the compacted-powder elements will be brought up to date in a subsequent issue.

Although interest in packed-powder technology is comparatively recent, advances in the state of the art have progressed at a relatively rapid rate. This has been due in part to the general insight into fuel-element behavior, which has been gained from experience with sintered-pellet elements. The existence of the successful sintered-pellet technology has established a number of technologic and economic standards which must be met or improved upon if widespread acceptance of the packed-powder concept is to be realized.

Early work established that metal-jacketed UO_2 fuel elements could be produced by either swaging or vibratory compaction, although neither method gave preirradiation UO_2 densities that approached those attainable by cold-pressing and sintering. As a result of this and other factors not yet completely explained, the quantity of gas released from the packed-powder elements was observed to be considerably greater[1] than that released from the pressed and sintered material. An additional handicap was the meager amount of irradiation data available for the evaluation and prediction of in-reactor performance. The objectives of the more recently reported work have been to (1) improve existing techniques, (2) attain higher UO_2 densities, (3) establish the process limits necessary for the production of satisfactory elements, (4) investigate new methods, and (5) obtain supporting irradiation experience.

The fabrication of UO_2 elements by the packed-powder method consists of three essential steps: (1) UO_2 powder preparation, (2) jacket loading, and (3) densification. The powder consists of a blend of high-density UO_2 particles of various sizes. In the earlier work the powder was manufactured by grinding pressed and sintered UO_2 of about 92 to 95% of the theoretical density. Recently, UO_2 powder with particle densities that are near the theoretical density has been produced by high-energy forming, by electrodeposition, by fusion,[2a] and by calcining and reducing either uranium peroxide or uranium diuranate.[2b] At present, fused and ground UO_2 provides the highest "as-packed" density; it is therefore the most generally used starting material for the packed-powder programs.

Fused UO_2 is produced either by direct electric-arc heating or by the heat of recombination of previously dissociated hydrogen. The direct arc-fusion method has the disadvantage of high material losses by vaporization. The extensive vaporization in the arc results from the increase in the electrical conductivity of UO_2 with temperature. The arc tends to concentrate upon the regions of highest temperature within the ingot, and therefore it causes overheating and vaporization in these regions. Heating by the recombination of hydrogen is a purely thermal-conductance phenomenon, and it produces a uniform melting of all exposed UO_2 without overheating any particular fraction of the material. In this process[2b] UO_2 is continuously deposited on a water-cooled copper disk that rotates through a region of recombining hydrogen. The UO_2 is fused by the heat of recombination and is swept from the disk by a stationary baffle plate as the disk continues to rotate. The mixture is collected and separated into fused and nonfused fractions. The nonfused fraction is returned to the disk. The fused fraction, in the form of platelets approximately 0.1 in. thick, 1 in. long, and 0.3 in. wide, is crushed to powder that is less than 0.06 in. in mean diameter. Fused material produced in this manner exhibits an oxygen-to-uranium ratio between 1.98 and 2.01. Contamination of tungsten occurs from the electrodes used to dissociate the hydrogen, but it appears to be limited to less than 100 ppm.

Satisfactory UO_2 powder can also be produced by calcining and reducing uranium peroxide or ammonium diuranate. The uranium peroxide is precipitated from a uranyl nitrate solution treated with hydrogen peroxide at a *p*H of 2 to 3. Calcining is accomplished at 1000 to 1050°C, and reduction at 900 to 950°C. The powder has an oxygen-to-uranium ratio of less than 2.01 and a Brunauer-Emmett-Teller surface area of about 0.25 m^2/g. Particles range from 1 to 10 μ in size. Powder prepared from ammonium diuranate consists of calcining at 700°C and reducing at 600°C to UO_2. The product is further refined by annealing in hydrogen for 2 hr at 1500°C. An oxygen-to-uranium ratio of 2.00 can be attained. This material is often referred to as "high-fired UO_2."

Reporting investigators generally agree that the particle size and the distribution of the various sizes in the working powder strongly influence the attainable as-packed density when vibratory-compaction techniques are used.[2c–f,3]

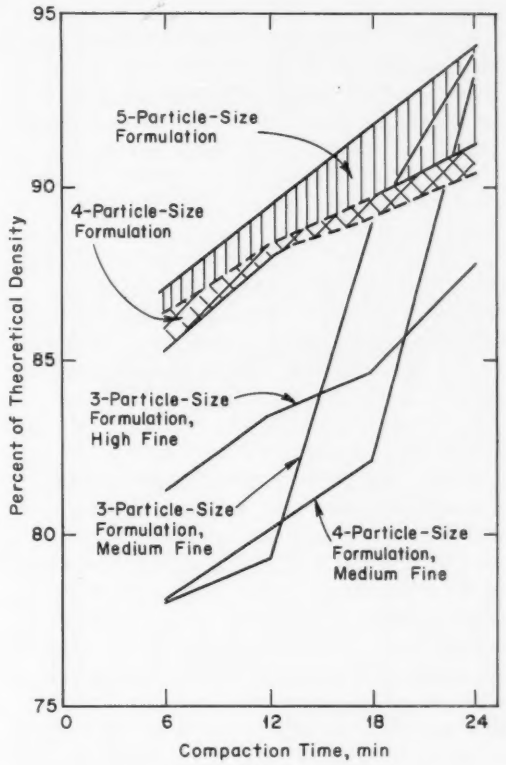

Fig. IV-1 Density vs. compaction time for several particle-size formulations.[2c]

The results of various methods of compaction using blends (or "formulations") of powder containing from two to seven different particle-size groups have been reported. The particle sizes range from less than 0.0029 in. in mean diameter to about 0.132 in. in mean diameter. A seven-particle-size blend of fused UO_2 using particles in this size range produced as-packed densities of 90 to 91% of theoretical after 12 min of vibratory compaction, and 93% of theoretical density was attained after 24 min of compaction.[2c] The effect of various particle-size blends upon density is shown in Fig. IV-1. A five-particle-size blend ranging in size from −6 to 24 mesh has yielded densities up to 93.4% of theoretical.

The investigations reported in Ref. 2*c* also disclosed that a reduction in particle size occurred as a consequence of the vibratory-compaction process. This effect is shown in Fig. IV-2. As a result of this particle breakdown, there is a tendency to form an optimum particle-

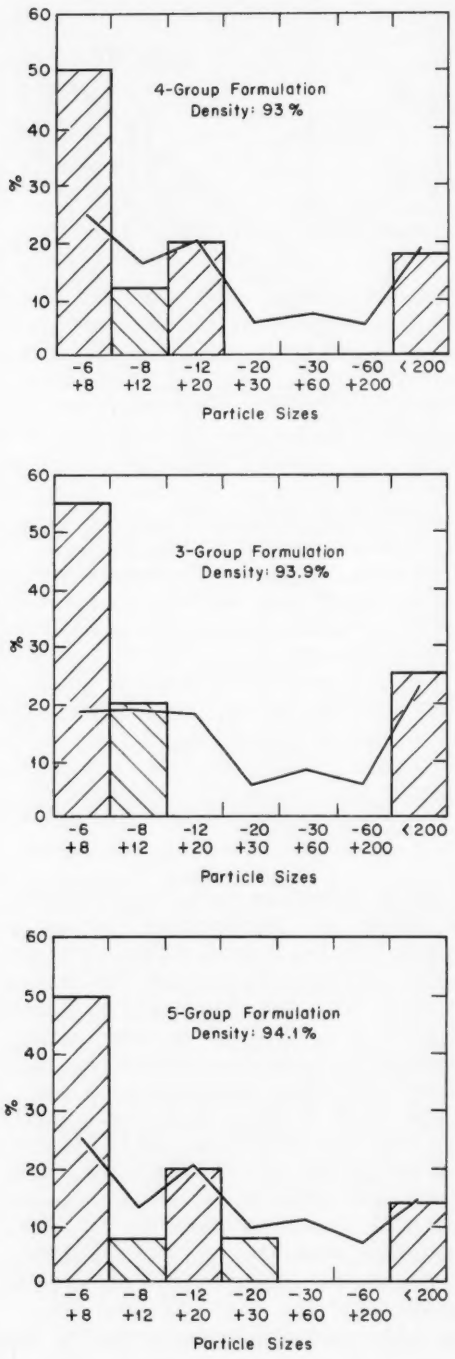

Fig. IV-2 Effect of compaction on change in particle size.[2c] Cross-hatched areas, original particle-size distribution; solid lines, final particle-size distribution.

size distribution that is capable of attaining densities in excess of 90% of theoretical regardless of the initial size distribution. Although densities of up to 94% of theoretical are reported when specialized compaction techniques and seven-particle blends are used, economic considerations make it difficult to justify this approach as a means to increase density. Consequently a three-grade particle blend containing a powder-size distribution of 50 to 65% coarse (>30 mesh), 10 to 35% medium (30 to 100 mesh), and 15 to 30% fine (<100 mesh) is usually preferred.

The effect of particle size and blending upon attainable densities when compaction is accomplished by swaging techniques has also been investigated. Generally, powder sizes no greater than −3 mesh are used. Reference 2*g* reports a vibratory-loaded cold-swaged density of 93.5% of theoretical when using a blend in which this particle size was the maximum. The same reference reports a cold-swaged density of 95% of theoretical with a powder blend of about the same composition as the five-particle mixture described previously. Reference 2*b* reports hot-swaged (750°C) densities greater than 94% with a powder composed of particles ranging in mean diameter from no greater than 0.06 in. to less than 0.00036 in. Reference 2*g* also supports the findings of the vibratory-compaction studies with regard to the breakdown of coarse particles under compaction. Size reductions occurred during both the preswaging vibratory-loading step and the swaging process. The effect upon particle size of both the vibratory-loading and swaging steps is shown in Figs. IV-3 to IV-5.

Densification by vibratory compaction has been accomplished mainly by either pneumatic or sonic electromechanical equipment. Generally the pneumatic units cost less and produce higher accelerations (up to 35,000 *g* for high-impact machines). Conversely the electromechanical units can be controlled more precisely, although high-impact pneumatic units have been operated with both frequency and impact independently controlled. However, the 500-cpm (8.3 cps) frequency of vibration associated with the high-impact pneumatic units is low compared to the frequencies attained by pneumatic vibrators (about 100 cps) and electromechanical machines (as high as 3000 cps).

A typical arrangement of the work and of the compaction equipment when pneumatic vibrators are used is described in Ref. 2*c*. In this instance

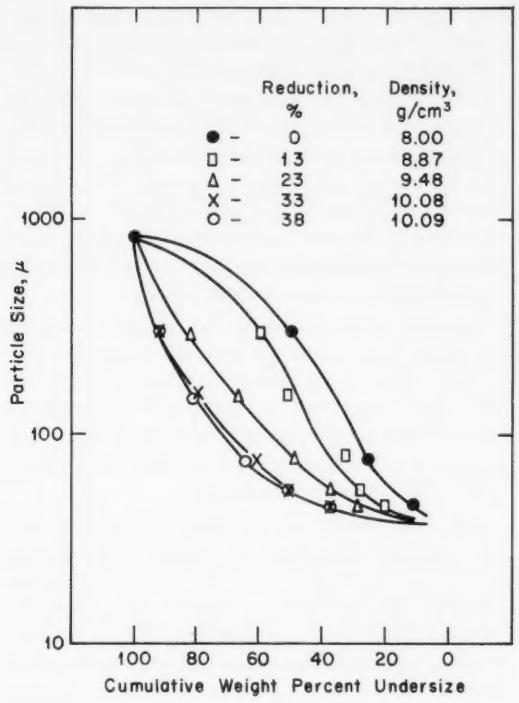

Fig. IV-3 Variation in particle-size distribution of fused UO_2 during cold swaging in a 2.54-cm-OD tube.[2g] Fine-powder blend (largest particle passes 20-mesh sieve).

the jacket tube is slipped over the lower (impact) ram. The jacket tube is then filled with loose UO_2 powder, and the upper (frequency) ram is inserted into the remaining tube length. The upper ram is brought to bear against UO_2, and a small static load is applied to the UO_2 and is maintained during the compaction process. Densification is obtained by operating both rams simultaneously so as to superimpose a high-energy shock load upon the existing static load. In some cases, only the lower ram is vibrated and the upper ram is only used to apply a static load to the powder.

These same techniques can also be applied to jacket tubes having one end cap installed prior to UO_2 powder loading.[2c] This configuration permits the capped jacket tube to be loaded with powder prior to insertion in the compaction equipment, and it reduces the time the vibratory-compaction equipment is used to that required for actual densification. The capped-tube alternate can be accommodated by replacing the cylindrical insert portion of the lower ram with a cup-shaped workpiece that has been fabricated to fit the shape of the capped tube. The tube end cap then becomes, in effect, the cylindrical insert during the compaction process. This technique has been used to produce average densities of 90% of theoretical in 5-ft-long by 0.399-in.-diameter tubes when subjected to static loads of 250 to 300 lb and accelerations of 28,000 g for about 14 min.

Electronic vibrational-compaction equipment has been used to produce both solid cylindrical rod type elements and tubular elements.[3] Densities in excess of 90% of theoretical are reported for the rod type elements; tubular-element densities are generally 3 to 5% lower. Maximum density was obtained by sweeping the frequency range from 300 to 1500 cps at an acceleration level of about 30 g. Continuous frequency sweeping was found to be essential for attaining high density. Maintaining frequency at a resonant point for more than 2 or 3 sec resulted in particle segregation and an attendant nonrecoverable density loss.

The technique used for compacting end-capped elements with the electronic vibrator differs from that used in conjunction with pneumatic equipment in that usually only a lower connection is used: no static load is impressed upon the powder during the densification process, densification being accomplished by lower-end impact energy only. A typical compaction cycle using this equipment consists of filling the jacket with powder and accomplishing preliminary packing at a frequency of 200 cps and at an acceleration level of 5 to 10 g. After the initial rapid settling is terminated (in about 30 sec), the frequency is increased to 1000 cps and is swept rapidly between 300 and 1500 cps, at accelerations varying from 30 to 80 g, until densification is accomplished. The optimum acceleration has been found to depend on both the frequency of vibration and the fuel-element resonances.

Reductions in powder densities were observed whenever resonant frequencies were held for short periods of time. This is attributed to unsettling of the powder. Resonances in 4-ft-long elements, both tubular and of rod form, were encountered at 340, 580, and 1400 cps. Vibration concurrent with powder loading resulted in lower final densities than those obtained when the elements were vibrated only after complete loading of the powder had been accomplished. The variance of this result with observations made by

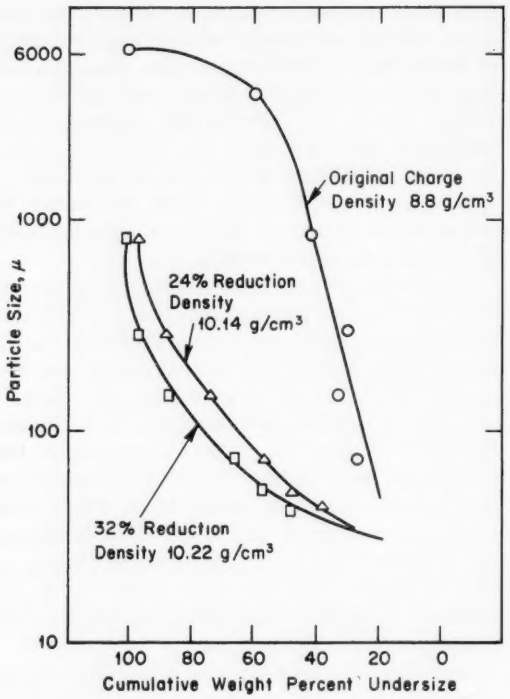

Fig. IV-4 Variation in particle-size distribution of fused UO_2 during cold swaging in a 1.83-cm-OD tube.[2g] Coarse-powder blend (largest particle passes 3-mesh sieve).

other experimenters[4] may indicate that, in this regard, the fuel-element length determines the optimum loading technique.

The shape of the input wave form and the jacket wall thickness were also observed to have an effect upon the attainable as-packed density. A chopped sine input generally produced the highest density in the shortest time (3 to 10 min of compaction), and jacket wall thicknesses of 0.010 to 0.014 in. were found to be more favorable for high density than thicknesses of either 0.020 or 0.007 in. Although this effect is not understood, it is probably related to variations in the modes of lateral vibration of the tubes.

The application of ultrasonic vibration techniques to the loading of metal-jacketed rod type UO_2 fuel elements is reported in Ref. 5. The method is reported to be "... superior to both low frequency vibrating compaction and cold pressing as well as to have certain advantages over the sintered pellet process." When fused UO_2 powder was used, the maximum density obtained was 92.3% of theoretical. When a 50–50 mixture of ground and fused UO_2 and "ceramic-grade" UO_2 powder was used, a maximum density of only 84.7% of theoretical was obtained. Ultrasonic compaction of pellet-grade ThO_2–3.4 wt.% UO_2 produced a maximum density of 91.9% of theoretical. A slight increase (91.1 to 91.4%) in the density of previously vibratory-compacted UO_2 was attained when the compact was subjected to additional ultrasonic compaction.

Further information on the use of ultrasonic vibration techniques for both hot and cold compaction of ceramic materials other than UO_2 or ThO_2 is presented in Refs. 6 and 7. Although the effects upon nuclear fuel materials were not investigated, this work may have some application to UO_2 fuel-element technology.

The fabrication of packed-powder UO_2 fuel by swaging was among the first of the powder techniques investigated. Basically the process consists of preloading a capped tube with UO_2 powder, tamping or packing to minimum volume, closing the remaining open end, and swaging the closed UO_2-filled tube to maximum density without destroying the jacket-tube integrity. Following swaging, the tube is trimmed to length, and permanent end closure are made. Variations of this basic process have been used for all swaging work reported up to the present time.

The most important variables affecting density and product integrity appear to be (1) the characteristics of the UO_2 powder, (2) the swaging temperature, (3) the jacket material, and (4) the reduction in area. When compaction is to be accomplished by swaging only, the highest densities (above 90% of theoretical) are obtained using coarse powder (about –3 mesh) of high tap density. However, the probability and severity of jacket damage is greater for large-particle powder blends than for small-particle blends.

The effects of swaging temperatures are of similar complexity in that the benefits to density, as temperature is increased, are offset by the decrease in strength of the jacket materials. This follows from the circumstance that densification during the swaging process is a function of the ability of the jacket to restrain the UO_2, at least at temperatures below the sintering point. Since, for the jacket materials of interest, the ability of the jacket to restrain the UO_2 is reduced importantly at elevated

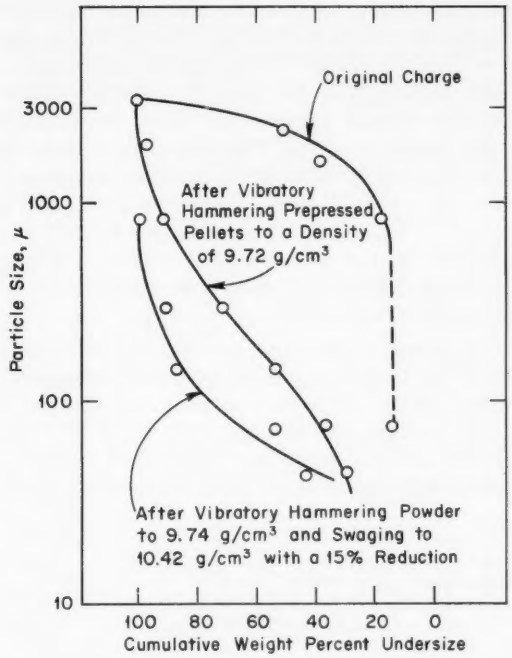

Fig. IV-5 Variation in particle-size distribution of fused UO_2 vibratory-hammered and cold-swaged inside a 1.83-cm-OD tube.[2g] Medium-powder blend (largest particle passes 6-mesh sieve).

temperatures, only modest increases in UO_2 density are obtained by hot swaging.

The effect of reduction in area upon density varies with the type of powder used as well as with the particle-size blend. Fused UO_2 appears to attain its maximum density between 40 and 50% reduction in area. The densities of high-fired and peroxide-based UO_2 continue to increase at area reductions as high as 58%, although they remain lower than the densities of fused material at comparable reductions in area. However, high density attained by large reductions in area is usually accomplished at the expense of jacket integrity.

The production of packed-powder fuel by swaging only is reported in Refs. 2*b*, 2*h*, 2*i*, and 8. In Ref. 2*b* a representative process is described which consists of filling 0.7-in.-diameter stainless-steel tubes, which have walls that are 0.06 to 0.008 in. thick, with fused UO_2 powder and tamping until a density in the range of 70 to 75% of theoretical is reached. After complete filling the tubes are evacuated, backfilled with argon, and both ends are welded shut. The loaded tubes are then reduced in cross-sectional area on a rotary, four-die swaging machine until the maximum density is obtained. When all swaging was accomplished cold, a cross-sectional area reduction of 30% or more was required to produce densities of about 92% of theoretical. However, when an initial cold reduction of 20 to 30% was followed by a hot (750°C) reduction of another 20 to 30%, densities in excess of 94% of theoretical were obtained without extreme damage to the jacket. In the process described,[2g] the elements were prepared for the hot-swaging step by heating in an argon-atmosphere furnace.

The reference also states that successful swaging of uranium peroxide powder and "high-fired" powder can be accomplished using pre-swaging densities of only 50 to 55% of theoretical. However, 60% reductions in area are required. These reductions produce hot-swaged densities in the range of 90% of theoretical with peroxide-based powder and 87% of theoretical with high-fired powder.

Reference 8 summarizes work done on the fabrication of tubular, stainless-steel-jacketed UO_2 elements by swaging techniques. The elements produced were 2.138 in. in outside diameter, 1.458 in. in inside diameter, and ranged in length from 5 to 10 ft. The walls of the inner and outer jacket tubes, which were made of type 304 stainless steel, were approximately 0.02 in. thick. The fuel material used was arc-fused UO_2. The elements were swaged on a rotary four-die machine that impacted upon the outer jacket tube. The inner jacket tube was supported by a reusable steel mandrel that was withdrawn from the tube after the swaging operation. The production process is outlined in Fig. IV-6. The effects of the swaging operation on UO_2 density, jacket elongation, and jacket thickness are given in Fig. IV-7 as functions of reduction in tube area.

As shown in the figure, a 43% reduction in area produced UO_2 densities of 91% of theoretical. Ten tubes fabricated by the process for irradiation tests averaged 88.5 ± 0.5% of theoretical density. The average oxygen-to-uranium ratio for all 10 tubes, analyzed by the ignition of UO_2 to U_3O_8, was 2.019 ± 0.005. The results of the dimensional inspections of these tubes are given in Table IV-1. The reference states that, in general, the external appearance of the specimens was good. However, extensive indentation of the inner surfaces of the jacket tubes

by the UO_2 was noted. Individual indentations as deep as 0.005 in. were observed in both jackets.

In summary, the "swaging only" experience has shown that densities in excess of 91% of theoretical can be attained using coarse-powder blends of fused UO_2, either stainless-steel or Zircaloy-2 jacketing materials, and area reductions in the range of 30 to 40%. Slightly higher densities (about 95% of theoretical density) can be obtained if swaging is done at elevated temperatures or at 40% or greater reductions in area. However, the probability of jacket damage increases with either process temperature or area reduction.

The need to eliminate jacket damage and the hope of obtaining a slight decrease in cost have given impetus to a compaction process utilizing both vibratory techniques and swaging.[2g,2j-l] This approach is predicated upon the observations that 85 to 88% of theoretical density can be attained rather easily and quickly by vibratory compaction and that the majority of the jacket damage appears to result from large reductions in area. Therefore, if swaging is preceded by a vibratory-compaction step yielding the above density, it seems possible that a single swaging pass producing about a 20% reduction in area will give the desired final density of more than 91% of theoretical with little or no damage to the jacket.

A typical combination process is described in Ref. 2*j*. In these experiments type 304 stainless-steel tubes, which were 0.516 in. to 0.539 in. in outside diameter, approximately 4.5 ft long, and which had a nominal wall thickness of 0.028 in., were reduced to 0.500 in. in outside diameter.

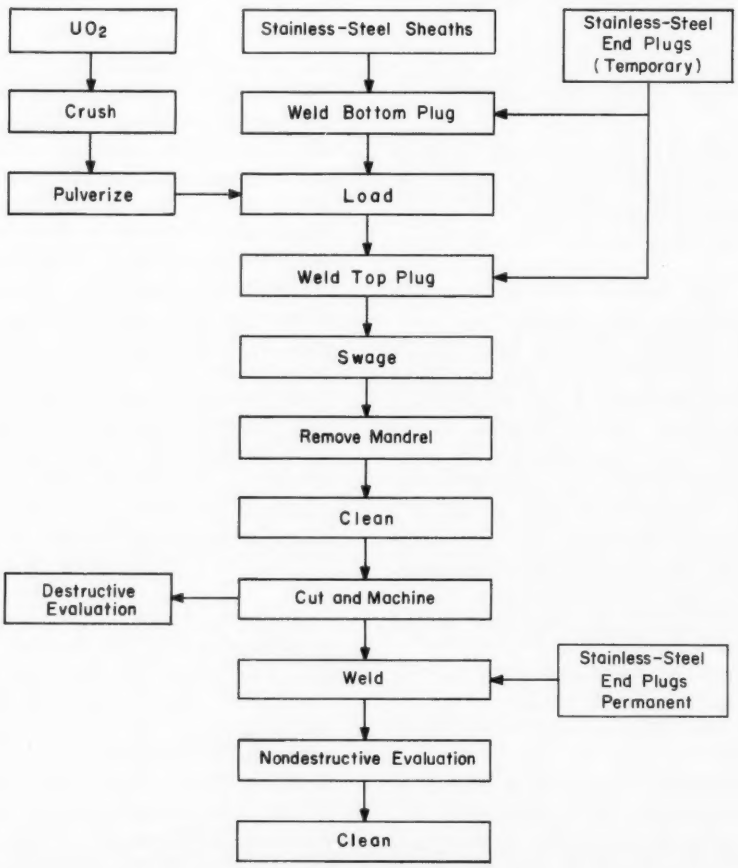

Fig. IV-6 Process flow sheet for swaged UO_2 tubes clad in stainless steel.[8]

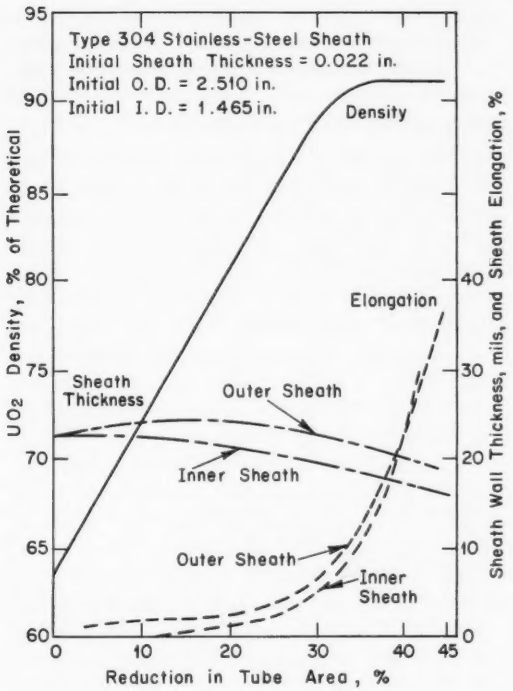

Fig. IV-7 Swaging behavior of tubes.[8] Fused UO_2 core.

Densities in excess of 90% of theoretical were attained. The as-received tubes were loaded with either a four-particle-size or three-particle-size blend of fused UO_2. The former were vibrated to 88% of theoretical density on standard vibratory-compaction machines. The tubes containing three-particle blends were compacted for 15 to 20 sec to about 85% of theoretical density on a small portable vibrator. The tubes were then reduced in cross section from 5 to 15% by cold swaging. The densities obtained are shown in Fig. IV-8. These densities are typical of all the referenced reports. The samples preswaged to 85% of theoretical density yielded about the same swaged density as the 88% samples.

The reports indicate that preswaging compaction may be accomplished by (1) pneumatic vibratory compaction, with or without a static load, (2) impact compaction, or (3) a combination of impact and vibration (vibratory hammering).[2g] The vibratory-hammering process yielded the highest densities and also had the added advantage of producing the previously mentioned blend refinement by fracturing the large particles into finer sizes.[2g] This refinement mitigates to a large extent the need for the more expensive small-size blends. Swaging can be done on either a rotary two-die or four-die machine. However, the four-die machine is generally considered to give better results, and it is preferred, particularly if the jacket tubes have thin walls.[2b]

The extrusion techniques for fabrication of UO_2, reported in Refs. 9*a* and 9*b*, are, in actuality, alternate methods of producing pressed and sintered material. However, they offer the attraction that considerably longer compacts can be made per pass through the dies. Consequently fewer compacts are needed to produce a given fuel loading, and the handling costs associated with the UO_2 are minimized. An additional advantage claimed for the process, which is a result of the absence of voids created by the nonperpendicularity of abutting compact end faces, compact edge chipping, and other surface defects is better utilization of the available fuel volume within the jacket tube. It is also reported that, with sufficient ball milling to produce particle sizes of about 1 μ, almost any type of urania may be used.[9c]

Table IV-1 DIMENSIONS OF 10 TYPE 304 STAINLESS-STEEL-CLAD UO_2 TUBES[8]

Dimension, in.	Average	Maximum	Minimum	Confidence limits*	No. of measurements
Outer diameter	2.138	2.142	2.131	±0.005	100
Inner diameter	1.458	1.461	1.453	±0.003	100
Eccentricity	0.009	0.015	0.001	±0.007	20
Wall thickness	0.339	0.354	0.320	±0.014	160
Bow, single throw	0.007	0.015	0.003		20
Cladding thickness:†					
Outer	0.021	0.022	0.018	±0.002	160
Inner	0.017	0.018	0.015	±0.002	160

*These are 2σ limits that include 95% of the data.
†Micrometer measurements.

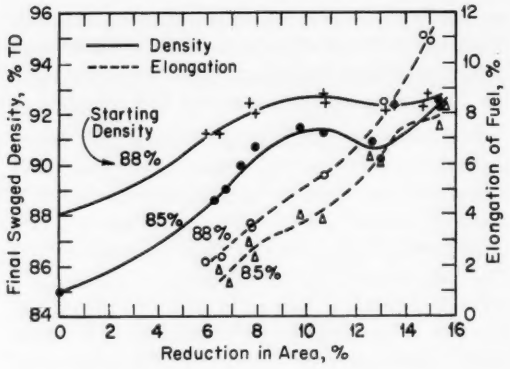

Fig. IV-8 Variation in UO_2 density and elongation with reduction in area.[2j]

The basic steps in the process consist of powder preparation, extrusion, sintering, and finishing. The powder is prepared by ball milling in the presence of binders and die lubricants in a manner quite similar to the methods used for pressed and sintered pellet compacts. Ball milling produces the small-particle size and the intimate mixing of UO_2, binder, and lubricant, which are necessary to attain a high density and an acceptable surface. The binder is used to preserve the shape of the green compacts during presintering handling and sintering. Lubricants are incorporated to reduce die wear and to eliminate "chattering" and consequent loss of surface finish as the extrusion passes through the die.

The most effective binders are reported to be dragant gum[9a] or methylcellulose.[9b] The preferred lubricants are urea[9a] or ammonium alginate.[9b] The addition of titanium oxide in concentrations of at least 0.20 wt.% is reported to be beneficial to densification.[9b] However, the high neutron-absorption cross section of TiO_2 is disadvantageous from the standpoint of reactor neutron economy.

Cold extrusion is used, through hardened steel or carbide dies, at pressures in the range of 24 tons/sq in. Green compacts are produced which have densities ranging from 3 to 6 g/cm^3. The reported experience indicates that the plasticity of the UO_2, the die angle, and the ratio of die cylindrical length to die diameter are important parameters.[9a] Splitting of the extrusion occurs[9a] if the die length-to-diameter ratio falls outside the range of 5 to 7. A 120° die angle and a very plastic paste extruded under high pressure produce an extrusion that exhibits a sintered density in excess of 90% of theoretical.[9a] Flow through the die was also investigated to determine if irregularities such as mixing occurred. None were found.[9a]

Prior to sintering the green extrusions are cut to length and are dried at low temperatures (up to 130°F) to reduce the content of moisture and other volatiles. Sintering is accomplished in an atmosphere of cracked ammonia at temperatures up to 3100°F. The effect of sintering temperature upon density[9b] is given in Table IV-2. However, different sintering methods and temperature schedules are used at different laboratories. Reference 9*a* gives an elaborate procedure involving slow heatup (50°C/hr) to 800°C, holding for 2 hr at this temperature, followed by an increase (at 65°C/hr) to 1650°C and cooling for three days. On the other hand, in the procedure of Ref. 9*b*, the extrusions travel through a tunnel furnace, heated to 2900°F, at the rate of 0.1 in./min for a period of time not to exceed 90 min. The reference further states that a density decrease is observed if the 90-min sintering time is exceeded. The addition of the TiO_2 densifier reported in Ref. 9*b* may be the basis for the difference of procedure. Various positions and methods of suspension of the extruded rods were studied during the sintering operation, and the smallest bending type deformations obtained were less than 0.02 in.

The sintered extrusions are finished by grinding the diameter to the required dimensions and the ends to the required perpendicularity. Both centered and centerless grinding have been used,

Table IV-2 DENSITIES OF SINTERED 6-IN. EXTRUSIONS*,[9b]

Batch	Urania vendor	Sintered density, g/cm^3, for the indicated sintering temperature				
		2700°F	2800°F	2875°F	3000°F	3110°F
100	D	10.00	10.28	10.57†	10.49	10.47
101	D	9.14	9.38	9.95	10.00	10.28
102	D	10.02	10.47	10.33	10.34	10.32
107	B	9.76	9.90	10.10	10.17	10.22
113	B	9.62	10.02	10.15	10.20	10.23

*Each value in the table is computed from the averages of five separate sets of measurements of the dimensions and weight of a single specimen typical of all extrusions in the same batch.

†The corresponding density determined by the water-displacement method is 10.55 g/cm^3; this value is also the average of five separate measurements.

depending upon the length of the extrusion. Rods as long as 10 in. have been mounted in a horizontal lathe and surface ground to remove as much as a 0.12-in. bow.[9a] Experience indicates that 10 to 20% of the UO_2 can be removed from the as-sintered extrusion in producing the sized and finished compact ready for loading. This material is recycled to the extrusion process, and it apparently presents no problem. Powder blends containing up to 30% of sintered and ground recycle material have been made without causing deterioration of the sintered densities.[9a,9b]

The reported extrusion methods have produced solid cylindrical rods of UO_2 up to 12 in. long and 0.471 in. in diameter. The as-sintered rods exhibited a total indicated reading within about ±0.002 in. of the nominal dimensions.[9b] Cored cylindrical rods and tubes, 0.6 in. in outside diameter, 0.4 in. in inside diameter, and 10 in. long, have also been produced. As-sintered densities have exceeded 95% of theoretical without additives and 97% of theoretical when TiO_2 was used to aid densification. Comparisons of the physical and chemical properties of pressed and sintered compacts and extruded compacts indicate the extruded material to be at least the equivalent of the pressed and sintered product.[9a-c] It is reported that the extruded material exhibits greater thermal-shock resistance, less open porosity, higher thermal conductivity, more uniform microstructure, and better as-sintered surface finish than the pressed and sintered UO_2. Preliminary work on ThO_2-UO_2 is reported to be yielding similarly promising results.[9b]

A variation of the extrusion technique for the preparation of packed-powder fuel elements is a hot coextrusion method[10] that offers the possibility of producing a metal-jacketed UO_2 rod in one operation. This process consists of forcing a composite extrusion billet, composed of the extrusion container, stainless-steel jacket material, and UO_2 powder, through an appropriately shaped extrusion die. Although sintered and ground UO_2 was used for the experiments, it is believed that almost any ground UO_2 powder may be utilized.

Matching of the dissimilar extrusion characteristics of the billet components is basic to the process; it requires that the three components be heated to different temperatures. This was accomplished by heating the powdered UO_2 in a special graphite furnace to 1875°C. The UO_2 was pushed out of the furnace and into the 750°C stainless-steel jacket can that, together with the extrusion container, had been previously heated in a separate furnace. The composite billet thus formed was pushed directly through the die, at the rate of 2.3 in./sec, in the same motion and by the same ram used to remove the UO_2 from the furnace.

At entry into the die, the composite billet was 2.615 in. in diameter and 6 in. long. The stainless-steel jacket can was 1.6 in. in inside diameter, 1.75 in. in outside diameter, and 5 in. long. A radial clearance of 0.010 in. was provided between the jacket can and the extrusion can. The UO_2 fuel slug was 1.496 in. in diameter and, including front and rear molybdenum end plugs, was 6 in. long. After the extrusion can was removed, the as-extruded rod was 0.410 in. in average diameter and about 40 in. long. The finished rod diameter, following four passes through a surface-conditioning sanding belt, measured 0.42 ± 0.002 in.

Two new and interesting approaches to the fabrication of packed-UO_2-powder fuel elements are gas consolidation[9d] and tandem rolling.[11] The gas-consolidation process appears to be a variation of isostatic pressing, which utilizes helium at high pressure to simultaneously compact both the UO_2 and the jacket. Fabrication of the prepressed element consists of filling the jacket tube with UO_2 powder, packing to minimum volume, and installing end closures as in the swaging processes. The sealed element is then subjected to external pressure up to 10,000 psi and at temperatures to 2300°F, which produces compaction and low-temperature sintering of the UO_2.

When ceramic-grade powder was used, densities as high as 99.5% of theoretical have been obtained after 1 to 3 hr at pressure. However, owing to the excessive shortening and diametral reduction of the element, the low initial (green) density of the prepressed oxide resulted in extensive wrinkling of the jacket tube. Fused and ground UO_2 eliminated the jacket damage, but at the cost of decreased density. A mixture of 60% fused, 40% ceramic powder effected the best compromise between jacket integrity and density. This powder blend, when compacted to a green density of 75% of theoretical, is expected to yield satisfactory elements of 95% of theoretical density after gas consolidation. Green densities in this range are easily achieved by inexpensive vibratory-compaction equipment.

Table IV-3 RÉSUMÉ OF TANDEM ROLLING DATA FOR ENRICHED FUEL RODS[11]

Starting rod diameter, in.	0.503
Starting rod length, in.	31
Starting tube wall thickness, in.	0.015
UO_2 powder	Spencer fused grade
UO_2 powder enrichment, %	3.5
Starting UO_2 particle size	−6 mesh
Finished rod diameter, in.	0.401
Finished rod length, in.	$38\frac{3}{8}$
No. of rods rolled	26
Density of rolled rods, % of theoretical density (maximum)	89.6
Density of rolled rods, % of theoretical density (minimum)	87.8
Density of rolled rods, % of theoretical density (average)	88.7

A combined process consisting of vibratory compaction and gas consolidation may be of as much interest as the combination of vibratory compaction and swaging.

The tandem rolling process is an adaptation of a method that has long been used for the commercial production of ceramic-insulated heating elements in stainless-steel or Inconel jackets. The process consists of passing a sealed, oxide-filled, metal-jacketed rod through a series of rolls, each of which reduces the rod cross section about 5%. For the experiments described,[11] 10 sets of rolls were used. Reduction is accomplished cold at a speed of about 50 ft/min.

The reference discusses the development and the production of 26 stainless-steel-jacketed, fused and ground UO_2 rods intended for irradiation in the Vallecitos Boiling-Water Reactor. The rods were $38\frac{3}{8}$ in. long and 0.401 in. in diameter. A density of 88% of theoretical was achieved for this run, but it is expected that larger-diameter rods will exhibit densities of at least 90% of theoretical. Other data of interest are given in Table IV-3. Of particular note is the estimated process production rate of 350,000 ft/month quoted in the report for this type of fuel.

References

1. R. T. Pennington, Nuclear Superheat Project Ninth Quarterly Progress Report, July–September 1961, USAEC Report GEAP-3877, General Electric Co., Atomic Power Equipment Dept.
2. Combustion Engineering, Inc., Symposium on Powder Packed Uranium Dioxide Fuel Elements, November 30–December 1, 1961, Volume I, USAEC Report CEND-153(Vol. I):
   a. J. J. Hauth, Fabrication Techniques for Packed-Powder Fuel Elements, 1961.
   b. F. Hofmann, H. Kroll, and B. Leibmann, Fuel Element Fabrication by Cold and Hot Swaging of Specially Prepared UO_2 Powders, 1961.
   c. R. C. Brayer and B. E. Murtha, Pneumatic Vibratory-Compaction of UO_2, 1961.
   d. W. S. Ernst, Jr. and R. L. Beatty, Vibratory-Compaction Studies at the Oak Ridge National Laboratory, 1961.
   e. W. R. DeHollander, Particle Size Relationships in the Packing of UO_2, 1961.
   f. Emile Vandenbemden, Sonic and Ultrasonic Compaction of UO_2, 1961.
   g. M. A. Feraday, Cold Swaging UO_2 in Zircaloy: The Effect of Some Process Variables on Fuel Density and Sheath Integrity (an Interim Report), 1961.
   h. J. V. Denero and F. J. Hartwig, Study of Variables in the Swaging of Zircaloy-2 Clad UO_2 Fuel Pins, 1961.
   i. J. M. Leblanc, UO_2 Compaction by Hot and Cold Swaging, 1961.
   j. E. I. Veil and R. H. Gale, Fabrication of UO_2 Fuel Elements by the "Vibswage" Process, 1961.
   k. R. L. Eichinger, Vibratory and Swage Compaction of Small Diameter Stainless Steel Clad Fuel Rods, 1961.
   l. G. Frigerio, Cold Swaging of Uranium Dioxide, 1961.
3. H. G. Marsh, Fabrication of UO_2 Fuel Elements by Vibrational Compaction, USAEC Report DP-681, Savannah River Laboratory, February 1962.
4. Hanford Atomic Products Operation, Novel Ceramic Fuel Fabrication Processes, USAEC Report HW-64629, Apr. 15, 1960.
5. W. B. Tarpley and R. Pheasant, Applications of Ultrasonic Energy. Ultrasonic Filling of Tubular Cladding with Ceramic Fuel Powders, USAEC Report NYO-9587, Aeroprojects, Inc., November 1961.
6. W. B. Tarpley and H. Kartluke, Application of Ultrasonic Vibration to Cold Pressing of Ceramic Pellets, USAEC Report NYO-10005, Aeroprojects, Inc., November 1961.
7. W. B. Tarpley and H. Kartluke, Ultrasonic Hot Pressing of Metals and Ceramics, USAEC Report NYO-10007, Aeroprojects, Inc., December 1961.
8. A. S. Ferrara, Savannah River Laboratory, August 1960. (Unpublished)
9. Combustion Engineering, Inc., Symposium on Powder Packed Uranium Dioxide Fuel Elements, November 30–December 1, 1961, Volume II, USAEC Report CEND-153(Vol. II):
   a. R. Hauser, The Extrusion of Uranium Dioxide: Technique of Extrusion, 1961.

b. W. J. O'Leary and R. S. Miller, Extrusion of UO_2 and ThO_2-UO_2 Nuclear Fuels, 1961.

c. A. Porneuf, The Extrusion of Uranium Dioxide: Physicochemical Properties of Extruded Uranium Dioxide, 1961.

d. S. W. Porembka and C. B. Boyer, Consolidation of Uranium Dioxide by Gas-Pressure Bonding, 1961.

10. J. G. Hunt, D. F. Kaufman, and P. Loewenstein, Hot Extrusion of UO_2 Fuel Elements. Fundamental and Applied Research in Metallurgy, USAEC Report NMI-1245, Nuclear Metals, Inc., Oct. 31, 1961.
11. J. W. Lingafelter, Fabrication of Fuel Rods by Tandem Rolling, USAEC Report GEAP-3775, General Electric Co., Atomic Power Equipment Dept., July 1961.

Section

V

Power Reactor Technology

Materials

Beryllium Oxide

The major question in the performance of beryllium oxide as a moderator is the degree to which its properties deteriorate by radiation damage over long exposure times. A program at Oak Ridge National Laboratory[1] has investigated the effects of irradiation at temperatures up to 1025°C. Two types of BeO were tested: (1) a high-density hot-pressed material at a density of 2.9 g/cm^3, and (2) some specially prepared lower-density material (2.65 to 2.70 g/cm^3) made by sintering isostatically pressed granules. The granules were prepared, in turn, from isostatically pressed BeO powder. On the basis of a quite recent figure[2] for the theoretical density of BeO, 3.0100 ± 0.0003 g/cm^3, these densities correspond to 96.4% and 88 to 89.7% of the theoretical density.

Since one of the major interests of the program was thermal stress, the BeO was irradiated in the form of cylinders whose diameters were selected to produce the required stresses at the test temperatures. Pellet diameters ranged from 0.428 to 1.180 in. The smaller diameter is calculated to correspond to a stress of 7600 psi at 900°C and a gamma heat of 25 watts/g, whereas the larger diameter is equivalent to 57,700 psi under the same conditions. Since there was some doubt concerning the values used in the calculations and since stress relaxation might take place, a wide range of calculated stresses was employed so that both failed and unfailed specimens would be recovered from the tests. Irradiations were carried out in the Engineering Test Reactor (ETR), and integrated fast fluxes (>1 Mev) (as monitored with Mn^{54}) from 1.1 to 10^{20} to 2.8×10^{21} nvt were attained. Center temperatures of the specimens ranged from 110 to 1025°C in the tests. Temperature control was effected by automatically regulating the dilution of the coolant helium in the capsule with argon. The gamma flux of the ETR was high enough to provide the desired temperatures without supplemental heating, and the coolant-dilution scheme of temperature control was sufficiently effective so that the temperature of one capsule could be varied from 790°C with pure argon to 300°C with pure helium. The response time of the control system was found to be adequate for normal reactor behavior. Five experiments at five exposure levels of from 411 to 10,032 Mwd were carried out. The test involving the largest exposure consisted of some seven capsules containing three specimens each. A total of some 57 BeO specimens was exposed and reported.

Postirradiation examination included measurements of changes in physical dimensions, the determination of the amount of gas released in the specimens, and determinations of the changes in thermal conductivity and in crystal structure. Visual examination of the specimens when removed from the irradiation capsules showed that damage varied from simple cracking, through general fracturing, to partial or complete powdering of the material. For the lower exposure levels (4.4×10^{20} nvt), even at low temperatures (120°C), the BeO pellets survived without visible damage. At 950°C and 2.1×10^{21} nvt, two of the three specimens in one capsule had random breaks. One of the specimens showed evidence of powdering. However, the third specimen remained sound with sharp edges. It appeared that failures did not take place early in the exposure as would be expected if breakage were due to thermal stress alone. Evidently there is a deterioration in physical properties due to radiation damage. Some experimental indication of decreased thermal conductivity with irradiation was found. Dimensional changes in the pellets, which could be expected to lead to ultimate failure of the pellets, were found to increase with

radiation exposure at all temperatures, but the changes were more evident below 400°C. A related effect, sensitive to irradiation temperature, is the expansion of the c axis of the hexagonal BeO lattice. Expansions under irradiation of from 0.2 to 0.6% were found. Plots of the changes in the c parameter against temperature show that increases were most marked below 400°C and that the changes became greater with decreasing temperature. Above 400°C the changes reached saturation at a relatively low expansion.

The role of radiolytic gas may be important in explaining deterioration. The two nuclear reactions of importance are (1) the $(n, 2n)$ reaction, which produces helium, and (2) the (n,α) reaction, which produces helium and tritium. The helium was retained within the BeO matrix even at high temperatures, and solution of the oxide in molten salt was necessary to release it for measurement. Escape of the tritium formed was high at the higher temperatures. The $(n, 2n)$ reaction is by far the major contributor of helium. The diffusion of the helium to submicroscopic voids is indicated in several electron photomicrographs at 17,500 to 35,000 ×. The increasing size of these voids with exposure and the pressure in them would account for much of the decrease in mechanical properties and thermal conductivity and possibly for the increase in physical dimensions of the specimens.

In view of the high incidence of failure in the irradiated specimens, which progressed to the point of degradation to a fine powder under some conditions, the authors appear justified in concluding[1] that great caution must be exercised in designing BeO moderators for nuclear reactors. For the greatest life of the moderator, its temperature should, from the evidence reported, be kept above 400°C, and much greater safety is indicated at temperatures above 800°C.

Experimental work on BeO irradiations has also been reported by General Atomic[3] with somewhat more optimistic results. However, since the pellets that were irradiated were small, in the range 0.24 in. in diameter, the lower incidence of cracking found would not be unexpected in view of the lower thermal stresses in the pellets. About 45 BeO pellets were irradiated in the General Electric Testing Reactor for exposures from 1 to 2 × 10^{21} nvt (>1 Mev) (as determined by nickel monitors) at temperatures from 1000 to 1900°F. The pellets were fabricated by a variety of methods, such as by sintering cold-pressed, isostatically pressed, and extruded oxides and by hot-pressing the oxide. Some of the specimens contained MgO, Al_2O_3, and bentonite as additives. In operation, heating was provided by gamma heating in a mandrel that surrounded both the specimens and a graphite sleeve used as a thermal bond between the specimens and the mandrel. Although a resistance heater had been provided for the capsule, its use was not required. Ten thermocouples were installed for the test, but they all had failed by the start of the fourth and final cycle.

When removed from the capsule after the test, several of the pellets irradiated at 560 to 720°C were found to be broken into chips or granules. Axial crushing tests on the sound pellets showed decreases of from 21 to 81% of the strength of unirradiated control specimens. The strongest specimens were those containing 1% MgO; these specimens retained 81% of their unirradiated strength. The next strongest specimens contained 1% bentonite, and they had a crushing strength equal to 41% of that of unirradiated material. However, because of the anomalous behavior of some specimens containing varying amounts of MgO, the authors[3] believe bentonite to be the best additive. It was also found that, although additives decrease the unirradiated thermal diffusivity of BeO, they may decrease the radiation damage sufficiently so that the highest irradiated thermal diffusivities are exhibited by pellets containing additives. Two percent bentonite gave a thermal diffusivity for irradiated specimens equal to 85% of that of unirradiated specimens. The effects of additives on density and dimensional changes under irradiation could not be assessed because the sensitivity of the measurements was good to only about 1% for dimensional changes and to about 3% for decreases in density. The changes produced by irradiation were in this range or lower.

Although additives such as bentonite had a markedly beneficial effect, the small diameter of the specimens leaves in doubt the significance of this improvement for larger bodies which would be subject to higher thermal stresses. The powdering of a pure BeO specimen at the lowest irradiation temperature used, 570°C (1059°F), and the cracking of 2% bentonite additive specimen at the same temperature is in agreement with the Oak Ridge work discussed above.

Another program to determine the effects of radiation on BeO at high temperatures is under

way at General Electric Nuclear Materials and Propulsion Operation. A recent progress report[4] discusses irradiations in progress in the ETR and presents results of orientation studies. Since anisotropic properties are to be expected in the hexagonal BeO lattice, any significant degree of preferred orientation in a BeO body might result in dimensional instability under irradiation. A relatively high degree of preferred orientation was found in certain extruded BeO bodies, but, of those examined, it was found only in specimens made from one grade of BeO, the UOX grade. The observation that bodies made from other grades of BeO show far less orientation is surprising since the extrusion process usually tends to produce definite orientation.

Data are also presented on compressive creep behavior at 1200°C for various grades of oxide, different grain sizes, and various stress levels. Randomly selected values are presented below to give a general idea of the spread in creep behavior of BeO at 1200°C.

Stress, psi	Creep, % in 500 hr
3,000	0.62
6,000	0.09
10,000	0.13
1,000	0.18

The discrepancies apparent in the tabulation can be attributed, at least to some extent, to grain size effects, different porosities, and differences in the grade of oxide.

A theoretical study based on a critical review of the literature on irradiation effects in BeO has been provided by Harwell.[5] Some 36 papers published prior to 1962 are referenced, but, unfortunately, most of the work reported was carried out at relatively low temperatures. However, surprising consistencies were discovered in some areas. A curve is given for the fractional macroscopic growth in BeO as a function of integrated neutron flux. Data for the 80 to 170°C range, as provided by five groups of workers, were plotted and are found to fall in a straight narrow band. This band of experimental data agrees up to 10^{20} nvt (>1 Mev) with the straight line developed theoretically.

Analysis of the available information indicated that the anisotropic growth of BeO is probably the major factor causing the powdering found in low-temperature (100°C) irradiations. Low-density (2.7 g/cm^3) material was susceptible to powdering. The clean fracturing of BeO bodies when irradiated at high temperatures, as reported in the papers discussed above, is thought to be a more complicated phenomenon in which thermal stresses are a contributing factor and in which gas formation can be involved, since gas agglomeration begins in the 700 to 1000°C range. The author[4] suggests that deterioration due to anisotropic growth may be important in other oxides used in reactors, such as Al_2O_3 for which anisotropic growth has been reported. However, the commonly used oxide, MgO, should be relatively immune to this difficulty because of its cubic structure.

Beryllium Metal

The Defense Metals Information Center has reviewed the literature on beryllium metal for structural applications[6] for the period 1958 to 1960, a continuation of former reviews on this subject. Although primarily concerned with the field of missile-aircraft applications, the brief but adequate reviews of some 186 papers cover fabrication techniques, alloy development, the development of composite materials such as beryllium-silver or beryllium-aluminum, and joining methods. Properties are given, and current projects are described.

Iron-Aluminum Alloys

The outstanding oxidation and corrosion resistances of the known iron-aluminum alloys, combined with the comparatively low-thermal-neutron cross sections to be expected from combinations containing appreciable amounts of aluminum, have made the iron-aluminum system of considerable interest to reactor metallurgists. One major characteristic has, however, prevented the use of iron-aluminum alloys: the brittleness, or lack of any but trace ductility, of most of the compositions of interest. The alloys have been as notorious for brittleness as they have been famous for oxidation resistance.

A recent paper from Saclay[7] shows, however, that brittleness is not necessarily inherent, even in alloys containing quite large percentages of aluminum. At 40 at.% aluminum (25 wt.%), it was possible to produce material with the following properties at room temperature: elastic limit,

38,400 psi; ultimate strength, 89,600 psi; and elongation, 11%. This ductility was produced by employing high-purity starting materials and by controlling in some manner the cooling rates so as to produce a fine equiaxed grain structure in the ingot. Rolling was carried out at 1000°C with significant reductions per pass. The product so prepared was found to be free of grain-boundary precipitates. Consequently the brittleness of previously prepared material is attributed in large part to the grain-boundary segregation of impurities.

The production of such comparatively high elongations in a 40 at.% aluminum–60 at.% iron alloy is obviously an impressive accomplishment metallurgically which has practical implications for several technologies. Until further data become available, some speculation would seem permissible as to the possible properties of such an alloy for reactor use. In addition to corrosion resistance in oxidizing media and a fairly low cross section (roughly half that of type 304 stainless steel), resistance, or immunity, to chloride stress-corrosion may be indicated by the ferritic nature of the alloy. However, comparatively low high-temperature strength may also be implied by the structure. In any case further developments will be watched with considerable interest.

Stress Relief of Pressure Vessels

The large size (up to 70 ft in diameter) of the pressure vessels used for the Magnox series of British gas-cooled reactors requires that stress relief be carried out *in situ*. On-site stress relieving requires far longer heating and cooling cycles than are necessary for similar operations when furnaces can be used. Total times in the 100-hr range may be required for complete heating and cooling, and the time at peak temperature is proportionally long. Studies have therefore been made at Culcheth[8] on the effect of such long stress-relieving times on the tensile, impact, creep, and stress-rupture properties of the pressure-vessel steels and on the properties of pressure-vessel weldments.

The steel tested was a 0.14% maximum carbon, 1 to 1.4% manganese steel, as silicon killed and as aluminum grain-refined. The usual strength of such steels is in the 26- to 32-tsi range. Test times at stress-relieving temperature varied from 36 to 72 hr. The weld metal showed the greatest deterioration on prolonged heat-treatment, with drops in ultimate tensile strength as great as 6.7 tsi (maximum) to 3.2 tsi (minimum). Transition temperatures for notch ductility were increased 20°C on the average by the 600 to 650°C treatment. With respect to creep behavior, although it had previously been shown that silicon steels might increase in creep rate by factors of from 4 to 50 times after treatment at 600 to 650°C, it was found that the aluminum grain-refined steels showed little effect from prolonged heat-treatments. The differences between the steels were also apparent in the stress-rupture results. Silicon-killed steels showed a significant decrease in stress-rupture strength as stress relieved, whereas the aluminum grain-refined steels showed only slight effects.

Since British practice sets the allowable minimum operating temperatures for such pressure vessels by testing Charpy specimens cut from the vessels themselves, the safety aspect of the results is not uppermost. The work, however, indicates the importance of the stress-relieving cycle.

Work on the problem of stress relaxation under irradiation has been reported by Savannah River[9] for stainless steel under torsional stress at low temperatures. Type 304 stainless-steel tubular specimens were exposed to total integrated fluxes of 2.7, 5.1, and 10.0×10^{20} nvt (>0.1 Mev) (as calculated from flux traverses) to an accuracy of ±35%. The exposure temperatures were calculated to be less than 100°C. Before exposure the bar specimens were twisted through a known angle so that the extent to which the bar did not spring back to its original position after exposure could be used as a measure of the stress relaxation due to irradiation. It was found that, at 5000-psi shear stress, the relaxation was too small to be measured. The measurements made above this stress level showed the relaxation to increase with the initially applied stress somewhat faster than proportionately. Relaxation apparently reached saturation at 5×10^{20} nvt, but relaxations as great as 7500 psi from an initial stress of 22,000 psi were measured. Compared to tensile-stress relaxations, the 30% decrease observed at 20,000-psi initial stress was about the same as that found for previously reported tensile loading. At half this initial stress, however, the torsional stress decrease (20% at 10,000 psi) was less than half that encountered in tensile loading.

References

1. R. P. Shields, J. E. Lee, Jr., and W. E. Browning, Jr., Effects of Fast-Neutron Irradiation and High Temperature on Beryllium Oxide, USAEC Report ORNL-3164, Oak Ridge National Laboratory, Apr. 2, 1962.
2. B. Bellamy, T. W. Baker, and D. T. Livey, The Lattice Parameter and Density of Beryllium Oxide Determined by Precise X-Ray Methods, *J. Nucl. Mater.*, 6(1): 1 (1962).
3. J. M. Tobin, Some Effects of Neutron Irradiation on Selected Beryllia Materials, USAEC Report GA-2648, General Atomic Div., General Dynamics Corp., Apr. 30, 1962.
4. General Electric Co., Flight Propulsion Laboratory Dept., High-Temperature Materials Program. Progress Report No. 12, Part A, USAEC Report GEMP-12A, June 15, 1962.
5. F. J. P. Clarke, Irradiation Damage in Beryllium Oxide, British Report AERE-R-3971, February 1962; also to be published in *Progress in Nuclear Energy, Series IV, Technology and Engineering*, Vol. 5.
6. W. Hodge, Beryllium for Structural Applications, Report DMIC-168, Battelle Memorial Institute, Defense Metals Information Center, May 18, 1962.
7. G. Cabane, P. Mouturat, P. Pepin, J. Petit, G. Sainfort, and M. Salesse, Fragilite de la Solution Solide Feraluminum, *Compt. Rend.*, 254(19): 3360–3362 (May 7, 1962).
8. B. Watkins, D. S. Wood, and R. W. Nichols, The Effects of Prolonged Stress Relieving Treatments on the Mechanical Properties of Reactor Pressure Vessel Steels, British Report TRG-262 (C), 1962.
9. R. E. Schreiber, Relaxation of Torsional Stresses in Stainless Steel During Irradiation, USAEC Report DP-669, Savannah River Laboratory, April 1962.

Section

VI

Power Reactor Technology

Design Practice: The N.S. Savannah

The N.S. *Savannah*, the first merchant ship to use nuclear power for propulsion, was launched in July 1959. Since that time construction and testing have been completed, and the ship is currently in service. Although the general characteristics of the propulsion plant are well known, it is worthwhile to examine some of the significant details of the plant as examples of design practice in pressurized-water reactors and particularly as examples of practice in a marine application. The following section summarizes a number of such details, extracted from the Safety Assessment report.[1] Reference 2 also contains design information on the plant.

It may be informative to compare the characteristics of the *Savannah* power plant with those of the Yankee Nuclear Power Station (reviewed in the June 1961 issue of *Power Reactor Technology*, Vol. 4, No. 3, pages 47 to 55), which, although a much larger plant, employs the same basic materials in its reactor.

The *Savannah* is a combination passenger-cargo ship, 595 ft long and 78 ft wide, displacing 21,850 long tons at full load (60 passengers and 9250 long tons of cargo). At the normal cruising speed of 20 knots, the propulsion turbine delivers 20,000 shp, and the reactor (which supplies steam for the ship's electric generators and the hotel load as well as the propulsion equipment) operates at 64 Mw. The maximum powers are 70 Mw and 22,000 shp. The crew consists of 105 on-board members plus staff consultants on shore. Without passengers the ship would probably require a crew of 55 to 60. This is comparable to a crew of 53 that is normal for a mariner-class vessel (a slightly smaller ship with accommodations for only 12 passengers). A single-batch refueling scheme is to be used which will replace all fuel elements at one time. In the design of the reactor, a major objective was to achieve an energy production of 52,000 Mwd from the first core to give a core life of 1200 days at 44 Mw, the average reactor power requirement expected in operating the ship. The power density in the core and the specific power are relatively low, about half those of the Yankee reactor. A low specific power makes possible a large total energy output (megawatt days) without requiring an excessively large average fuel exposure (megawatt days per ton). The design value of the average exposure is 7352 Mwt/ton. The reactor core contains a relatively large fraction of stainless steel, which is utilized for a permanent eggcrate structure as well as for fuel jackets; the fuel jackets are sufficiently thick (35 mils) to be free-standing under operating pressure after furnace brazing at 1950°F. No reactivity control other than the 21 control rods is required for normal operation.

The general features of the reactor are shown in Figs. VI-1 and VI-2. The installation of the reactor in the containment shell is shown in Fig. VI-3, and its location in the ship is shown in Fig. VI-4.

Fuel Elements

The rod type fuel elements are each composed of a closed stainless-steel tube, of full core length, which contains uranium dioxide fuel in the form of pressed and sintered pellets. A hollow stainless-steel spacer below the pellets insulates the bottom end plug, and an Inconel X spring at the top of the pellet column serves as an insulator and pushes the fuel pellets of the column together. The fuel tubes are sealed at the ends by heliarc-welded end plugs.

Pellet density	10 g/cm^3
Pellet dimensions	0.4245 in. in diameter by about 0.5 in. long

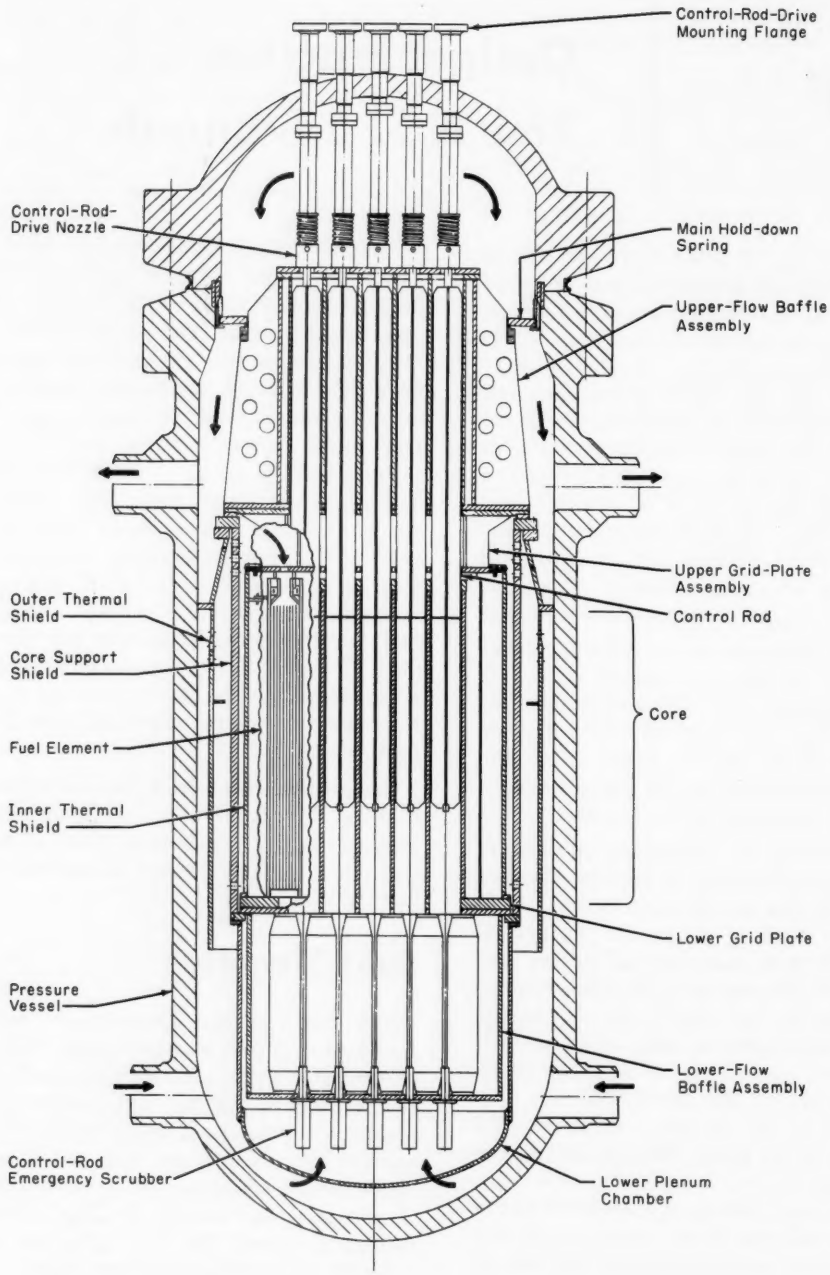

Fig. VI-1 Vertical cross section through the N.S. *Savannah* reactor.

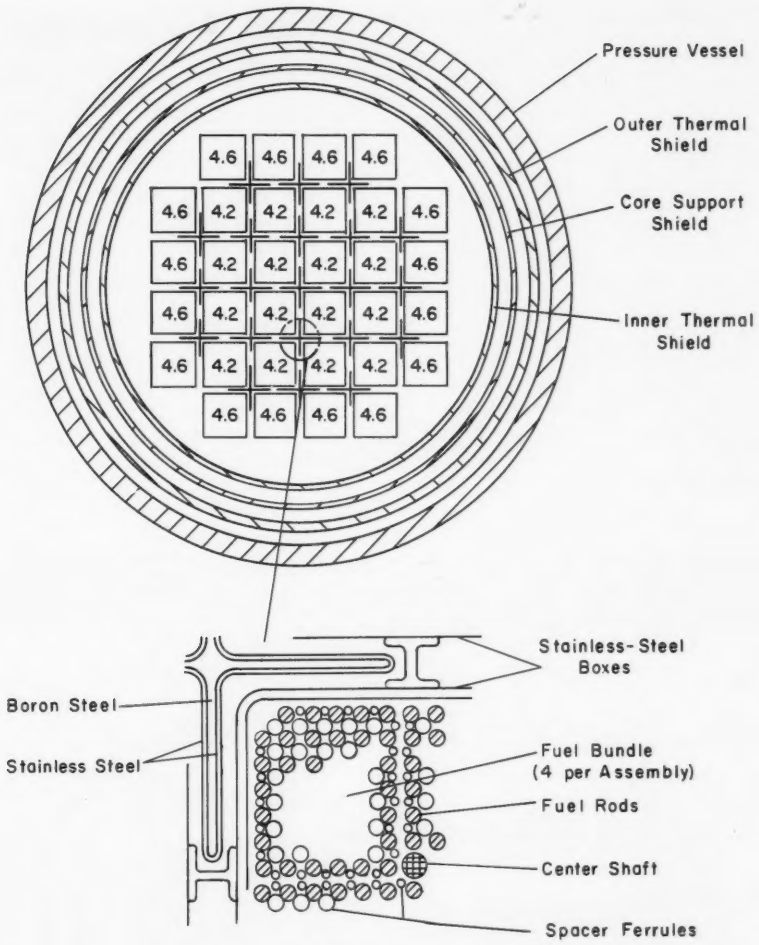

Fig. VI-2 Horizontal cross section through the N.S. *Savannah* reactor. The numbers represent fuel enrichments.

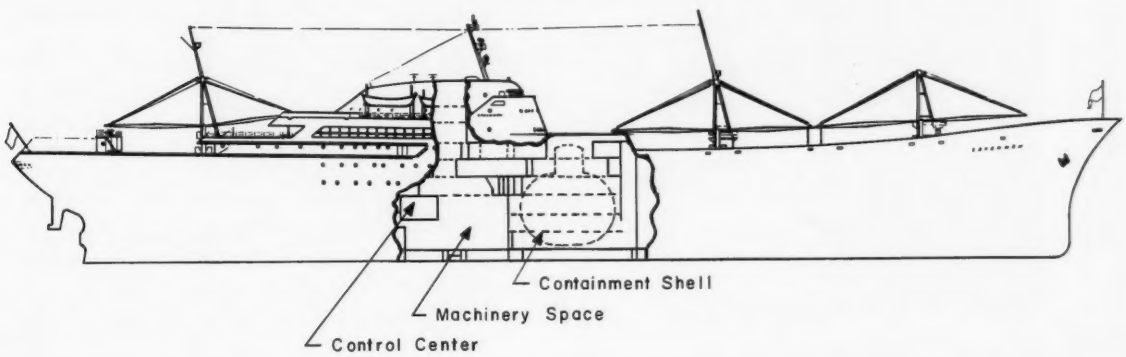

Fig. VI-3 Location of reactor and propulsion equipment on the N.S. *Savannah*.

Element dimensions	0.500 in. in outside diameter by 69 in. long
Jacket material	Type 304 stainless steel
Wall thickness	0.035 in. (free standing)
Jacket thickness/OD ratio	0.070
Nominal pellet-jacket clearance (assembly)	0.0027 in. on radius
Additional gas space (cold)	Approximately 3 in. of fuel-element length
Filling gas	Helium
Length of UO_2 per element (cold)	66 in.
Total elements in core	5248
UO_2 pellets per element (approximately)	132
Total UO_2 pellets in core (approximately)	6.93×10^5
Total length of UO_2 pellet column in core	2.89×10^4 ft

Fuel Assemblies

The fuel rods are joined into 41-rod bundles (six by seven array with one corner rod omitted) by brazing with 1-in.-long ferrule spacers at 8-in. intervals. Four bundles are arranged in a 164-rod assembly by support frames at the ends. The assembly is held together by one central shaft that connects the support frames. A fuel assembly is shown in Fig. VI-5.

Number of fuel elements per assembly	164
Fuel-rod lattice	Square
Lattice pitch	0.663 in.
Cross-sectional dimensions of assembly	Approximately 8.5 in. square

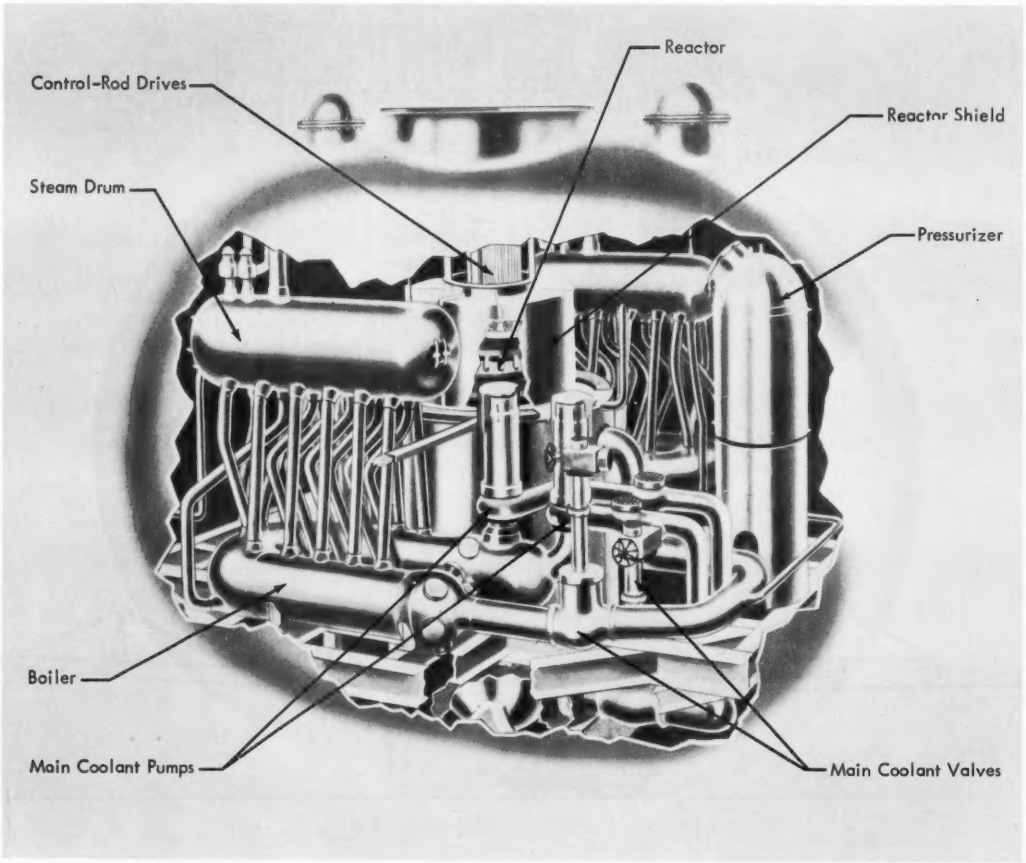

Fig. VI-4 Cutaway view of reactor containment vessel for the N.S. *Savannah*, showing arrangement of equipment.

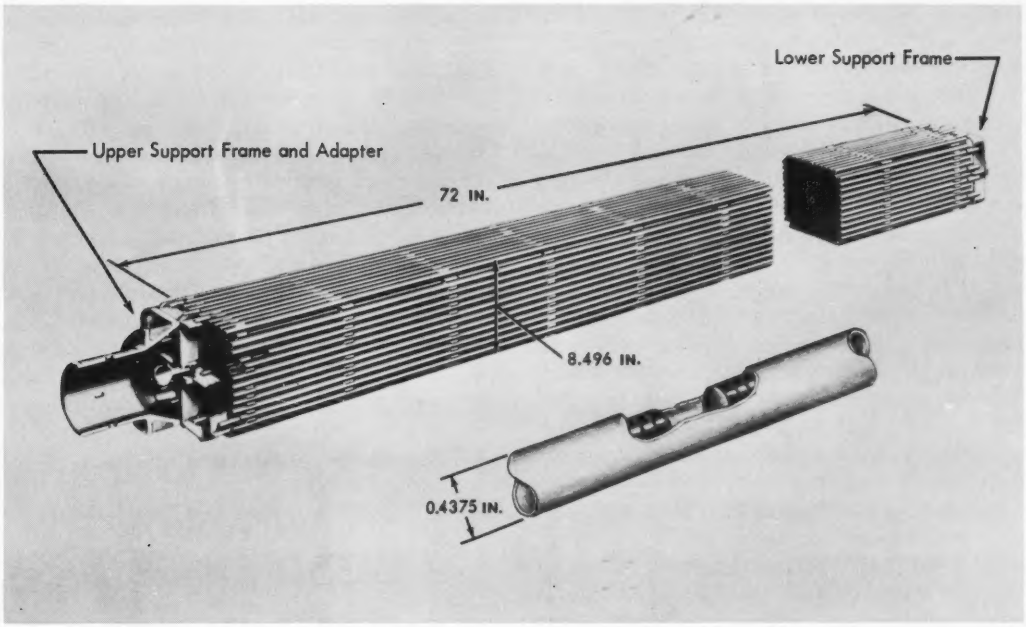

Fig. VI-5 N.S. *Savannah* reactor fuel assembly.

Method of spacing fuel rods	Brazed, tubular, type 307 stainless-steel ferrules
Ferrule dimensions	0.4375 in. in outside diameter by 0.3975 in. in inside diameter by 1 in. long (smaller ferrules used at periphery of assembly)
Ferrule braze material	Kanigen (0.90 nickel – 0.10 phosphorus)
Total assemblies in core	32

Control Rods

The reactor is controlled by 21 cruciform rods (Fig. VI-6), one at each core-lattice position, which is surrounded by a complete set of four fuel assemblies (Fig. VI-2). The poison material is boron, enriched to 92% B^{10}, in a 1.5 wt.% boron–stainless steel alloy. A stainless-steel jacket that surrounds the boron–stainless steel serves as a structural material. Finned dowels through the boron–stainless steel are welded to the two jacket surfaces. Any differential expansion between the jacket and the poison section will result in crushing of the fins without excessive stresses on the assembly.

Below the poison section there is a follower section formed from four angle sections of Zircaloy-2. The center of the follower is filled with aluminum oxide to minimize flux peaking.

Type	Cruciform, with follower
Arrangement	Square array, 9.7-in. pitch
Dimensions of absorbing section	8.00-in. span by 0.375 in. thick by 62 in. long
Absorber material	Boron–stainless steel, 0.188 in. thick, 1.5 wt.% boron, 92% enriched in B^{10}
Cladding material	Type 304 stainless steel, 0.094 in. thick
Follower materials	Zircaloy-2 with central filler of Al_2O_3
Number of control rods	21
Driven from	Top
Downward motion of rods	Decreases reactivity
Rod travel	Adjustable, 72-in. maximum

Core Structure

The reactor coolant makes three passes in the pressure vessel. Two of the passes are in

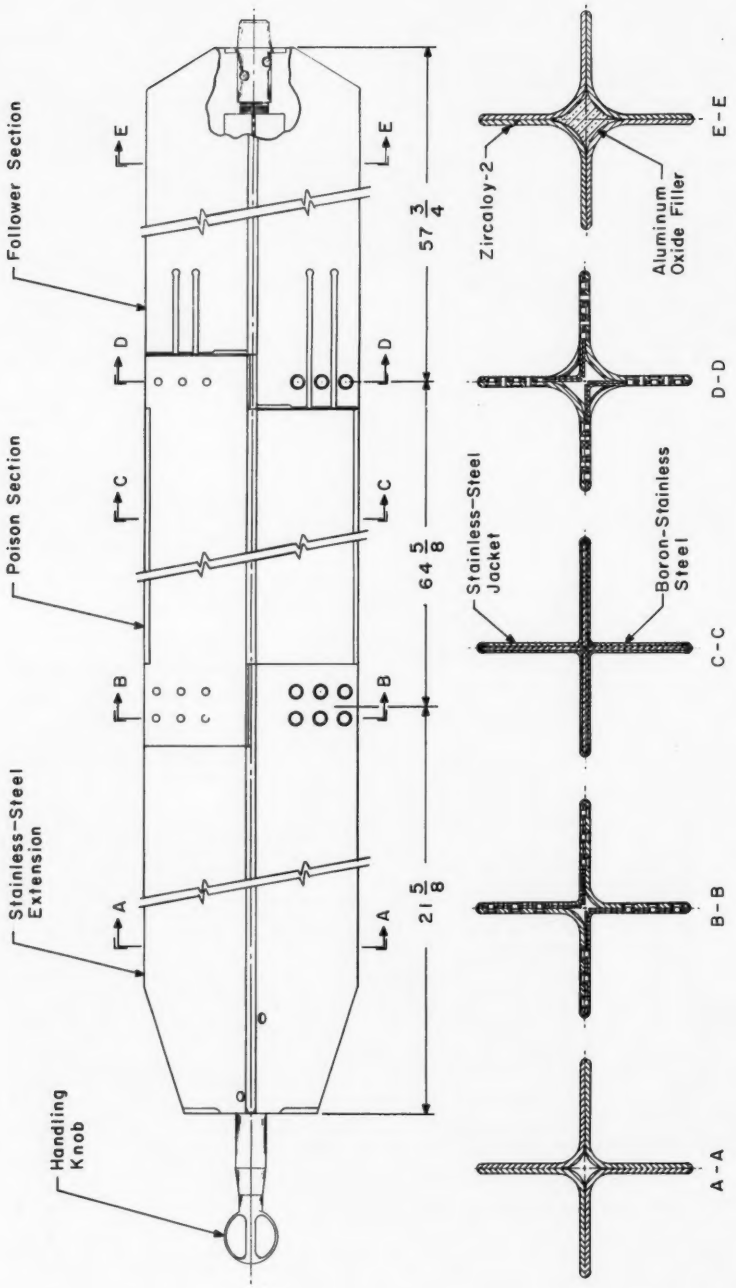

Fig. VI-6 N.S. *Savannah* reactor control rod.

the core. This requires that the core structure separate the coolant passes as well as position the core components. In the first pass the coolant flows upward outside the core, cooling the thermal shields. The second-pass flow is downward through the outer 16 fuel assemblies, and the third pass is upward through the inner 16 assemblies with a small amount of coolant flow in the control-rod channels bypassing the third pass.

The outer thermal shield and conical support ring are welded to the pressure vessel. The core support shield assembly, which supports all other core structures, is bolted at its top to the conical ring and is suspended from it, making all structures in the vessel removable except the conical ring and outer thermal shield (Fig. VI-1). The fuel-container assembly, consisting of the inner thermal shield, the core bottom plate, and the fuel-container eggcrate, is located inside the core support shield. The eggcrate consists of stainless-steel boxes of square cross section joined by stainless-steel H beams (Fig. VI-2). Each box contains one fuel element. The control rods are located in the channels formed by the boxes and H beams. The fuel elements are located at the bottom by a positioning device that mates with the support frame. Below the active core the lower flow-baffle assembly provides flow tubes out of the second pass and into the third to prevent flow across the control-rod followers. Snubbers are provided to prevent damage to any control rod if it is accidentally dropped during installation or removal. The lower plenum chamber separates the reactor inlet flow from the flow entering the third pass. Above the core the upper grid plate has a vertical baffle that channels flow from the first pass in and down to the outer 16 fuel assemblies (second pass). Flow from the inner 16 assemblies (third pass) is carried upward in flow tubes. The bottom plate seals against the fuel-assembly nozzles to prevent leakage between the fuel assemblies and the control-rod channels below the upper grid plate. Above the upper grid plate assembly, flow across the control-rod channels is prevented by the upper flow-baffle assembly. A large belleville spring between the upper flow baffle and the vessel head holds the entire core in place with the reactor in any position.

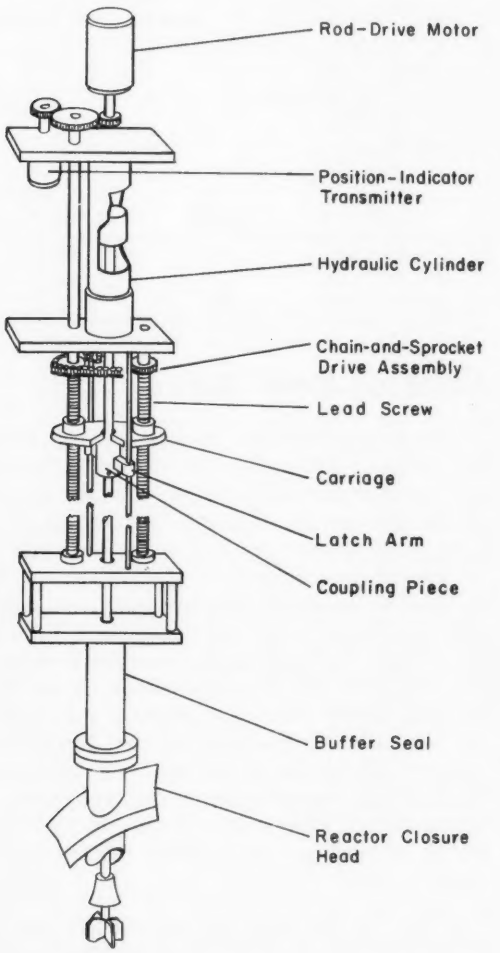

Fig. VI-7 N.S. *Savannah* reactor control-rod drive mechanism.

Core Characteristics

Active fuel length	66 in.
Core equivalent diameter	62 in.
Number of fuel assemblies	32
Fuel enrichment (inner 16 assemblies)	4.2%
Fuel enrichment (outer 16 assemblies)	4.6%
Volume fractions (active core):	
Water	56.7%
Control rods and followers	4.1%
Fuel	24.7%
Stainless steel	14.5%
Initial U^{235} loading	312.4 kg

Initial U^{238} loading	6787.5 kg
Average burnup	7352 Mwd/metric ton
Final enrichment (av.)	3.63%

Rod Programming

The center rod and the outer 12 rods are used as shim rods under manual control at all times, whereas the remaining eight rods may be positioned either under servo control or under manual control. The servo-controllable rods are divided into two groups of four: one group is normally under automatic control and one is operator controlled. The automatic control system positions its group of rods to maintain reactor temperature constant and to follow steam demand. The operator periodically positions the other servo-controllable rods to limit the reactivity swing required of the automatic control system.

Heat Removal

Maximum reactor power	70 Mw
Operating pressure	1750 psia
Maximum fuel temperature	3794°F
Coolant inlet temperature (full power)	496.3°F
Coolant outlet temperature (full power)	519.7°F
Maximum clad temperature	623°F
Maximum coolant temperature	541°F
Power peaking factors:	
Radial	2.0
Axial	1.5
Local (not including effects of manufacturing tolerances)	1.25
Total	4.75
Average heat flux at maximum power	63,500 Btu/(hr)(sq ft)
Maximum heat flux at maximum power (nominal dimensions)	238,000 Btu/(hr)(sq ft)
Maximum heat flux at maximum power (including accumulated effects of tolerances)	277,000 Btu/(hr)(sq ft)
Total coolant flow	8,640,000 lb/hr
Average coolant velocity, outer pass	10.0 ft/sec
Average coolant velocity, inner pass	9.0 ft/sec

Pressure Vessel

Shape	Cylindrical, with hemispherical top and bottom heads
Design codes	U. S. Coast Guard and American Bureau of Shipping
Design pressure	2000 psig
Hydrostatic test pressure	3000 psig
Top head seal	Double O rings and welded outer membrane
Inside diameter	98 in.
Total height	26 ft $10\frac{1}{2}$ in.
Material	Carbon steel, A-212 Grade B
Internal clad material	Stainless steel, type 304
Wall thickness, cylindrical portion	6.50 in.
Wall thickness, heads	6.25 in.
Clad thickness	0.11 in.
Nozzles:	

Type	Quantity	Size (inside diameter), in.
Coolant inlet	2	$12\frac{3}{16}$
Coolant outlet	2	$12\frac{3}{16}$
Control rods	21	~4

Control-Rod Drives*

The control-rod drive mechanism (Fig. VI-7) has electric and hydraulic elements. During normal operation the control rods are forced upward by reactor pressure, holding the coupling piece against the carriage which is driven by the electric motor at a speed of 5 to 15 in./min. To scram the reactor, hydraulic pressure is applied to the cylinder, pushing the rod down where it is held by the hydraulic pressure until the carriage is driven down against the coupling piece. The time required for three-fourths rod insertion is 0.807 sec. In addition to providing scram action, the hydraulic system partially counterbalances reactor pressure, which, in turn, reduces the load on the carriage during normal operation. When reactor pres-

*It has recently been reported that the original drive system will be replaced by an all-electric system at some time in the future. This all-electric system will improve accessibility of important items during operation.[3]

sure is low, hydraulic pressure is applied under the piston to hold the coupling piece against the carriage. Hydraulic pressure is supplied by any one of three power units. Each unit is equipped with oil reservoir, pump, filters, etc. Each control-rod drive is equipped with an accumulator so that the reactor can be scrammed even if the hydraulic power units fail.

The control-rod drive shafts move vertically through penetrations in the reactor-vessel head which are sealed by the buffer seal assembly (Fig. VI-8). The primary seal is made by four

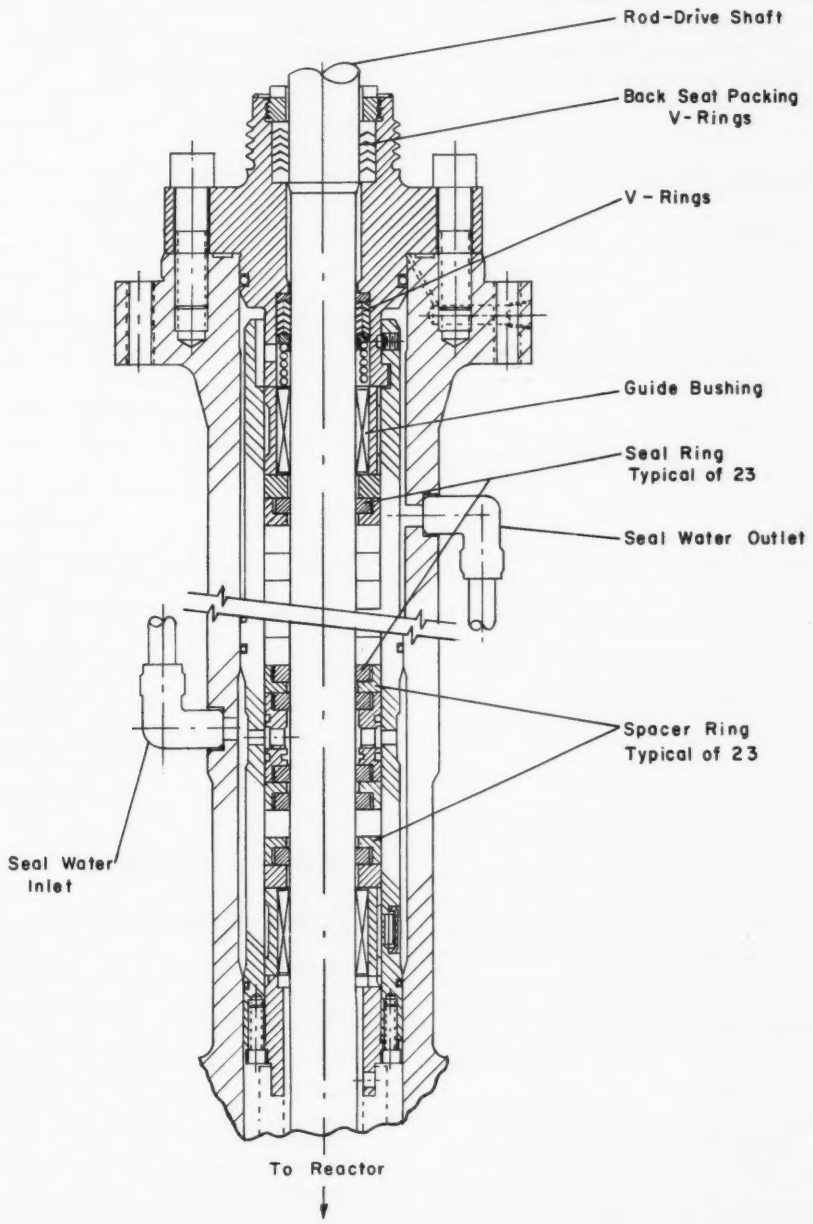

Fig. VI-8 Buffer seal assembly for penetrations through the N.S. *Savannah* reactor-vessel head.

sealing-ring units between the vessel interior and the seal water injection point and by 18 sets of rings between the injection point and the outside. The seal rings are stellite, and the spacer rings are 17-4 PH steel. Buna-n/asbestos V rings form the low-pressure seal between the seal water outlet and the atmosphere. Another set of V rings mates with a shoulder on the shaft when the control rods are fully inserted to form a high-pressure seal. Thus, if the seal water supply fails, reactor pressure can be held with all rods in.

Instrumentation and Control

Startup range:

Two channels using BF_3 chambers cover the source level to 10^{-7} × full power. Two channels using fission chambers cover the range 10^{-9} to 10^{-4} × full power.

Intermediate range:

Three channels using compensated ion chambers cover the range from 10^{-6} to 1.5 × full power.

Power range:

Three channels using uncompensated ion chambers cover the range from 10^{-4} to 1.5 × full power.

Startup neutron source:

Two 100-curie polonium-beryllium sources located at diametrically opposed points in the core.

Chamber location:

All chambers are located in instrument wells in the neutron shield tank just outside the pressure vessel.

Rod insertion and scram:

All rods are electrically inserted at the maximum rate on period signals from the startup and intermediate channels. The hydraulic scram system is actuated by: (1) period signals from the two startup channels that use fission chambers; (2) period signals in a two-out-of-three coincidence from the intermediate-range channels; and (3) high reactor-power signals in a two-out-of-three coincidence from the power-range signals.

k_{eff} cold and clean	1.112
Temperature coefficient (room temperature)	-2.3×10^{-5}/°F
Reactivity requirements:	
Moderator temperature (68 to 508°F)	0.032
Equilibrium xenon and samarium	0.020
Fuel temperature	0.013
Fuel burnout and poison buildup	0.047
Total excess reactivity	0.112
Total control-rod worth	0.146

Primary Coolant Circuit

Number of coolant loops	2
Number of steam generators per loop	1
Number of pumps per loop	2
Valves per loop	2 gate valves (remotely operated), 1 check valve at each pump discharge
Main piping size	$12^{9}/_{16}$ in. in inside diameter
Pipe construction and material	Hollow forged ASTM A-376 type 304 stainless steel
Main circulating pumps	Canned motor, 5000 gal/min each at 495°F (~2×10^6 lb/hr) with half-speed winding for shutdown cooling of the reactor
Steam generators	U-tube boiler and steam drum with scrubbers and centrifugal moisture separators; primary coolant in U tubes
Pressurization	Electric heater in separate pressurizer vessel
Relief valves	One pilot-operated valve on pressurizer set to open at 1930 psia; two self-actuated valves set to open at 2000 psia; a three-way remote-operated valve allows isolation of either self-actuated valve

Primary System Water Treatment

Dissolved solids content	1 ppm
Purification method	Bypass flow of cooled, depressurized water to mixed-bed demineralizers. Flow rate, 20 to 60 gal/min
Demineralizer life	150 to 300 days
Spent-resin disposal method	Sluicing to shore storage and disposal facilities or removal of complete demineralizers

Hydrogen content	20 to 40 cm^3/liter (STP)
Hydrogen-addition method	Added to return from demineralizers

Reactor Shielding

Primary shielding	Outside the reactor pressure vessel: 33-in.-thick water neutron shield surrounded by 1- to 4-in.-thick lead shield
Secondary shielding	Outside the upper half of containment vessel: 8 in. of polyethylene plus 5.2 to 6 in. of lead. Outside lower half of containment vessel: concrete, 33 to 48 in. thick

Shield design rates:

Area	Dose rate	Reactor power
Passenger spaces	0.5 rem/year	Full power
Crew areas	5 rem/year	50 Mw (expected av.)
Temporary access (food storage, etc.)	1 rem/week	
Stevedore spaces	0.5 rem/year	14 Mw (ship in port)
Inside containment vessel	0.2 rem/hr	½ hr after reactor shutdown

Maintenance and Refueling

Both periodic and unscheduled maintenance will be required. Some of the periodic maintenance items are:

Item	Interval	Location
Waste transfer	100 days	As required
Inspection	Annually	As required
Refueling	30 to 40 months	Refueling site
Removal of demineralizers and charcoal traps	No regular interval	Refueling site
Drydocking	Annually or as required	As required

In general, maintenance operations in which the containment is breached are performed at the refueling site. Other operations may be performed at any location where adequate facilities are available.

To provide a mobile nuclear servicing facility, a 650-ton barge, the nuclear service vessel *Atomic Servant* was built. The 129-ft-long by 36-ft-wide barge is equipped to receive the *Savannah's* demineralizer resins and one core loading of spent fuel. Facilities are provided to store, process, and package waste for disposal and to dilute and dispose of low-level liquid wastes. Health physics, decontamination, and other facilities are provided to allow any shipyard to work on the *Savannah*.

Refueling will be done at the shore facility, where the refueling equipment is stored. The shore facility also is equipped to transfer spent fuel for disposal, to store fresh fuel, and to provide other facilities required for refueling and reactor-system maintenance.

Power Plant

Propulsion turbine:
Cross compound type, directly coupled to the propeller shaft through double-reduction gearing. Maximum continuous rating is 22,000 shp at 110 rpm with steam pressure of 445 psia.

Turbogenerators:
Two 1500-kw turbogenerators use secondary steam to provide electric power for reactor auxiliaries and ship's load.

Low-pressure steam generator:
Steam is generated at 100 psig for laundry and various heating uses on the ship. Maximum capacity is 7500 lb/hr.

Condensers:
Propulsion turbine and turbogenerators are each equipped with a separate condenser, air-removal equipment, and condensate pumps.

Feedwater system:
One low-pressure feedwater heater, one direct-contact deaerating heater, one turbine-driven boiler feed pump, and one high-pressure feedwater heater.

Steam dump system:
Up to 190,000 lb of steam per hour from the steam generators can be bypassed directly to the main condenser.

Auxiliary equipment:
Two 750-kw diesel generators provide electric power to the ship and to a 750-hp "take home"

electric motor if the reactor or the steam turbogenerators are disabled. A 300-kw diesel generator, located on the bridge deck, provides electric power for essential services if all other generators fail. An oil-fired boiler provides steam for ship's service when the reactor is not operating.

General Arrangement

The general arrangement of the ship is shown in Fig. VI-3. The reactor and power plant are located amidships in order for the ship to maintain an approximately even keel in the loaded and unloaded conditions. The containment vessel is ahead of the main propulsion turbine and other machinery to allow it to be placed as low as possible without interfering with the shaft tunnel. For refueling, it is advantageous to have overhead access with a minimum of restrictions; therefore the superstructure is placed over the machinery space, leaving vertical access to six of the seven cargo holds. The machinery space contains the reactor control center, the propulsion equipment, the auxiliaries, and the ship's service equipment.

The reactor containment shell is protected against damage in collision by special strengthening of decks outboard of the reactor compartment and by a vertical mat of steel and redwood. The bottom structure of the ship is strengthened in the area under the reactor to hold its weight under all conditions.

Containment

All high-pressure components of the primary loop are inside the reactor containment shell, which is a cylindrical vessel with hemispherical ends and a cupola mounted at its center to give vertical access to the pressure vessel. The containment shell and primary system components are shown in Fig. VI-7. Weight and space limitations on the ship dictated the use of a relatively small high-pressure vessel, accommodating the most compact practical arrangement of internal components. Except for an occasional flow of air to purge radioactive gases, the vessel is sealed during plant operation.

Diameter	35 ft
Length	50½ ft
Cupola diameter	13½ ft
Design pressure	186 psi
Maximum pressure occurring during accident	173 psi
Test pressure	173 psi
Design code	ASME code for unfired pressure vessels

The containment vessel, which lies lengthwise in the ship, rests on six longitudinal beams under the cylindrical portion. Additional support is provided by braces at the C deck level above the vessel center line, by two transverse saddles, and by chocks that follow the contours of the hemispherical ends. The vessel is bolted only to the rear saddle, and clearance is left between the vessel and the forward chock to allow for thermal expansion. The entire containment vessel is designed to be held in place with the ship in any position and to withstand 1-g accelerations, which are considerably above the maximum expected in heavy weather or collision.

The containment vessel is protected from crushing, in the event that the ship sinks, by two manways that open at a depth of 100 ft and reclose after the pressures are equalized.

References

1. The Atomic Energy Commission and the Maritime Administration, N.S. *Savannah* Safety Assessment, Vol. I, Engineering and Construction, August 1960; Vol. II, Operations, August 1961; Vol. III, Radiological Health, August 1961; and Vol. IV, Analyses of Hypothetical Accidents, November 1960.
2. A. W. Kramer, *Nuclear Propulsion for Merchant Ships*, U. S. Government Printing Office, Washington, 1962.
3. N.S. *Savannah* To Undergo Modifications, *Nucleonics*, 20(10): 30 (October 1962).

Section

VII

Power Reactor Technology

Operating Experience: Heavy-Water Losses from Power Reactors

The rate of loss of heavy water is one of the important uncertainties that affects the assessment of the practicality and the economic promise of heavy-water-cooled reactors. Several programs of laboratory tests have been performed in an effort to determine the suitability of various turbine-shaft, pump-shaft, and valve-stem seals for use in D_2O systems. Reports giving some of the results of these tests have been reviewed in the September 1961 issue of *Power Reactor Technology*, Vol. 4, No. 4, page 70, and in the June 1962 issue, Vol. 5, No. 3, page 35. Additional results of tests to determine the leakage of water from pump mechanical seals are given in Ref. 1.

The general usefulness of laboratory tests is limited by the specific nature of the items tested, the many variables that affect service performance, and the inconsistencies encountered in the tests. In some cases a test of a single seal may yield instantaneous D_2O-loss values that differ from minimum to maximum by more than three orders of magnitude. Yet, despite the restrictions placed upon the use of most of the test data, the tests have provided at least a basis for the selection of specific components and some basis for estimates of the D_2O-recovery facilities that would be required for heavy-water power-reactor plants.

Reference 2, which reports leakage experience with a complete D_2O reactor system of the pressure-tube type, is of particular interest. The report contains a discussion of the D_2O losses that occurred in the Plutonium Recycle Test Reactor (PRTR) during the period from November 1960 through November 1961. This period covers the time from initial criticality through several months of operation at rated power [70 Mw(t)]. Although the PRTR operates under power-reactor conditions (530°F and 1050 psi), it is intended for research and development purposes. Two features of the PRTR design which are not common to most proposed power reactors of the pressure-tube type are (1) the provision of helium pressurization for the primary coolant system and (2) the installation of easily removed pressure tubes. Both of these features may contribute to D_2O losses.

The major D_2O systems of the PRTR, each of which contains about 30,000 lb of D_2O, are:

1. The primary system, which is pressurized to about 1050 psi and which operates at 478 to 530°F
2. The moderator system, which is nominally unpressurized in the core region and which operates at a maximum temperature of about 160°F
3. The reflector system, which is also nominally unpressurized and which operates at a maximum temperature of about 160°F

Reference 2 contains detailed descriptions of the above systems, the helium systems, and the D_2O recovery system. In conjunction with the system descriptions, specific mention is made of those components from which losses of D_2O might be expected.

Although the D_2O losses from the PRTR have been very high, the attention given by its designers to component testing, D_2O-loss prediction, and D_2O recovery appears to be at least as great as that proposed for similar reactors in design studies. The large D_2O losses were contributed to by the failure of components to perform in the reactor as well as tests had indicated they would and by the spills and other errors that occurred during the early operating period of the reactor. However, other substantial losses of D_2O have come from a multitude of minor sources that would be present in any power reactor of the PRTR type.

Heavy-water loss rates are given in Ref. 2 for the period of rated-power operation covered

by the report (July 1961–November 1961). The loss rate was reduced from an initial value of over 200 lb/day to a value of nominally 50 lb/day. The authors state that they feel it is possible to reduce the loss rate further (to the design value of about 20 lb/day), but such decreases will become progressively more difficult. It should be noted that the design value (20 lb/day) represents an annual D_2O loss of about 8% of the total inventory and that the actual loss rate as of November 1961 was equivalent to about a 20% annual loss. Heavy water from the moderator and reflector systems constituted about 15 lb/day of the 50 lb/day nominal actual loss, and the remainder of the loss was heavy water from the primary system. Helium losses of 3000 scf/day or more were normal.

The recommendations that appear in Ref. 1, based on PRTR operating experience, are quoted below.

1. A continuing effort should be made during design and procurement periods to obtain systems and/or components that are (or can be) hermetically sealed. A substantial premium for such items may not be warranted, however, because a continuing effort to minimize D_2O losses will be necessary anyway for those items which are not or cannot be so sealed.
2. A record-keeping program of D_2O leakage (and repair) should be maintained for each piece of equipment or component to determine items that require replacement or modification.
3. Rather complex shrouds (for potentially high-leakage equipment) can be built with the expectancy of collecting high isotopic purity D_2O.
4. Continuous monitoring (in preference to batch monitoring) should be provided wherever possible as a signal of changing D_2O losses. This is true of both unrecoverable streams (stack exhaust) and recoverable streams (recovery systems).
5. A continuous inventory system (during shutdown and operation) is desirable to ensure that malfunction of monitoring instrumentation does not go undetected.
6. Shutdown losses resulting from maintenance and operating functions can be as great or greater than full power operation losses. Stringent procedures for maintaining and repairing the piping systems and the collection systems (D_2O recovery system, for instance) are required.

Reference 3 contains information concerning D_2O and helium losses from the PRTR for a 39-day period ending May 25, 1962. During this time the reactor was shut down for 20 days. Heavy-water losses were 2120 lb, or about 54 lb/day, and helium losses totaled 73,500 scf. A total of 20,900 lb of D_2O equivalent was shipped for reprocessing, and this amount covered all the degraded heavy water accumulated since startup of the PRTR. These values[2] indicate no improvement over the loss rates that were reported for November 1961.

It is hoped that, percentagewise, large D_2O power reactors can achieve loss rates substantially lower than those which have characterized the PRTR to date. Large D_2O-cooled reactors of the pressure-tube type appear to be capable of specific powers of about 0.5 kw(e) per pound of D_2O in the total reactor system. A loss rate of even 8% per year (the PRTR target value) in such a plant would contribute about 0.65 mill/kw-hr to the cost of power generation. However, it is not unreasonable to expect very substantial improvements in future designs, particularly those directed specifically toward plants for commercial power generation, on the basis of experience provided by reactors such as the PRTR. Further, there is no apparent fundamental reason for a direct proportionality between leakage rate and D_2O inventory. The common practice of estimating leakage as a percentage of inventory is evidence of the inadequacy of existing information, an inadequacy that operation of the early experimental and prototype D_2O power reactors should do much to remedy.

References

1. D. L. Burns, Leakage of Water from Pump Mechanical Seals, USAEC Report DP-666, Savannah River Laboratory, November 1961.
2. H. Harty, K. G. Toyoda, and R. D. Widrig, Heavy Water Losses in the PRTR, USAEC Report HW-73755, Hanford Atomic Products Operation, May 1962.
3. S. Goldsmith, Hanford Atomic Products Operation, July 2, 1962. (Unpublished)

Section

VIII

Power Reactor Technology

Sodium-Cooled Reactors

Fuel-Rod Bowing in SRE

The Sodium Reactor Experiment (SRE) was operated from April 1957 to July 1959 with its first core loading, which consisted of 43 seven-rod-cluster fuel elements of uranium metal enriched to 2.8% U^{235}. The uranium rods were jacketed in type 304 stainless steel with an NaK thermal bond. Measurements showed that the power coefficient of reactivity had two distinct components: (1) a fast negative effect associated with the fuel temperature, and (2) a much slower, positive contribution associated with the moderator. The net power coefficient was positive at operating powers below 12 Mw, and negative above. However, the reactor was, for practical purposes, very stable over the entire range because of the much faster response of the negative term.[1,2]

Operation with the second core loading[3] began in September 1960. The second loading consists of five-rod-cluster fuel elements containing thorium–7.6 wt.% uranium alloy slugs with a U^{235} enrichment of 93.1%. Like the core 1 elements, the core 2 elements use type 304 stainless-steel fuel tubes with an NaK thermal bond between fuel and tube surfaces. Figure VIII-1 shows cross sections of the seven-rod and five-rod clusters.

The early operation with core 2 was at relatively low power until some residual decomposition products of Tetralin, remaining from the earlier Tetralin-leakage problem, had been removed.* During this low-power operation, in December 1960, indications of reactor instability were observed at 2 Mw(t). The instability was attributed to a fast, positive power coefficient of reactivity that was caused by the thermal bowing of fuel elements. Previously it had been assumed that small changes in fuel position would cause negligible reactivity effects because of the long diffusion length in sodium graphite reactors. However, experiments proved that this is not true and that it was necessary to constrain the fuel rods to prevent reactor instability. This effect is discussed in Ref. 3, and the method used to prevent thermal bowing in the elements is presented in Ref. 4. Rigidity was achieved by installing a helical wire wrap around the fuel clusters. This reduced the power coefficient, measured at power levels to 5 Mw(t), from +16 cents/Mw to −2.1 cents/Mw. As of January 1962 the fuel-element modifications were completed, and the SRE was operating at a power level of 5 Mw(t) while carbon deposits were being removed from the sodium coolant.[5]

The initial indications of reactor instability were observed under manual control at a power level of 2 Mw(t) when flux- and temperature-monitoring instruments recorded oscillations having an amplitude of 5% of the average value and a frequency of one-fourth cycle per minute.[3] Two attempts to increase power resulted in minor flux transients with exit temperatures increasing 30°F. In view of these indications, the reactor was shut down temporarily, and a study was initiated to determine the cause of the instability. During subsequent tests the reactor was operated safely on manual control for steady-state operation at power levels below 3 Mw(t), and power changes were easily accomplished using automatic flux control.

Experimental measurements with an "on-line" analog simulator showed that the fast power coefficient was +16 cents/Mw. Since the estimated Doppler coefficient was −2 cents/Mw, this indi-

*The Tetralin leaks, and their effects, were discussed in previous issues of *Power Reactor Technology*, Vol. 3, No. 2, pages 60–64 (March 1960) and Vol. 5, No. 1, pages 84–87 (December 1961).

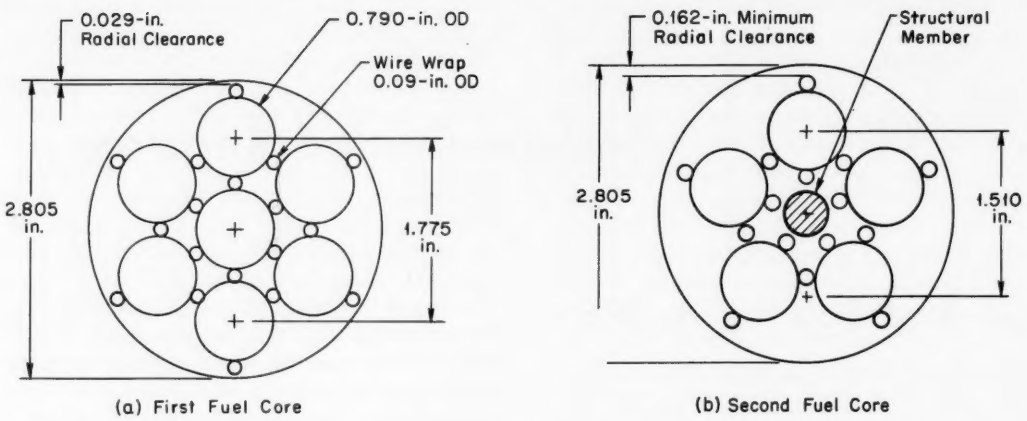

Fig. VIII-1 Cross sections of a seven-rod and a five-rod fuel element in a fuel channel.[4]

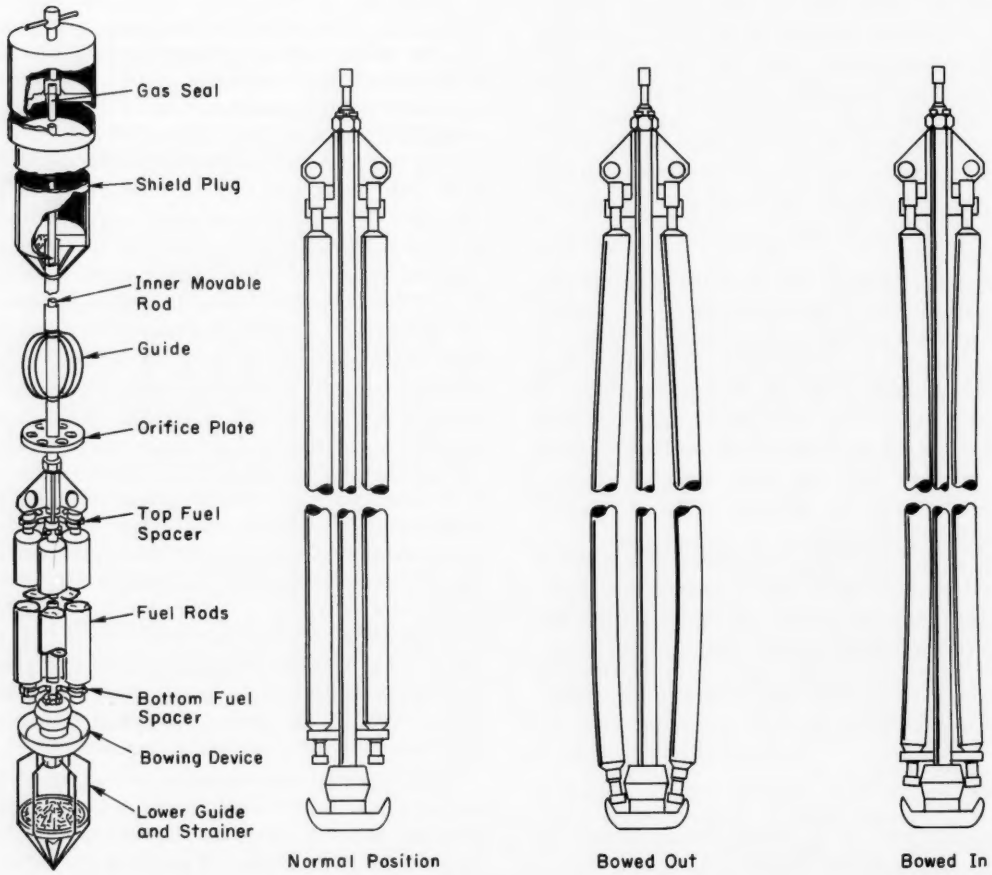

Fig. VIII-2 Fuel-rod bowing assembly.[3]

cated a positive component of +18 cents/Mw to be explained. This component of the coefficient was not evident during the measurement of the isothermal temperature coefficient. Therefore it was apparently associated with the temperature gradients in the fuel cluster, which were postulated to result in fuel-rod bowing. Theoretical analysis of the reactivity effects of outward fuel-rod bowing indicated the following components: (1) absorption of thermal neutrons by the fuel rods causes a depression in the thermal flux at the position of the fuel; as the rods move outward, the shadowing of each rod by adjacent rods becomes smaller, resulting in a rise in thermal flux and an increase in thermal utilization (a positive effect); (2) absorption of resonance neutrons also increases for the same reason, causing a decrease in the resonance escape probability (a negative effect); (3) outward movement of rods displaces sodium from

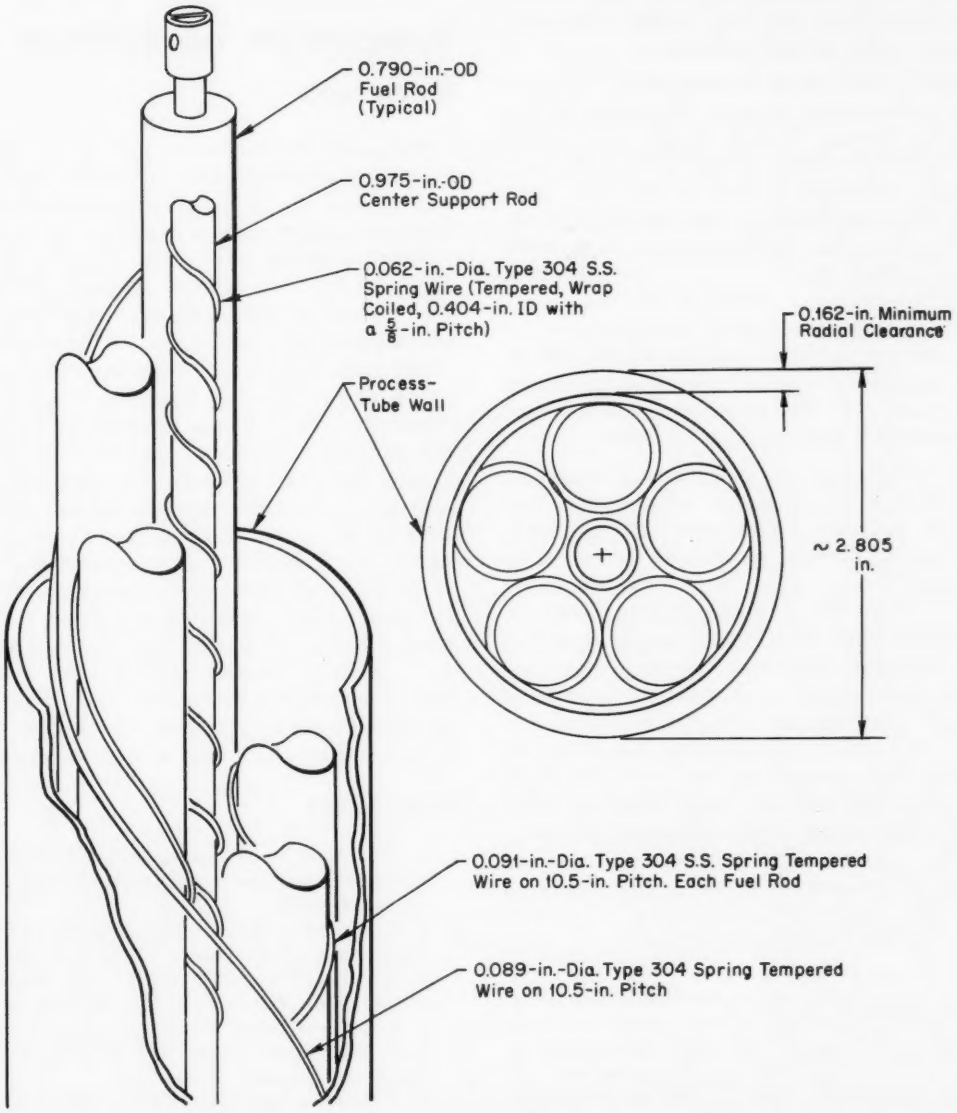

Fig. VIII-3 Wire-wrapped fuel cluster in a fuel channel.[4]

the outer annulus to the inner annulus, causing a reduction in the neutrons absorbed by sodium and an increase in thermal utilization (a positive effect). The net change in reactivity from these causes was calculated to be about +24 cents/Mw, which agreed reasonably with the experimental value of 18 cents/Mw for the observed positive component. Another source of reactivity increase was found to be due to hydraulic bowing of elements caused by a differential pressure between the inner flow annulus and the outer flow annulus (see Fig. VIII-1). This contribution was about 4 cents when going from zero flow to maximum flow.

Direct experimental measurements of bowing effects were undertaken also in the Sodium Graphite Reactor Critical Assembly (SGRCA). Two methods, period measurements and trace analysis, indicated a loss in reactivity from outward bowing, in direct contradiction to other results. However, the absence of sodium in the SGRCA caused doubt as to the applicability of these results. As a consequence a bowing experiment was performed in the SRE using an experimental assembly as shown in Fig. VIII-2. This experiment was performed at essentially zero power (10 kw) and showed that outward bowing caused an increase in reactivity.

On the basis of the experimental results, a program was undertaken to constrain the fuel rods by wrapping the clusters with stainless-steel wires.[4] The configuration of the wire wrap is shown in Fig. VIII-3. Thirty-five irradiated fuel elements were wire wrapped in a hot cell, and twelve unirradiated fuel elements were also wire wrapped. Low-power physics measurements were performed at power levels to 3 Mw with 40 wire-wrapped fuel elements in the reactor. The results indicated that the power coefficient was reduced to −2.1 cents/Mw from +16 cents/Mw* before wire wrapping. This modification restored the stability of the reactor. The loss in reactivity due to wire wrapping was approximately 95 cents, of which 22 cents was the poisoning effect of the stainless-steel wire. The geometry change effected by restricting the fuel-rod bowing was responsible for the remainder of the loss, 73 cents. This was additional proof that outward bowing caused the positive power coefficient.

The effects discussed above are also treated in a recent paper in *Nuclear Science and Engineering*.[8] This paper gives particular attention to the experimental investigation of the reactor behavior.

*The magnitudes of the power coefficients quoted here were furnished by private communication from Atomics International. They differ from those reported in Refs. 3 and 4 because they have been uniformly normalized to a power level of 5 Mw(t) and a coolant flow rate of 1000 gal/min to facilitate comparisons.

Symposium on Sodium Reactors

The proceedings of the Symposium on Sodium Reactors Technology, held in Lincoln, Nebr., on May 24 and 25, 1961, has been issued.[6] In the field of thermal-neutron reactors, the symposium covered the Hallam Nuclear Power Facility, the SRE, and related developmental work. The review of SRE operating experience has been summarized in *Nucleonics*.[7] The remainder of the papers treat fast-reactor projects. The Experimental Breeder Reactors I and II, including the Mark IV core for EBR-I (plutonium alloyed with 1.25% aluminum), are discussed. Related to these projects are discussions of fast-neutron critical experiments and discussions of the status of the fuel-cycle work involving pyrometallurgical reprocessing at Argonne National Laboratory. Status reports on the Enrico Fermi Atomic Power Plant, the Los Alamos Molten Plutonium Reactor Experiment No. 1, and the General Electric work on fast-oxide reactors are given, with related reports on research and development. The French fast-reactor project, Rapsodie, is also reviewed.

References

1. C. Starr and R. Dickinson, *Sodium Graphite Reactors*, Addison-Wesley Publishing Co. Inc., Reading, Mass., 1959.
2. L. E. Glasgow, Sodium Reactor Experiment, in Proceedings of Symposium on Sodium Reactors Technology, May 24–25, 1961, Lincoln, Nebraska, USAEC Report TID-7623, pp. 63–72, June 1962.
3. H. F. Donohue and R. W. Keaten, Fuel Rod Bowing in the SRE, USAEC Report NAA-SR-6878, Atomics International, June 1, 1962.
4. H. F. Donohue and H. A. Vislay, Stabilizing SRE Fuel Elements, USAEC Report NAA-SR-6879, Atomics International, Apr. 15, 1962.

5. SRE Operates Again with Core 2 but with 5-Mw(th) Power Limit, *Nucleonics*, 20(1): (January 1962).
6. Proceedings of Symposium on Sodium Reactors Technology, May 24–25, 1961, Lincoln, Nebraska, USAEC Report TID-7623, June 1962.
7. L. E. Glasgow, Experience with SRE, *Nucleonics*, 20(4): (April 1962).
8. C. W. Griffin, Analysis of the Sodium Reactor Experiment Prompt Power Coefficient, *Nucl. Sci. Eng.*, 14(3): 304 (November 1962).

Section

IX

Power Reactor Technology

Organic-Cooled Reactors

Current Status

By EDWARD A. MASON*

(Editor's Note: This review of the status of organic-cooled nuclear-reactor technology was presented as an invited paper at the 1962 annual meeting of the American Nuclear Society [Trans. Am. Nucl. Soc., *5(1): 101–103 (June 1962)]. It is reproduced here because it will serve as a point of departure for future reviews in* Power Reactor Technology *of the work in this rapidly developing area. It should also serve to draw into perspective the occasional past reviews of organic-cooled technology in this journal. In this connection, the editors have, with the author's consent, added a number of references to previous papers, many of which have been reviewed in past issues of* Power Reactor Technology.)

*Edward A. Mason is an associate professor in the Department of Nuclear Engineering at the Massachusetts Institute of Technology (MIT). He received the B.S. degree (1945) from the University of Rochester and the S.M. (1948) and Sc.D. (1950) degrees from MIT. He served as an assistant professor of chemical engineering at MIT (1950–1953) and as director of research for Ionics, Incorporated (1954–1957) before taking his present position in 1958. He has worked on the analysis and design of nuclear reactors for Brookhaven National Laboratory, Oak Ridge National Laboratory, and General Atomic Division of General Dynamics Corporation. His principal research interests are in the effects of radiation on materials, solvent extraction, and fuel-cycle analysis. He is supervisor of an AEC in-pile loop project at MIT, which is studying the effects of radiation and heat on organic coolants for nuclear reactors. He is a member of the American Nuclear Society, American Chemical Society, American Institute of Chemical Engineers, American Rocket Society, Sigma Xi, Phi Beta Kappa, and Tau Beta Pi.

The use of hydrocarbon liquids in nuclear reactors was originally considered during the Manhattan Project of World War II; however, it was only after enriched uranium became available as a reactor fuel and sufficient information concerning the radiation stability of a variety of organic fluids was acquired that development work began in earnest (about 1953). The technology is developing rapidly.[1–3]

Although hydrocarbon fluids can be used as both moderators and coolants in nuclear reactors, the coolant properties of these fluids provide the unique aspects of organic reactors. Except for somewhat larger values of neutron age and thermal-diffusion length, the basic reactor physics of organic-moderated reactors closely resembles, and has drawn extensively from, that for water-moderated reactors. The advantages that arise from the use of organic coolants are principally due to their low vapor pressures, which permit operation at temperatures of about 700°F with system pressures of 100 to 200 psi, low corrosion rates with most common materials of construction, and low coolant activation. These properties favor the achievement of low capital and maintenance costs for organic reactors. On the other hand, the organic coolants have relatively poor heat-transfer properties, and they suffer from decomposition induced by radiation and high temperatures.

Table IX-1 presents for comparison a list of some of the physical and engineering properties of water and the organic coolant used in the Organic-Moderated Reactor Experiment (OMRE). The differences in viscosity, thermal conductivity, and specific heat are all significant, and they contribute to the lower heat-transfer coefficients of organic coolants relative to water. Additional data on physical properties have been published.[4]

Table IX-1 PHYSICAL AND THERMAL PROPERTIES OF OMRE COOLANT AND WATER

	OMRE coolant[17]	Water
Composition	Diphenyl-terphenyl isomer mixture	H_2O
Operating temperature on which the properties listed below are based	500	580
Vapor pressure, psi	5.3	1330
Melting point, °F	~200	32
Thermal conductivity, Btu/(hr)(sq ft)(°F/ft)	0.069	0.31
Specific heat, Btu/(lb)(°F)	0.53	1.41
Viscosity, centipoises	0.46	0.091
Density, g/cm^3	0.89	0.70
Typical coefficient of heat transfer in reactor, Btu/(hr)(sq ft)(°F)	1000	8000

Efforts to develop organic-cooled reactors in the United States have centered around the use of the organic fluids as the moderator as well as the coolant. Such reactors have many of the characteristics of pressurized-water reactors. Table IX-2 lists the various reactors of this type for which definite commitments have been made. The first, and as yet the only operating, organic-cooled reactor is the OMRE. Atomics International (AI) has been responsible for most of the organic-reactor design and development work in the United States. The Piqua reactor,[5-13] also designed and built by AI, should achieve criticality during January 1963 and should operate in the power range in April 1963. The Experimental Organic-Cooled Reactor (EOCR) will serve as a test reactor for the U. S. organic-reactor program.[14-16] It should achieve criticality in April 1963. Two in-pile loops are now being constructed: one for fuel-element tests and the other for coolant-technology studies.

In addition to the three U. S. reactors that are either operating or are under construction, the Italian National Committee for Nuclear Energy (CNEN), which has an organic-reactor program, is planning the construction of the Organic-Reactor Program (PRO) organic-cooled and -moderated test reactor.[18] In Germany, engineering design studies of two organic-moderated central-station power reactors and one organic-moderated maritime propulsion plant are being carried out.

The other organic-cooled concept that has received considerable development employs heavy water as the moderator; both Canada and Euratom have large programs for the development of this concept.[19-24] This concept combines the features of operation with natural uranium with the higher temperatures and lower pressures of organic cooling. Relative to the D_2O-cooled concept, the organic-cooled concept results in increased thermal efficiency, which reduces the design pressure of the pressure tubes and eliminates the necessity of circulating high-pressure D_2O. Canada has recently authorized the construction of the Whiteshell Reactor No. 1 (WR-1) for its Organic-Cooled Deuterium Reactor (OCDR) program, and Euratom has decided to construct ESSOR

Table IX-2 ORGANIC-COOLED REACTORS

Reactor	Location	Power	Startup date	Purpose
Organic-moderated and -cooled reactors:				
OMRE	Idaho, USA	6.0 Mw(t)	1957	Concept demonstration and experiment
Piqua plant	Ohio, USA	11 Mw(e)	1963	Small reactor prototype
EOCR	Idaho, USA	40 Mw(t)	1963	Test reactor for USAEC's organic-reactor program
PRO Reactor	Italy	30 Mw(t)		Test reactor for Italy's organic-reactor program
Organic-cooled heavy-water-moderated reactors:				
Whiteshell Reactor No. 1 (WR-1)	Manitoba, Canada	40 Mw(t)	1965	Test reactor for Canadian OCDR program
ESSOR	Ispra, Italy	25 Mw(t)		Test reactor for Euratom's ORGEL program

(ESSai ORgel), a test reactor, for its ORGEL (ORGanique-Eau Lourde) program (see Table IX-2). Euratom is now building ECO (Expérience Critique Orgel), a critical experiment, for its ORGEL program. Spain's Junta de Energia Nuclear is planning a 30-Mw(e) power and test reactor, the DON, which will be of this type. The Junta has recently signed a contract with AI for a Title 1 design of the reactor and for consulting services.

E. I. du Pont de Nemours & Company, which has been investigating heavy-water-moderated reactors using natural-uranium fuel for the U. S. Atomic Energy Commission (USAEC), is evaluating the use of organic cooling in such reactors. Combustion Engineering has recently been awarded a contract by the USAEC for the conceptual design and economic evaluation of an organic-cooled heavy-water-moderated power reactor. This study, in conjunction with similar studies of cooling by pressurized D_2O, boiling D_2O, and CO_2, which are being carried out by the General Nuclear Engineering Corporation for the East Central Nuclear Group, will be used to compare the four different coolants for application to the D_2O-moderated reactor.

In addition to these reactor projects which are under way, Great Britain and Denmark have also studied various aspects of the use of organic coolants.

Since organic-moderated reactors can draw upon the reactor-physics work associated with the water-reactor programs, studies of the physics of organic reactors have constituted a relatively minor effort compared to that carried out in the water-reactor programs themselves and compared to the other areas that have been studied in the organic-reactor program. As interest in the organic-cooled D_2O-moderated reactor has grown, however, it has become apparent that the heterogeneous moderator structure of this reactor type presents a difficult reactor-physics problem, the importance of which is accentuated by the desire to use natural uranium as fuel and by the existence of positive reactivity coefficients associated with coolant temperature and coolant voiding. Most organizations considering this reactor type now have relatively strong reactor-physics programs, but the results have not yet reached the stage of publication in many cases. A number of papers pertaining to reactor physics, most of which apply mainly to the organic-moderated concept, are listed as Refs. 25 to 37.

One of the major efforts in the organic-reactor program has been directed to the determination of the effects of radiation on the organic materials at various temperatures. Aromatic hydrocarbons, particularly the polyphenyls, have so far been found to be the most stable types of organic liquids. These hydrocarbons also have the other properties required by coolants.

Table IX-3 shows the chemical structure of biphenyl and the three terphenyl isomers, ortho, meta, and para.

Although biphenyl appears to have slightly better radiation stability than the terphenyl isomers, its vapor pressure is appreciably greater. Consequently mixtures of terphenyl isomers are specified for organic-moderated and -cooled reactors in the United States and Italy and for the organic-cooled heavy-water-moderated reactors of Euratom, Canada, and Spain. Table IX-4 presents a listing of the composition of three terphenyl reactor coolants.

The main reaction induced by the irradiation of polyphenyls is that of polymerization to a variety of hydrocarbons having higher molecular weights, densities, and viscosities, and

Table IX-3 CHEMICAL STRUCTURE OF TERPHENYLS AND BIPHENYL

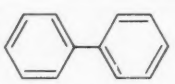

Biphenyl

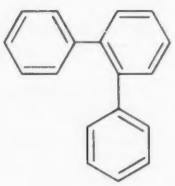

Orthoterphenyl

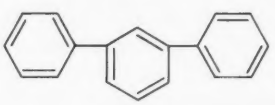

Metaterphenyl

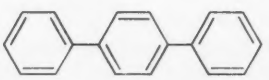

Paraterphenyl

Table IX-4 POLYPHENYL REACTOR COOLANTS

	Coolant		
	Santowax OMP	Santowax OM	OM-2
Reactor	Piqua, EOCR	WR-1	ESSOR
Approximate cost, $/lb	0.17	0.40	
Isomer	Weight percent in unirradiated coolant		
Ortho	12.5	60	15
Meta	62.5	30	80
Para	25		4
Biphenyl	<2	5–15	<1

hence poorer heat-transfer properties, than the original materials. There is also some formation of lower-molecular-weight species and of gases, largely hydrogen. The decomposition reactions are quite complex, largely irreversible, and are not well understood at the present time.

During the operation of organic-cooled reactors, a side stream of the coolant is subjected to vacuum distillation in order to separate the high-molecular-weight decomposition products, called high boilers, from the remaining coolant, which is recycled to the main primary coolant system. Fresh coolant is added as makeup for the high boilers removed. The high boilers are usually disposed of by burning after allowing any relatively short-lived radioactivity to decay. This makeup for high-boilers removal constitutes a significant cost factor for reactors cooled and moderated by organics;[38] estimates range from about 0.5 to nearly 1 mill/kw-hr(e). In organic-cooled heavy-water-moderated reactors, the organic makeup cost is lower since a smaller fraction of the reactor radiation is absorbed in the organic coolant.

Energy absorption from fast-neutron interactions has been found to cause more degradation of terphenyl coolants than does an equal amount of energy absorption from gamma interactions. The ratio of G values[39,40] for terphenyl disappearance, $G^n(-)/G^\gamma(-)$, has been found to be about 4 at 600°F. British data indicate that this ratio increases with increasing temperature.[40,41]

The magnitude of this fast-neutron effect and the temperature dependence of the degradation effects of both fast neutrons and gamma rays are of considerable importance in estimating the organic makeup costs for organic-cooled reactors under design and construction. The California Research Corporation is currently studying this fast-neutron effect under a wide variety of fast-neutron and gamma dose rates.

In addition to radiolysis, the thermal-degradation rates of organic materials generally increase with increasing temperature; with the polyphenyls the rates of thermal degradation do not become excessive until temperatures of about 460 to 490°C (860 to 914°F) are reached. At temperatures below about 400°C (752°F), the effects of thermal and radiation damage appear to be additive. The British, on the basis of limited data, have found a very rapid increase in the radiation-degradation factor, G (−coolant), with increasing temperature,[41] which begins just above 400°C and which appears to indicate a synergistic action of the radiolytic and thermal effects at the higher temperatures.

There is considerable interest in raising the maximum permissible coolant temperature in order to improve the thermal efficiency, as well as in reducing the cost of the organic required to make up for the degraded material. Atomics International, Phillips Petroleum Company, Monsanto Research Corporation, and California Research Corporation are examining a variety of organic fluids for thermal and radiation stability to determine their potential as low-cost alternatives to the polyphenyls. A number of petroleum-refinery and coal-tar fractions have been investigated. Although some of these materials are generally of lower unit cost than terphenyl coolants, none have been found which have sufficient stability to radiation and temperatures above about 650 to 700°F to indicate a lower makeup cost than terphenyls when used as a reactor coolant. The University of Utah has been carrying out theoretical studies of the thermal and radiation stability of various organic structures. These studies will aid in understanding the degradation processes that occur and will serve as a guide for the evaluation and selection of new coolant materials.

Since the cost of replacing the degraded polyphenyl coolant adds about 0.5 to 1 mill/kw-hr to the cost of electric energy generated from organic-moderated nuclear reactors, several groups are studying processes for recovering or regenerating the high-molecular-weight (or high boiler) degradation products for reuse as coolant. Monsanto Research Corporation has developed a process involving solvent extraction which removes the very high-molecular-

weight materials,[42] and studies of the use of high-vacuum distillation, hydrocracking, partial reduction, and redistribution are under way at Monsanto and Phillips Petroleum. Progress on organic-coolant reclamation has progressed to the point where pilot-plant operation appears to be the next logical step. Preliminary cost estimates have indicated that coolant can be reclaimed at a cost of $0.09 to $0.12/lb of reclaimed material, compared to a cost of $0.17/lb for fresh Santowax OMP. Recently research on a new reclamation process involving the use of corona discharge has been initiated by the General Electric Company under AEC sponsorship.

In organic-cooled heavy-water-moderated reactors, there is a relatively small fraction of organic material in the core. Much of the energy of neutron and gamma radiation is absorbed in the fuel and the moderator, with the result that the organic radiation degradation and makeup costs are less important than in organic-moderated reactors. Consequently thermal stability (for operation at high temperatures) and low melting point (for ease of operation) are more decisive factors in the selection of the hydrocarbon fluids for heavy-water-moderated reactors than for organic-moderated reactors. A terphenyl mixture (Santowax OM) with very little of the high-melting paraterphenyl isomer has been specified for the Canadian organic-cooled reactors, whereas a less expensive, but higher melting, mixture of all three terphenyl isomers (ortho, meta, and para) is generally specified for organic-moderated reactors (see Table IX-4).

The possibility of the use of additives, which would increase the radiation stability of the coolant, is also being studied by AI, Phillips Petroleum Company, and Monsanto Research Corporation. To date the work has not shown very much promise of reducing the cost of organic degradation. The polyphenyls themselves have high stability and are even used as liquid scintillators because of their ability to release absorbed energy as light.

The heat-transfer properties of the polyphenyls are poorer than those of water, principally because of the lower thermal conductivity and because of the increase of viscosity due to the high-molecular-weight degradation products. Extensive studies of the forced-convection heat transfer of the polyphenyls have indicated that their heat-transfer coefficients can be predicted using the conventional engineering correlations provided that the physical properties of the irradiated coolant are known.[19,43] In a program aimed at increasing the specific power of organic-cooled reactors, studies are under way at AI, Canadian General Electric, and Chalk River (AECL) on the behavior of organic coolants under conditions of local and bulk boiling, both out-of-pile and in-pile.[19] Additional reports on the heat-transfer properties of organic coolants are listed as Refs. 44 to 46.

The use of biphenyl as a reactor coolant in a direct-cycle reactor system has been proposed. The thermodynamic and physical properties of biphenyl are being studied by Monsanto Research Corporation[47] and the University of California to assist in the design and evaluation of this concept as well as for use in the correlation of heat-transfer and burnout data under boiling conditions.

One of the objectives of the OMRE was to determine if the thermal and radiolytic decomposition of the organic coolant resulted in the formation of any significant film on the heat-transfer surfaces which would seriously interfere with heat removal. Initial operation resulted in the formation of very thin films, which had a negligible effect on heat transfer. During the latter phases of core 1 operation, particulate matter was trapped by the aluminum cladding at the inlet ends of two experimental fuel elements of a finned type, and the deposits were serious enough to cause termination of the tests.[48–50] During the operation of the second core, serious fouling of some of the fuel elements occurred.[17,51]

The mechanism of fouling of fuel elements in organic-cooled reactors is not fully understood, and it is the subject of investigation by a large number of groups. It now appears that the film formation is related to the amount and type of particulate matter present in the coolant.[52,53] The OMRE films have been found to contain of the order of 25% inorganic matter (usually iron carbides or oxides). The coolant contains particulate matter that consists of an inorganic particle coated with organic polymeric material. Bench-scale pyrolytic testing of coolant from the OMRE has shown that the weight of film deposited during the test increases with increasing ash content of the coolant. Retesting of the batch of material showed decreases in both the ash and the amount of deposit formed

during the pyrolytic test. This indicates the removal of some of the film-forming constituents in the coolant. Reduction of the particulate content of the organic coolants has been found to be effective in reducing film formation. These findings suggest that it may be possible to control fouling in organic reactors by maintaining a low concentration of particulate matter in the coolant. At the present time, adsorption of coolant impurities by passage of the coolant through columns of Attapulgus clay appears to be an effective means for maintaining a low level of particulate matter in the coolant.[54] Equipment of this type has been installed[55] on the OMRE.

As with other reactor concepts, the development of materials and designs for fuel elements capable of operating at elevated temperatures for high burnups is required for the successful economic development of organic-cooled reactors. In the past, comparative economic evaluations of nuclear reactors have indicated that organic-cooled and -moderated reactors have capital costs as low as, or lower than, other reactor types, but low fuel burnup has produced fuel-cycle costs higher than those estimated for other enriched-reactor types. Fuel elements utilizing uranium-molybdenum alloys and uranium dioxide are being developed in the United States, whereas Canada and Euratom are looking primarily to uranium dioxide and more recently to uranium carbide as the fuel material. Because of the poor heat-transfer properties of the organic coolants, most reactor designs use extended-surface fuel elements and hence require a cladding of high thermal conductivity and low neutron absorption, with adequate strength at the highest temperatures at which the coolants themselves can operate. The cladding materials receiving most attention are, for the metallic fuels, aluminum bonded to the uranium alloy, and, for the ceramic fuels, materials made of aluminum–aluminum oxide powder mixtures by powder metallurgy methods.[56,57] In-pile tests of these materials and of beryllium and zirconium have been conducted.[54] The low burnups predicted for uranium–3.5% molybdenum fuel alloy and the relatively poor neutron economy of the uranium–10% molybdenum alloy appear to favor the use of UO_2, in spite of its low thermal conductivity, or the use of uranium carbide. References 58 and 59 are devoted to discussions of fuels for OMR reactors.

Comparative economic projections made under USAEC ground rules indicate that organic-cooled and -moderated reactors have the potential to compete favorably with fossil plants in the United States in the future, provided, mainly, that the fuel-cycle costs can be reduced by extending fuel life and that the prevention of fouling does not become an expensive item. The Canadians, who are enthusiastic about heavy-water-moderated reactors fueled with natural uranium as economic sources of power, have estimated that the use or organic cooling in such reactors, in place of heavy-water cooling, resulted in savings[9] of about 0.5 mill/kw-hr. Operation of the OMRE, Piqua, EOCR, WR-1, ESSOR, and PRO reactors will, in the next few years, provide additional much-needed information concerning the operation of organic-cooled reactors.

Recent Work

The subject of energy deposition in organic coolants was reviewed in the June 1962 issue of *Power Reactor Technology*, Vol. 5, No. 3, page 52, and continues to receive study. References 60 and 61 are recent additions to the literature on the subject.

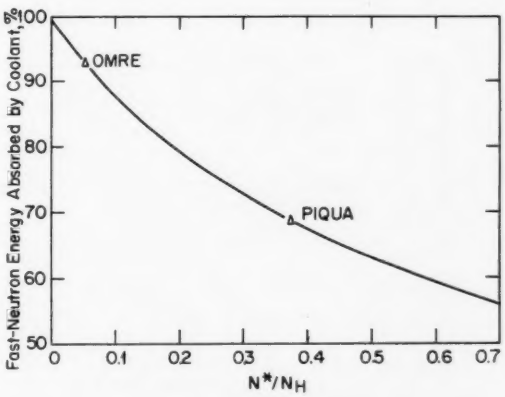

$$N^*/N_H = \frac{N_U + 0.26N_{Mo} + 0.203N_{Fe} + 0.140N_{Al} + 0.112N_O}{N_H}$$

Limits:

$N_C/N_H = 1.308$

$0 \leq N_U/N_H \leq 0.4$

$0 \leq N_{Mo}/N_H \leq 0.1$

$0 \leq N_{Al}/N_H \leq 2.0$

$0 \leq N_{Fe}/N_H \leq 0.4$

$0 \leq N_O/N_H \leq 0.6$

Fig. IX-1 Fast-neutron energy deposition in OMR coolants[60] (assuming no core leakage).

Reference 60 is an AI report dealing with analytical methods of calculating the energy absorption rates in OMR coolants as applied to the OMRE and the Piqua Nuclear Power Facility (PNPF). The author intended, however, to present the results in a general form that could be applied to energy absorption calculations for future OMR type reactors. Accordingly, the report is subdivided into parts. Each part treats separately the calculations of the energy absorbed from neutrons, gammas, and beta particles. A version of MUFT-4 was used to treat the slowing-down of neutrons by elastic and inelastic scattering, whereas a code called GRACE II was used to calculate gamma-energy absorption. The latter code handles spherical or cylindrical sources with varying distributions. These distributions represent the buildup factors by the use of double exponentials.

The results of the calculations are illustrated in Figs. IX-1 to IX-4. Pertinent data on the OMRE and PNPF cores are shown in Table IX-5. Table IX-6 illustrates the application of the data to neutron-energy deposition in the two reactors, and Table IX-7 summarizes the results and compares them with previous estimates. The calculations by Jones, which were reviewed in the June 1962 issue of *Power Reactor Technology*, Vol. 5, No. 3, are discussed briefly in Ref. 60, but, on the basis of the information available, the author is not able to identify the reason for the discrepancy (Table IX-7).

The benefit accruing to PNPF from the use of slightly enriched (rather than fully enriched) fuel is evident in Tables IX-6 and IX-7. The inelastic scattering in U^{238} accounts for a substantial reduction of the neutron energy in the PNPF, and the high gamma absorption by the uranium is also beneficial. The PNPF also

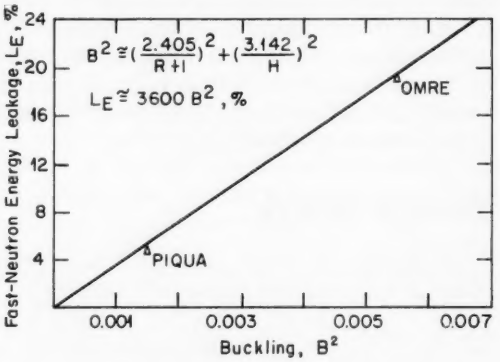

Fig. IX-2 Fast-neutron energy leakage versus buckling for organic-moderated reactors.[60]

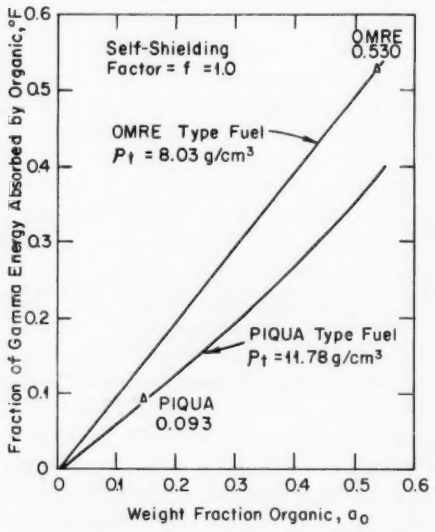

Fig. IX-3 Fraction of gamma energy absorbed by organic in OMR type cores.[60]

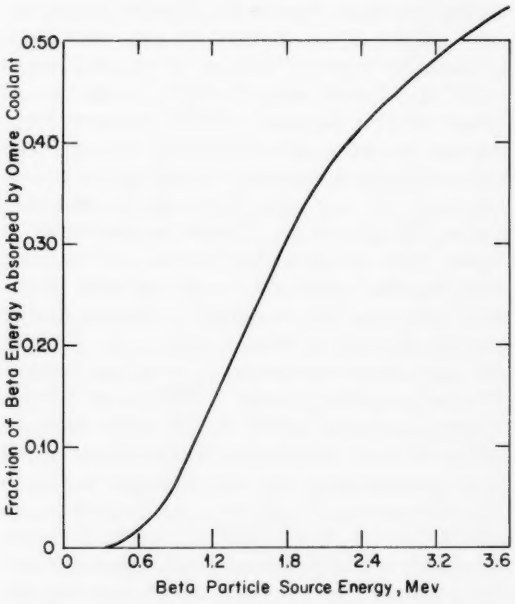

Fig. IX-4 Fractional energy absorption of beta energy in OMRE coolant.[60]

Table IX-5 DESCRIPTION OF OMRE AND PNPF CORES[60]

	OMRE	PNPF
Power level, Mw(t)	6.0	45.5
Core geometry:		
Radius, cm	35.9	74.0
Height, cm	9.0	137.0
Fuel:		
Type	Plate	Concentric cylinders
Material	25 wt.% UO_2 – 75 wt.% S.S.	U – 3.5 wt.% Mo
Thickness, mils	20	208
Cladding:		
Type	Flat	Finned
Material	Stainless steel	Aluminum
Thickness, mils	5	35
Core density, g/cm^3	1.54	4.24
Weight fractions:		
Coolant	0.539	0.149
Stainless steel	0.406	0.018
Aluminum		0.076
UO_2	0.055	
Uranium – Molybdenum		0.757
Atom density, atoms/cm^3($\times 10^{-24}$):		
Hydrogen	0.0299	0.0231
Carbon	0.0391	0.0302
Oxygen	0.00038	
Aluminum		0.00723
Iron	0.00673	0.00085
Molybdenum		0.000661
U^{235}	0.000177	0.000143
U^{238}	0.000013	0.00724

benefits from the lower energy leakage from the core (since most of the leakage energy is absorbed in the organic in the reflector); this improvement is due mainly to the larger core size.

Reference 61 is one of a series of Atomic Energy Research Establishment reports on the radiation and thermal stability of organic moderator-coolant materials. Previous decomposition data for pile radiation[64] were available only up to 27% high-boiler concentration. The latest experiments,[61] however, were extended to absorbed doses that were higher by about a factor of 3, and they provide information on the decomposition up to 55% high-boiler concentration. The difference between the American and British calculations for the power absorbed by the coolant is also noted in Ref. 61, but the earlier figure of 7.85% is referenced as the U. S. value for the total power absorbed by the coolant (Table IX-7) since Ref. 60 presumably was not available at the time. Figure IX-5 shows a comparison between neutron G values obtained from the calculations of Jones on OMRE data. The neutron G values were derived by assuming additivity of the effects of neutrons and gammas, and these values show the neutrons to be more damaging.

Reference 61 also considers the shape of the dose-decomposition curves, and it is concluded that the second-order law, $-dx/dt = kx^2$, where x is the fraction of the original material present, t is the dose, and k is a constant, gives the best fit. Analyses of the high-boiler residue indicated conversion to products with high molecular weights, and it is postulated[61] that these contain hydrogenated ring compounds.

At the 1962 annual meeting of the American Nuclear Society (ANS), results of irradiations of Santowax OMP in the Massachusetts Institute of Technology Reactor were reported.[39] As the irradiation progressed and the high-boiler concentration built up, samples were analyzed by

Table IX-6 FAST-NEUTRON ENERGY DEPOSITION IN THE OMRE AND PNPF REACTORS[60]

	Percentage of neutron energy assigned to process	
Process	OMRE	PNPF
Elastic scattering:		
Hydrogen	59.95	52.23
Oxygen	0.12	
Carbon	14.92	12.80
Iron	0.74	0.10
Aluminum		1.85
Molybdenum		0.10
U^{235}	0.01	0.01
U^{238}	0.00	0.42
Subtotal	75.74	67.51
Inelastic scattering:		
Iron	4.71	0.60
Aluminum		2.28
U^{235}	0.01	0.01
U^{238}	0.03	18.39
Subtotal	4.75	21.28
Resonance absorption and fast fission	0.01	5.61
Core leakage	19.50	5.60
Total	100.00	100.00
Percent absorbed by coolant	92.4 (4.56 Mev/fission)	69.5 (3.43 Mev/fission)

gas chromatography to determine the concentrations of the terphenyl isomers, and G values were determined for the individual isomers. The measurements indicated that the apparent differences in the degradation rates for the individual isomers were due, within the standard deviation of the experimental data, to the differences in the concentrations of the isomers present in the mixture. It was concluded that, under the conditions of the experiments so far investigated, no significant differences had been observed in the radiation stability of the individual terphenyl isomers in the coolant mixture and no significant effect of the degradation product buildup on the radiation stability of the isomers had been observed other than the dilution effect. These results are illustrated by Fig. IX-6.* The figure shows not only the normal G values for the isomers but also a quantity G', which is the ratio of the G value to the weight fraction of the isomer in the mixture. It can be seen that within the standard deviation G' is the same for all isomers, and it does not change as the concentration of degradation product decreases. These results appear to shed important light on the radiation-damage process.

Table IX-7 PERCENT OF TOTAL POWER ABSORBED BY COOLANT*[60]

	Keshishian,[62] OMRE	Jones,[63] OMRE	Duncan[60] OMRE	Duncan[60] PNPF
Gamma energy:				
Inside core	5.69	2.60	3.77	0.98
Outside core		1.25	2.27	0.24
Neutron energy:				
Inside core	1.41	1.95	1.85	1.61
Outside core	0.75	0.28	0.43	0.11
Beta energy		0.50	0.72	Negligible
Total	7.85	6.58	9.04	2.94

*The total energy produced per fission was assumed to be 200 Mev.

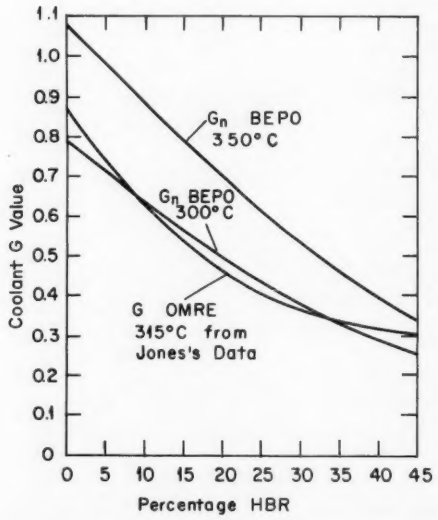

Fig. IX-5 Derived fast-neutron G values.[61]

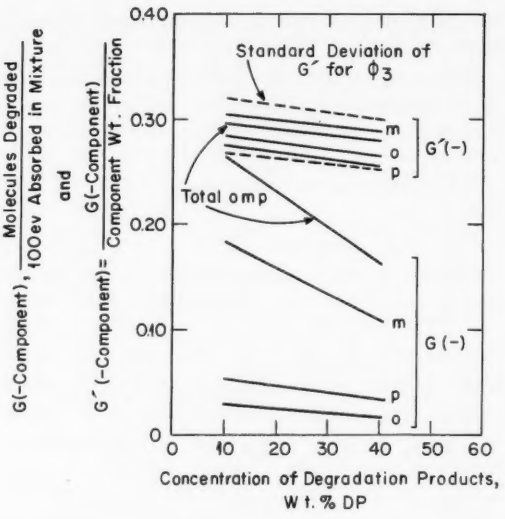

Fig. IX-6 Results of Santowax OMP irradiation in MITR.[39] The letters o, m, and p designate the ortho, meta, and para isomers of terphenyl.

Recent estimates of organic-coolant makeup rates by Atomics International for several organic-moderated concepts were also reported at the meeting.[40] The estimates were based on OMRE measurements, in-pile capsule irradiations, electron irradiations, and alpha-particle irradiations. The results for the Piqua reactor, for a prototype organic-moderated power reactor, and for two organic-moderated power reactors of larger sizes are given in Table IX-8. Both the decomposition rates and the

*Figure IX-6 (Ref. 39) and Table IX-8 (Ref. 40) are reprinted here by permission from the American Nuclear Society.

Table IX-8 OMR COOLANT MAKEUP RATE AND COSTS[40]

Reactor	POPR, 51.3 Mw(e)		PNPF, 11.4 Mw(e)		OMR 150 Mw(e)		OMR 300 Mw(e)	
Average in-core temp., °F	672		547		597		653	
Decomposition rate, lb/hr at full power	A* 250	B† 171	A* 40.9	B† 49.7	A* 520	B† 517	A* 1265	B† 1024
Coolant makeup cost, mills/kw(e)-hr	0.83	0.56	0.61	0.74	0.56	0.56	0.69	0.56

*A: Using G_n values derived from in-pile irradiations.
†B: Using G_n values derived from alpha-particle irradiations.

coolant makeup costs (in mills per kilowatt hour) are given.

Another interesting report[19] at the ANS meeting covered Canadian tests on materials for core components of organic-cooled D_2O-moderated reactors. On the basis of short tests, rather encouraging results were reported for Zircaloy. Recent irradiation tests of Zircaloy in contact with organic coolants in the Canadian National Research Experimental Reactor showed almost no hydrogen pickup after 24 days at 250°C. Aluminum-coated Zircaloy samples showed comparable results after 43 days of irradiation at temperatures up to 370°C. The possibilities of zirconium alloys are being evaluated both for pressure tubes and for fuel jackets.

References

1. K. Maddocks (Comp.), Organic Liquids as Reactor Coolants. Review of Technological Information Available July 1959, British Report AERE-R-3633, April 1961.
2. R. H. J. Gercke, Status of Organic Coolant Technology, in Proceedings of the Organic Cooled Reactor Forum, October 6–7, 1960, USAEC Report NAA-SR-5688, pp. 5–43, Atomics International, December 1960.
3. Argonne National Laboratory, Organic Nuclear Reactors: An Evaluation of Current Development Programs, USAEC Report ANL-6360, May 1961.
4. R. H. J. Gercke and G. Asanovich, Thermo-Physical Properties of Irradiated Polyphenyl Coolants, USAEC Report NAA-SR-4484, Atomics International, Dec. 1, 1960.
5. Atomics International, Final Safeguards Summary Report for the Piqua Nuclear Power Facility, USAEC Report NAA-SR-5608, Aug. 1, 1961.
6. E. F. Weisner, The Piqua Nuclear Power Facility, in Proceedings of the Organic Cooled Reactor Forum, October 6–7, 1960, USAEC Report NAA-SR-5688, pp. 211–224, Atomics International, December 1960.
7. W. N. Bley and R. W. Burkhardt, Piqua OMR Purification System Development, USAEC Report NAA-SR-5073, Atomics International, Nov. 1, 1960.
8. R. R. Stiens, Piqua OMR High Boiler Handling, USAEC Report NAA-SR-4791, Atomics International, Aug. 30, 1960.
9. G. W. Corporales and P. R. Benson, Operation of the Piqua OMR Degasification System Prototype, USAEC Report NAA-SR-4894, Aug. 30, 1960.
10. H. M. Gilroy and J. H. Wilson, Piqua OMR Waste Gas Disposal, USAEC Report NAA-SR-4576, Atomics International, July 15, 1960.
11. E. B. Baumeister and J. D. Wilde, Selection of the Piqua OMR Fuel Element, USAEC Report NAA-SR-4239, Atomics International, Mar. 15, 1960.
12. M. H. Binstock, Fuel Element Development for Piqua OMR, USAEC Report NAA-SR-5119, Atomics International, June 30, 1960.
13. R. R. Stiens, Disposal of OMR High Boilers by Combustion, USAEC Report NAA-SR-5410, Atomics International, Nov. 15, 1961.
14. W. E. Nyer and J. H. Rainwater, Experimental Organic Cooled Reactor Conceptual Design, USAEC Report IDO-16570, Phillips Petroleum Co., Dec. 1, 1959.
15. M. R. Dusbabek, Experimental Organic Cooled Reactor, in Proceedings of the Organic Cooled Reactor Forum, October 6–7, 1960, USAEC Report NAA-SR-5688, pp. 189–210, Atomics International, December 1960.
16. Fluor Corporation, Ltd., November 1960. (Unpublished)
17. Evaluation of the Organic Fouling Problem in the OMRE, USAEC Report TID-6882, Mar. 24, 1961.
18. A. Pedretti and D. DiMenza, Progress on the Italian Organic Reactor Program, *Trans Am. Nucl. Soc.*, 5(1): 106 (June 1962).
19. W. M. Campbell, Canada's Organic Cooled Reactor Program, *Trans. Am. Nucl. Soc.*, 5(1): 104 (June 1962).

20. J. C. Leny, ORGEL: A European Power Reactor Design, *Trans. Am. Nucl. Soc.*, 5(1): 103 (June 1962).
21. G. A. Pon and D. B. Primeau, Economic Analysis of Organic-Cooled Heavy-Water Moderated Natural-Uranium Reactors, *Trans. Am. Nucl. Soc.*, 5(1): 105 (June 1962).
22. J. C. Leny, ESSOR: Specific Test Reactor for the ORGEL Program, *Trans. Am. Nucl. Soc.*, 5(1): 103 (June 1962).
23. J. R. Dickinson and R. F. Scarth, OCDR Power Plant Study, in Proceedings of the Organic Cooled Reactor Forum, October 6–7, 1960, USAEC Report NAA-SR-5688, pp. 275–306, Atomics International, December 1960.
24. W. M. Campbell, Canada's Research and Development Program for an Organic Liquid Cooled Nuclear Reactor, in Proceedings of the Organic Cooled Reactor Forum, October 6–7, 1960, USAEC Report NAA-SR-5688, pp. 171–187, Atomics International, December 1960.
25. H. N. Royden, Current Status of OMR Experimental Physics, in Proceedings of the Organic Cooled Reactor Forum, October 6–7, 1960, USAEC Report NAA-SR-5688, pp. 125–141, Atomics International, December 1960.
26. R. O. Williams, Jr. and R. F. Wilson, A Summary of Nuclear Calculations for the Organic Moderated Reactor Experiment (OMRE), USAEC Report NAA-SR-4066, Atomics International, May 15, 1960.
27. T. J. Connolly, Plutonium-Enriched OMR Cores, USAEC Report NAA-SR-4812, Atomics International, May 1, 1960.
28. Bechtel Corp. and Atomics International, Organic Cooled Power Reactor Study, 75 Mw Power Plant Conceptual Design, USAEC Report TID-8501, pt.4, July 1959.
29. B. L. Hoffman, Design and Analysis of a Uranium–3.5% Molybdenum Alloy OMRE Core, USAEC Report NAA-SR-5174, Atomics International, Jan. 30, 1961.
30. R. W. Campbell and C. H. Skeen, Exponential Experiments with Heavy-Water, Graphite-and-Diphenyl Moderated, Uranium Metal Lattices, USAEC Report NAA-SR-6446, Atomics International, Sept. 15, 1961.
31. R. A. Blaine and J. L. Watts, Calculated Nuclear Properties of Low-Enrichment Metal-Plate Lattices in the OMR Critical Assembly, USAEC Report NAA-SR-6330, Atomics International, Aug. 15, 1961.
32. R. R. Hood and L. Isakoff (Comps.), Heavy Water Moderated Power Reactors. Progress Report, June 1962, USAEC Report DP-755, E. I. du Pont de Nemours & Co., July 1962.
33. H. Alter, J. Dudek, and G. Joanou, Monte Carlo Calculation of the Slowing Down Moments in Hydrocarbons, USAEC Report NAA-SR-Memo-5655, Atomics International, Dec. 12, 1960.
34. W. W. Brown, Neutron Age and Diffusion Length Measurements in Diphenyl, *Proceedings of the Second United Nations International Conference on the Peaceful Uses of Atomic Energy, Geneva, 1958*, Vol. 16, p. 403, United Nations, New York, 1958.
35. N. C. Francis, M. L. Storm, and P. F. Zweifel, Neutron Age in Diphenyl, *Nucl. Sci. Eng.*, 2(6): 745 (1957).
36. B. G. Dubovskii and M. N. Lantsov, Organic Compounds as Moderators in Nuclear Reactors, *J. Nucl. Energy: Pt. A: Reactor Sci.*, 12(3): 122 (June 1960).
37. H. Goldstein, J. G. Sullivan, Jr., R. R. Coveyou, W. E. Kinney, and R. R. Bate, Calculations of Neutron Age in H_2O and Other Materials, USAEC Report ORNL-2639, Oak Ridge National Laboratory, July 12, 1961.
38. R. H. J. Gercke and J. F. Zack, Jr., Coolant Decomposition Rates and Make-up Costs for Organic Reactors, USAEC Report NAA-SR-6920, Atomics International.
39. E. A. Mason, D. T. Morgan, W. N. Bley, T. W. Carroll, J. P. Casey, E. Sefchovich, and A. Turricchia, In-pile Irradiation of Santowax OMP, *Trans. Am. Nucl. Soc.*, 5(1): 106 (June 1962).
40. R. H. J. Gercke and J. F. Zack, Jr., Coolant Decomposition Rates and Make-up Costs for Organic Reactors, *Trans. Am. Nucl. Soc.*, 5(1): 108 (June 1962).
41. W. G. Burns, W. Wild, and T. F. Williams, The Effect of Fast Electrons and Fast Neutrons on Polyphenyls at High Temperatures, in *Proceedings of the Second United Nations International Conference on the Peaceful Uses of Atomic Energy, Geneva, 1958*, Vol. 29, p. 266, United Nations, New York, 1958.
42. R. J. Wineman, D. A. Scola, and J. S. Adams, Reclamation of Organic Nuclear Reactor Coolant, *Trans. Am. Nucl. Soc.*, 5(1): 112 (June 1962).
43. E. A. Mason, D. T. Morgan, W. N. Bley, T. J. Swierzawski, and J. P. Casey, Heat Transfer Characteristics of Irradiated Santowax OMP, *Trans. Am. Nucl. Soc.*, 5(1): 107 (June 1962).
44. W. R. Martini, Status of Heat Transfer Development for Organic Reactors, in Proceedings of the Organic Cooled Reactor Forum, October 6–7, 1960, USAEC Report NAA-SR-5688, pp. 45–67, Atomics International, December 1960.
45. C. Grove-Palmer and H. Pass, Heat-Transfer Properties of Santowax R, *Nucl. Power*, 4(44): 118–121 (December 1959).
46. T. C. Core and K. Sato, Determination of Burnout Limits of Polyphenyl Coolants. Summary Report, USAEC Report IDO-28007, Aerojet-General Corp., Feb. 14, 1958.
47. J. A. Ellard and M. V. Milnes, Physical and Thermodynamic Properties of Biphenyl, *Trans. Am. Nucl. Soc.*, 5(1): 112 (June 1962).

48. A. A. Jarrett, SRE Fuel Element Damage. Interim Report, USAEC Report NAA-SR-4488, Atomics International, Nov. 30, 1959.

49. R. L. Ashley, R. J. Beeley, F. L. Fillmore, W. J. Hallett, B. R. Hayward, Jr., and A. A. Jarrett, SRE Fuel Element Damage. Final Report, USAEC Report NAA-SR-4488(Suppl.), Atomics International, June 30, 1961.

50. J. H. Walter, E. E. Garrett, and J. M. Davis, Evaluation of Irradiated Experimental OMR Fuel Elements, USAEC Report NAA-SR-4670, Atomics International, Apr. 1, 1960.

51. R. O. Williams, Jr., OMRE Operating Experience, in Proceedings of the Organic Cooled Reactor Forum, October 6–7, 1960, USAEC Report NAA-SR-5688, pp. 143–170, Atomics International, December 1960.

52. A. M. Aikin and D. H. Charlesworth, Fouling of Heat Transfer Surfaces by Organic Coolants, *Trans. Am. Nucl. Soc.*, 5(1): 110 (June 1962).

53. R. A. Mengelkamp, P. S. Hudson, and J. C. Hillyer, An Out-of-Pile Electron Irradiation Circulating Loop for Fouling Studies, *Trans. Am. Nucl. Soc.*, 5(1): 111 (June 1962).

54. R. F. S. Robertson, H. E. Thexton, and D. E. Lew, An Irradiation of Highly Rated, SAP-Clad UO_2 Fuel Specimens in Organic Coolant, *Trans. Am. Nucl. Soc.*, 5(1): 110 (June 1962).

55. H. Cataldo, Design and Construction of the OMRE Particulate Removal Loop, USAEC Report NAA-SR-6646, Atomics International, Dec. 30, 1961.

56. S. O. Arneson, Development of APM-Clad UO_2 Fuel Elements, *Trans. Am. Nucl. Soc.*, 5(1): 113 (June 1962).

57. C. Moranville, Development of Fuel and Cladding Materials for the ORGEN Project, *Trans. Am. Nucl. Soc.*, 5(1): 114 (June 1962).

58. H. Pearlman, Status of OMR Fuel Element Development at Atomics International, in Proceedings of the Organic Cooled Reactor Forum, October 6–7, 1960, USAEC Report NAA-SR-5688, pp. 89–124, Atomics International, December 1960.

59. J. Kroehler, Jr., Dispersion Fuels for Advanced Organic Moderated Reactor, USAEC Report NAA-SR-5018, Atomics International, June 30, 1960.

60. D. Duncan, Energy Absorption Rates in OMR Coolants, USAEC Report NAA-SR-6893, Atomics International, Mar. 15, 1962.

61. T. H. Bates, W. G. Burns, M. East, B. Morris, C. R. Reed, P. Stanaway, R. W. Wilkinson, and J. A. Winter, The Radiation and Thermal Stability of Some Potential Organic Moderator Coolants, Part V. Pile and Electron Irradiation of Biphenyl, Orthoterphenyl, Metaterphenyl, and Pile Irradiation of Santowax R to High HBR Content, British Report AERE-R-3743, March 1962.

62. V. Keshishian, Organic Energy Absorption in OMRE and in Metal and UO_2 Fueled OMR, USAEC Report NAA-SR-Memo-2484, Atomics International, May 1, 1958.

63. J. D. Jones, Energy Deposition and Radiation Damage in Organic Cooled Reactors, British Report AEEW-R-52, September 1960.

64. T. H. Bates, W. G. Burns, B. Morris, R. W. Wilkinson, and T. F. Williams, The Radiation and Thermal Stability of Some Potenital Organic Moderator Coolants, Part II, Pile Irradiation of Para-Terphenyl and Santowax-R, British Report AERE-C/R-2185, July 1959.

Section

X

Power Reactor Technology

Gas-Cooled Reactors

The Dragon Reactor

The High-Temperature Gas-Cooled Reactor (HTGCR) or Dragon Reactor Experiment[1–6] as it is more commonly called is now well along in construction at the United Kingdom Atomic Energy Authority's installation at Winfrith, Dorset, England. The reactor pressure vessel was lifted into the reactor building on Mar. 1, 1962, and the plant is expected to go into operation late in 1963. Most of the basic features of the reactor design have not changed substantially from those reported earlier,[2–6] but the recent annual report on the project[1] describes the progress made in proving out these features, describes the status of the design and construction of the plant, and gives details in some of the more important areas.

The Dragon Reactor Experiment and its associated extensive research and development program are a joint undertaking of the European Nuclear Energy Agency (ENEA) of the Organization for Economic Cooperation and Development (OECD), which superseded the Organization for European Economic Cooperation (OEEC). The international character of the effort is demonstrated by the research and development work that is being performed for this project at various installations throughout the member nations and by the 40 to 50 members of the Dragon project staff at Winfrith who are not United Kingdom personnel but who are on loan from member countries.

The Dragon Reactor Experiment is a 20-Mw high-temperature gas-cooled reactor. The core is composed of fuel-moderator elements in which graphite is used as the moderator, the structural material, the fuel diluent, and the fuel jacket. The fuel is a mixture of enriched uranium and thorium with graphite. The coolant gas is helium, and a bleed flow of helium gas is arranged to purge fission products from each fuel element. The nominal pressure of the helium coolant gas is 20 atm. The gas enters the reactor at 350°C and leaves at 750°C.

Dragon is the same type as the Peach Bottom reactor (HTGR) which is under construction in the United States and which was discussed in the June 1962 issue of *Power Reactor Technology*, Vol. 5, No. 3, pages 61 to 65. Special provisions have been made for the interchange of information and collaboration between these two projects. Table X-1 shows that the two plants have many similarities. The Dragon reactor is regarded as an experiment, and its power will be dumped to the atmosphere, whereas the considerably larger Peach Bottom reactor is part of a prototype electric-power-generating plant.

The general layout of the Dragon-reactor plant is shown in Fig. X-1.* One of the more unusual features of this plant, the double containment, is shown in this figure. An inner steel shell encloses the reactor and essentially all equipment that is, or may become, radioactive during normal operation. It was originally planned to fill this inner containment volume with nitrogen gas, primarily to preclude the possibility of generating explosive gas mixtures by the reaction of air and water with the hot carbon in the reactor core in the event of a rupture in the primary coolant loop. It was recently decided that the care which is being taken to ensure the integrity of the primary circuit will make it reasonable to fill this space with air instead of nitrogen, although the design allows for the use of either gas. Air will make the manual operations that are occasionally required within the containment volume, such as

*Figure X-1 is reprinted here by permission from *Nuclear Engineering*.[2]

those involved with refueling, much easier to perform.

The inner steel shell is surrounded by an outer containment building of sealed concrete. This building contains most of the normally nonradioactive components of the plant, some of which are control equipment. Operating personnel may enter this outer containment building during normal plant operation. The main control room and other auxiliary equipment and services are located in several conventional buildings around the containment structure.

Heat is removed from the reactor by six parallel primary coolant loops. Each coolant loop contains a primary heat exchanger and a gas circulator. The circulator is flanged directly to the heat exchanger, and the exchanger is close-connected to the reactor vessel by coaxial piping (Fig. X-1). In a typical loop the helium coolant gas flows from the circulator to the reactor vessel through the outer annulus of the coaxial piping, and it enters the reactor vessel at 350°C (662°F). It is baffled to flow first along the wall of the pressure vessel, and it then passes upward through the reactor core, where it is heated to a mixed-mean outlet temperature of 750°C (1382°F). From the reactor vessel it flows through the center pipe of the coaxial loop piping into the shell side of the heat exchanger. Water, under forced circulation, is boiled in the tubes of the primary exchanger. Six secondary heat exchangers are provided where the heat from the intermediate water circuit is transferred to a single tertiary pressurized water loop. This loop penetrates both containment vessels and carries the heat to a finned-tube forced-draft air-cooler bank where it is finally dumped to the atmosphere. An emergency tertiary loop is also provided. Reactor shutdown heat can be dissipated by natural circulation in the primary, secondary, and emergency tertiary loops in case of power failure.

Table X-1 COMPARISON OF DRAGON REACTOR EXPERIMENT WITH PEACH BOTTOM HTGR PLANT

Plant characteristic	Dragon	Peach Bottom
Reactor thermal power, Mw	20	115
Net electric power, Mw	None	40
Coolant gas	Helium	Helium
Pressure, psia	300	350
Inlet temp., °F	662 (350°C)	660
Outlet temp., °F	1382 (750°C)	1380
Fuel	Uranium-thorium	Uranium-thorium
Atom ratio	1:7	1:8 to 1:10
Maximum temp., °F	3100	3150
Fuel cladding	Graphite	Graphite
Moderator	Graphite	Graphite
Construction started	April 1960	February 1962
Estimated criticality date	Late 1963	1964 (at earliest)

The characteristic and essential feature of the Dragon Reactor Experiment is its fuel element, which might more properly be called a fuel-moderator element. The fuel-element assemblies consist of clusters of seven hexagonal graphite tubes. These tubes are loaded with graphite fuel boxes that contain annular fuel inserts and supporting graphite spines. The fuel inserts are prepared from a homogeneous mixture of enriched uranium, thorium, and graphite powders. The details of the fuel-element assembly are still being developed,[1,7] but Fig. X-2 shows one of the latest designs. This figure shows that metal components are located only at the ends of the fuel element. When the 37 elements are assembled, as shown in Figs. X-3 and X-4, an all-ceramic core approximately 3 ft 6 in. in diameter by 5 ft 3 in. high is formed. The only moderator in the core is the graphite in the fuel elements. The helium-coolant-gas flow is up through the fuel-element assemblies, over the surfaces of the graphite cladding tubes, and within the Y-shaped passages formed by the spacer ridges on the graphite tubes.

It is currently planned to use a two-zone core in the reactor. The 37 fuel-element assemblies will be divided between a central zone,

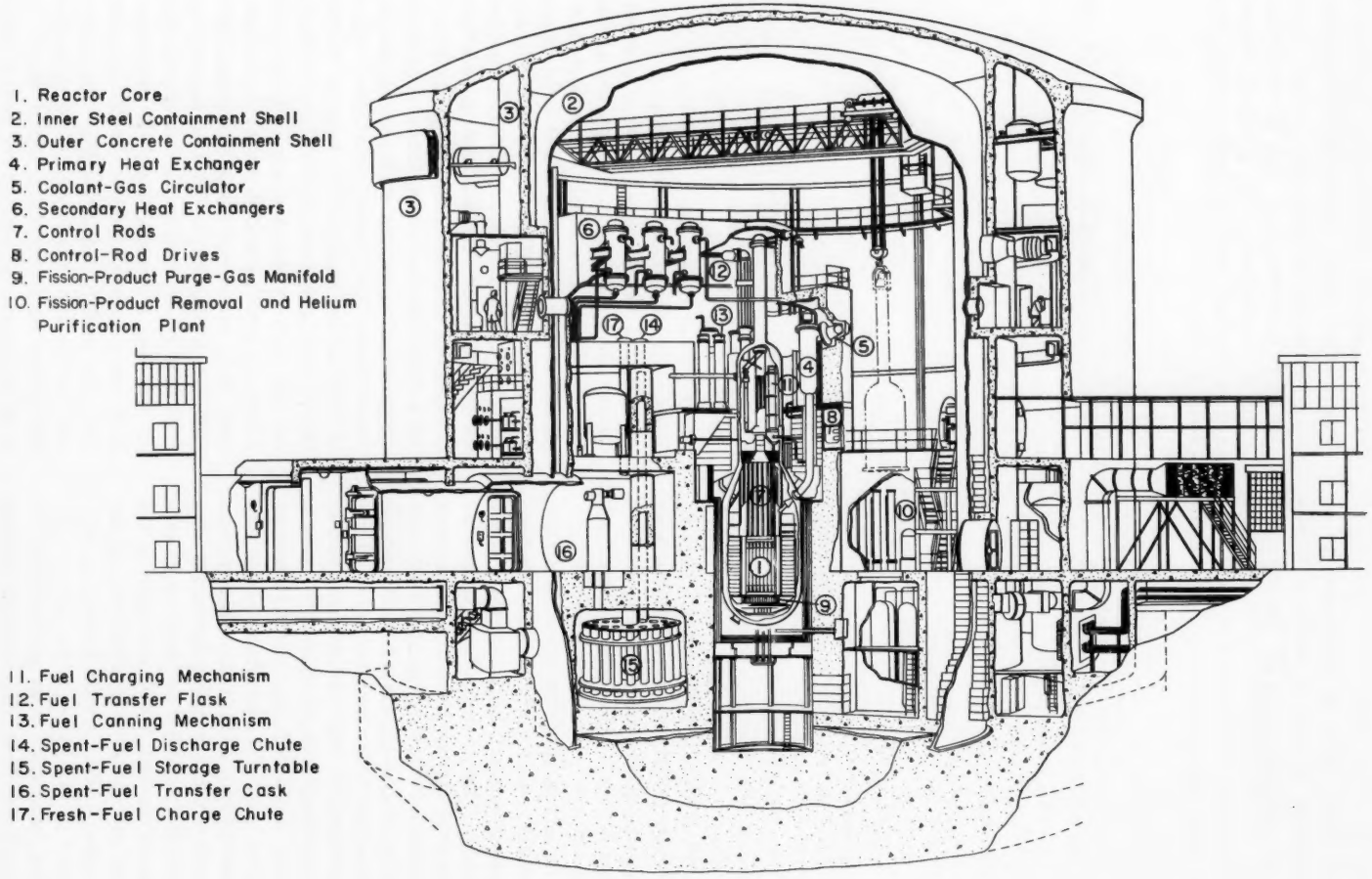

Fig. X-1 General arrangement of Dragon-reactor plant.[2]

which will undergo a higher burnup, and an outer zone, which will be changed more often. The outer zone will serve partly as a driver region for the central elements.

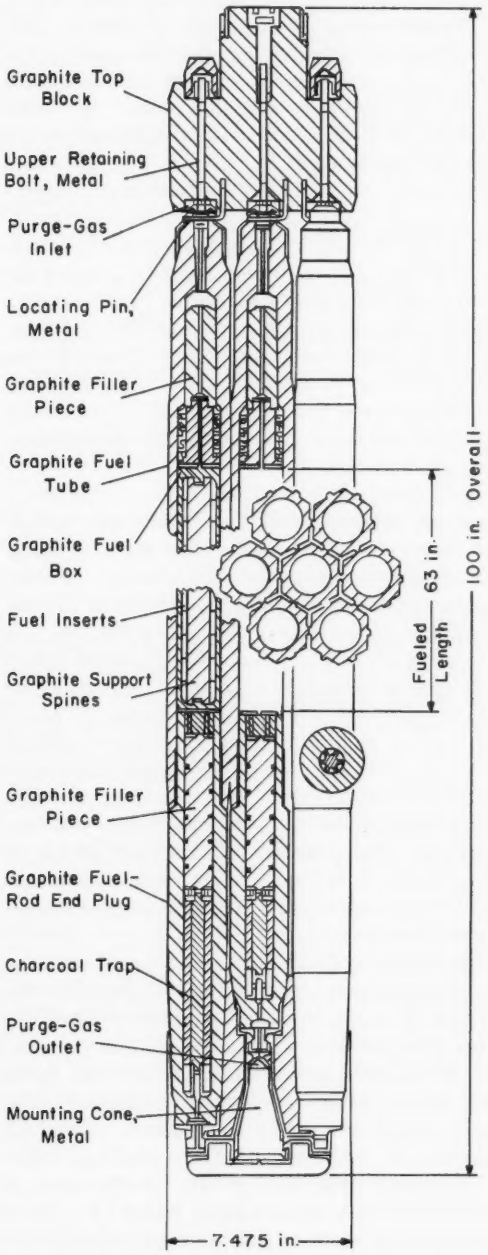

Fig. X-2 Dragon-reactor fuel element. (Adapted from Ref. 3 and modified by data from Ref. 1.)

The Dragon research and development program has developed two types of fuel inserts: (1) fission-product releasing and (2) fission-product retaining. Fission-product-retaining inserts are obtained by applying a pyrolytic carbon-graphite coating on the spherical particles of uranium and thorium dicarbides before they are compacted into the annular inserts. The fission-product-releasing fuel inserts require that the graphite fuel boxes be sealed and that their permeability be sufficiently low to delay the escape of fission products. No firm decision has yet been made as to which type of fuel will be used for the first fuel load.

Reactor control is provided by 24 absorber elements consisting of coaxial stainless-steel tubes packed with boron carbide. These are located vertically around the circumference of the core, moving in holes in the graphite reflector, as shown in Fig. X-4. The control-rod electric-motor drives are located radially around the reactor, as shown in Fig. X-1. These motors drive radial shafts that raise and lower the rods by cables. The motors and mechanisms are all within the helium-coolant-gas atmosphere, but at reduced temperatures, thereby eliminating the need for shaft seals.

A small amount of helium coolant gas enters the top of each fuel rod through the orifice screw (shown in Fig. X-2). This fission-product purge gas flows down through the inside of the fuel rods and over the graphite fuel boxes containing the fuel inserts. Before leaving the fuel rod the purge flow passes through an activated-charcoal trap located at the bottom, lower-temperature end of each fuel rod, as shown in Fig. X-2. This charcoal trap will delay some of the fission products and thus permit further decay before they are carried out of the fuel rods by the purge stream. The purge flow exits from the fuel rods through the fuel-element mounting spikes (shown in Fig. X-3). Each of these mounting-spike assemblies incorporates an instrumented orifice that restricts helium purge flow to a satisfactorily low amount and detects any variation from normal purge flow. Each spike assembly also contains a cyclone separator that will separate particles from the purge flow to prevent blockage of the restricting orifice. These spike assemblies can be changed by the fuel-changing machine when necessary. From the spike assemblies the purge flow is manifolded and passed to a precooler in the bottom of the reactor vessel, where a consid-

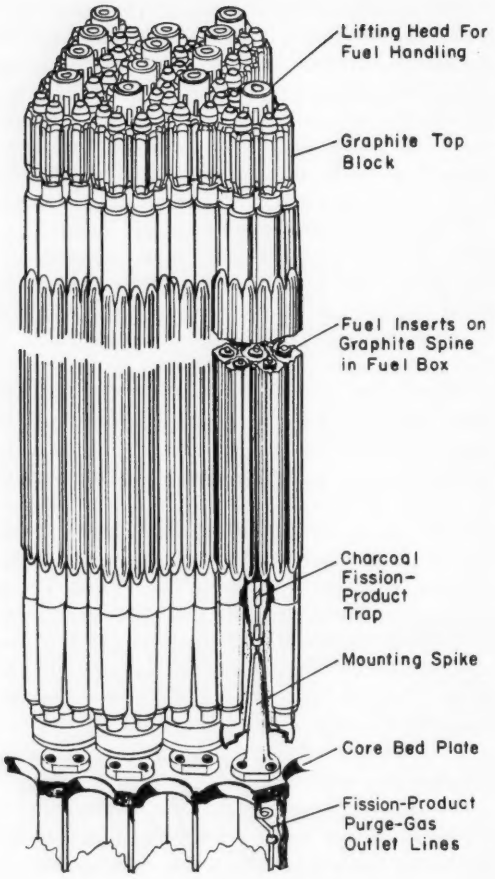

Fig. X-3 Assembly of fuel elements to form the Dragon-reactor core. (Adapted from Ref. 4).

erable fraction of the fission products will condense out. The flow then passes to the main fission-product-delay beds. These are water-cooled charcoal-filled traps that will delay the remaining fission products long enough for a large fraction of their activity and heat generation to decay. The purge-gas flow coming out of these main fission-product-delay beds is then passed to a helium-purification system. Here the impurities are separated from the helium purge gas before it is returned to the primary coolant system. The separated gaseous impurities are ultimately disposed of by being passed up the plant stack with diluting air.

The problem of handling fission products, which involves the design and performance of the fuel elements as well as the coolant-purification system, is the central one in reactors of the Dragon type. Some aspects of the purification system were discussed briefly in a previous issue of *Power Reactor Technology*, Vol. 5, No. 4, and the purification system and related helium systems are described in Ref. 1. A British report[7] released in November 1961 describes the exploration of techniques for the fabrication of the fuel elements and the testing of fuel-element components made by those techniques. It also describes the procedure for fuel-element assembly. Another report[8] is a review of the existing information on the transport and diffusion of fission products in graphite, directed toward those processes which may be important in the Dragon reactor. The subject is complex and has many areas of quantitative uncertainty. It seems probable that reactor-operating experience will make possible the first reliable assessment of the problem of fission-product management and will present the most favorable opportunity for improvement of the technology.

Fuel handling in the Dragon Reactor Experiment is accomplished only after the reactor has been shut down and cooled off. The fuel-grappling machinery is permanently located within the upper, bell-shaped portion of the reactor pressure vessel, shown in Fig. X-1. A fuel element is discharged by (1) lifting it into this charge-machine chamber, (2) passing it into the gas lock of the transfer flask, (3) passing it into a canning cell where it is enclosed in a sealed container, and (4) lowering it down the discharge chute into the spent-fuel storage turntable. All these operations are performed remotely from the charge-machine control room in the outer, concrete containment building with the assistance of television and optical viewing systems.

There are a number of engineering and mechanical problems associated with plants of the Dragon type. In terms of component development, the problem of the coolant-gas circulators is probably one of the more critical. However low, the fission-product contamination in the primary coolant circuit demands that a high standard of leaktightness be maintained. This requirement resulted in the specification of gas-bearing gas circulators. There is practically no operating experience with this type of equipment in the required size range. The development and fabrication of gas-bearing circulators for the primary coolant loop and of

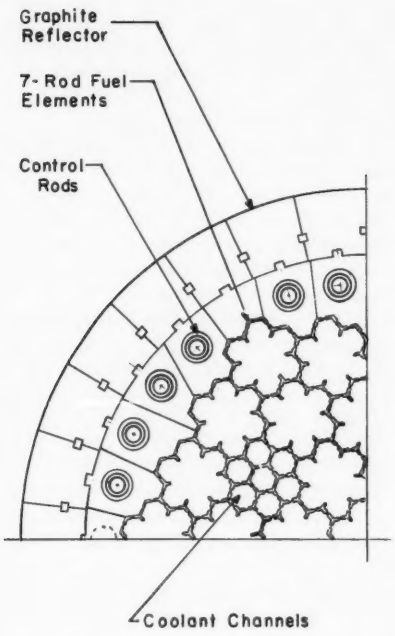

Fig. X-4 Cross section of the Dragon-reactor core. (Adapted from Ref. 2.)

smaller gas-bearing circulators used in the fission-product purge-gas system was subcontracted to Société Rateau, France. Work is reported to be proceeding satisfactorily on the testing of a full-scale prototype circulator unit in helium under operating conditions.

The declared purpose of the Dragon project is to investigate and resolve the problems that are involved in the development of high-temperature gas-cooled reactors for power or propulsion purposes. Significant steps toward achieving this objective are: (1) the process of designing and building the 20-Mw reactor experiment and (2) the research and development work that is being performed in order to arrive at the design. The overall program may be expected to go on to include operational experiments on components and materials. The original international agreement that set up the Dragon project was signed on Mar. 23, 1959, and provided for a five-year period. The various aspects of an extension to this agreement are already under active investigation. Preliminary studies of large power reactors [1000 Mw(t)] of the HTGCR type are already being performed under the project, and it has been reported[9] that the Dragon project will be extended to include designing a large power reactor.

Gas-Circulating Machinery

Reference 10 presents the findings of a survey, made by the Franklin Institute and completed in June 1961, on the requirements and availability of bearings and seals for use in primary loop components of gas-cooled nuclear-reactor power plants. The conclusion that resulted from this survey was that there were few, if any, off-the-shelf components to satisfy the specifications of reactor systems then under development and that there were none to satisfy the more extreme conditions of the proposed future generation of advanced gas-cooled-reactor plants. The survey was therefore restricted to the discussion of seal and bearing designs that were, at the time, unproved for the service intended. The equipment used in the Calder Hall gas-cooled-reactor plants and in the French G2 and G3 plants is not mentioned in the survey.

On Apr. 2, 3, and 4, 1962, a meeting was held at Oak Ridge National Laboratory (ORNL) to discuss progress in the development of rotating machinery for gas-cooled reactors. The meeting was cosponsored by the U. S. Atomic Energy Commission and ORNL. This was the second meeting of its kind, and it appears that such meetings may become regular events. The proceedings of the first meeting[11] were reviewed in the December 1961 issue of *Power Reactor Technology*, Vol. 5, No. 1, pages 82 and 83.

Reference 12 contains the complete proceedings of the second meeting. The equipment covered in the papers presented by the participants again included main blowers, shaft seals, gas turbines, gas-bearing compressors, and other types of special compressors for reactor and other applications. The meeting included French representatives from the Société Rateau, but no contributors reported on actual operating experience of rotating machinery in the French or British gas-cooled-reactor applications. The Société Rateau is developing and fabricating the gas-bearing circulators for the OECD Dragon reactor project, as discussed above.

An examination of the papers presented at the meeting shows that valuable data and experience are being accumulated in the United

States on rotating equipment, bearings, and seals intended for reactor-plant applications, but only while these components are operating on test stands and in experimental loops. Thus it appears that equipment to meet the design requirements for the intended applications is being developed. It will, however, still be some time before any amount of operating experience is accumulated in the United States in an actual reactor-plant application.

The first-to-be-completed U. S. gas-cooled-reactor plant that will include rotating equipment as a primary component is likely to be the ML-1 (Mobile Low-Power Plant No. 1), which is being developed by Aerojet-General Corporation for the U. S. Army. (This reactor was reviewed in the September 1959 issue of *Power Reactor Technology*, Vol. 2, No. 4, pages 79 to 82.) This is a nitrogen-cooled light-water-moderated reactor plant that uses a closed-cycle gas-turbine system to generate 330 to 500 kw(e). Initial full-power operation of this plant was scheduled for late 1962. This startup date has resulted[13] from a delay of about a year primarily because of problems with the gas turbine-compressor set. Apparently more than another year is required for the completion of construction and the start of operating-experience accumulation at any of the larger U. S. gas-cooled-reactor plants (EGCR, HTGR, and MGCR) which include gas-circulating equipment as a primary component.

References

1. Organization for Economic Cooperation and Development, European Nuclear Energy Agency, O.E.C.D. Dragon High Temperature Reactor Project, Third Annual Report, 1961–1962.
2. *Nucl. Eng.*, 5(50): 299–315 (July 1960).
3. The Dragon Project: Progress Report, *Nucl. Eng.*, 6(66): 454 (November 1961).
4. G. E. Lockett and R. A. U. Huddle, The Dragon Reactor Development and Design of the HTGC, *Nucl. Power*, 5(46): 112 (February 1960).
5. L. R. Shepherd and P. J. Marien, Research and Development Aspects on the Dragon Reactor Experiment, Proceedings Series, in Symposium on Power Reactor Experiments, Vol. I, Vienna, October 23–27, 1961, International Atomic Energy Agency, Vienna, 1962.
6. G. E. Lockett, Engineering Aspects of the Dragon Reactor Experiment, Proceedings Series, in Symposium on Power Reactor Experiments, Vol. I, Vienna, October 23–27, 1961, International Atomic Energy Agency, Vienna, 1962.
7. H. Lloyd, T. Thorpe, C. C. H. Wheatley, J. W. Bloodworth, H.T.G.C.R. Fuel Element Development, British Report AERE-R-3826, November 1961.
8. J. Bromley, Transport and Diffusion of Fission Products in Graphite, British Report AERE-R-4004, March 1962.
9. Dragon Project Extended to Design of Power Reactor, *Nucleonics Week*, 3(19): 1 (May 10, 1962).
10. S. B. Malanoski and D. D. Fuller, Survey of Component Requirements and Availability for Gas-Cooled Nuclear Reactor Power Plants, USAEC Report NYO-9792, Franklin Institute, June 1961.
11. Shaft Seals for Compressors and Turbines for Gas-Cooled Reactor Application. Proceedings of Meeting at Oak Ridge National Laboratory, December 16–17, 1959, USAEC Report TID-7604.
12. Rotating Machinery for Gas-Cooled Reactor Application. Proceedings of Meeting at Oak Ridge National Laboratory, Apr. 2–4, 1962, USAEC Report TID-7631.
13. ML-1, Pioneer Mobile Reactor, Reactor News, *Nucleonics Week*, 3(32): 3 (Aug. 9, 1962).

Section

XI

Power Reactor Technology

Advanced Ship-Propulsion Studies

References 1 to 6 give the results of an AEC-sponsored design analysis by Combustion Engineering, Inc., of advanced concepts for pressurized-water ship-propulsion reactors. The work extends that previously reported[7] by the application of later information from operating reactors and from various AEC-sponsored research and development programs.

The common characterizing features of the several designs analyzed in the later study are (1) the self-pressurization of the reactor and (2) the superheating of the secondary steam by the primary coolant water. As shown in Fig. XI-1, the entire primary coolant flow passes first through the superheater and then through the steam generator. For the design represented in the figure, the self-pressurized reactor operates at 2100 psi, and secondary steam is produced at a temperature of 605°F and 600 psi. Although nucleate boiling occurs in the reactor and the reactor is self-pressurized by a steam dome in the top of the reactor vessel,

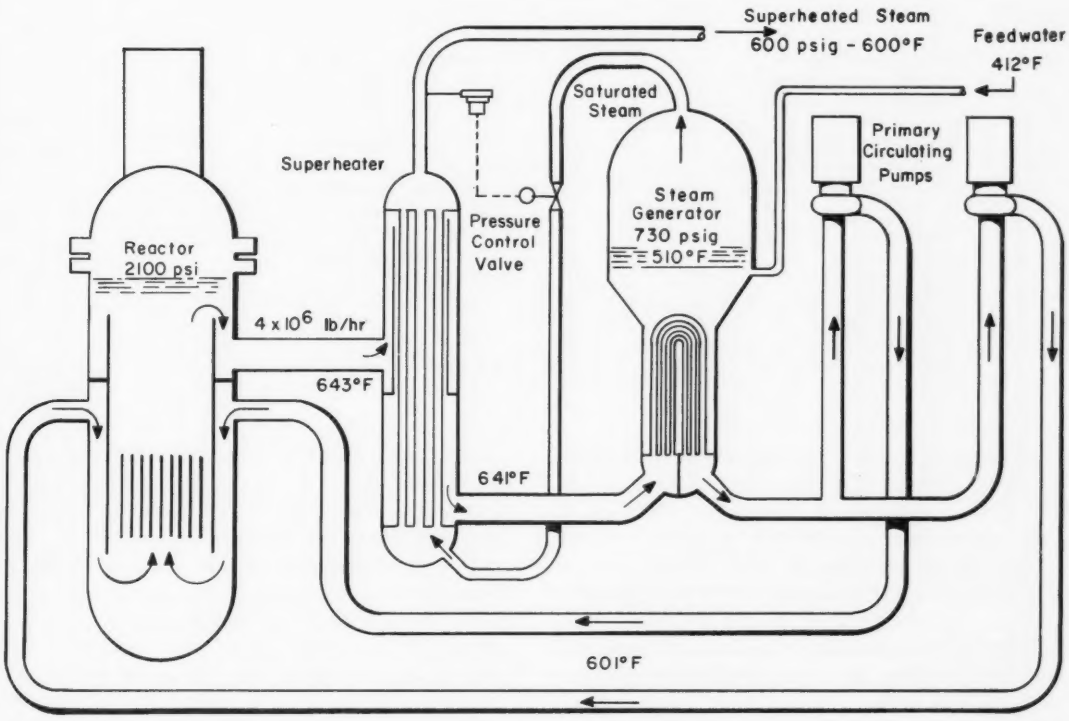

Fig. XI-1 Self-pressurized reactor system flow diagram (maximum core power and 2100 psi).

there is no significant transport of heat as latent heat in the primary coolant system. The primary coolant occupies the shell side of the superheater, whereas the secondary steam is superheated in the tubes. The system is so designed that, in case of troubles in the steam-generator system, the secondary feedwater can be admitted directly to the tube side of the superheater, which will then operate as a once-through saturated-steam generator of lower capacity. Likewise, if there are troubles in the superheater, saturated steam from the steam generator can be used directly in the turbine for return to port. It is thus expected that a system with a single primary loop, served by two parallel circulation pumps, will provide in effect the same duplication of capability as is ordinarily obtained with complete duplication of the coolant loops. Since the primary flow is through the superheater and steam generator in series, isolating valves are not required for these components in the primary circuit. The reduction in valve requirements and the use of a single primary loop are considered to have substantial economic benefits.

Aside from the unusual steam system, the plant is characterized by a rather compact reactor core. In the core, radial power flattening is obtained by three different radial zones of fuel enrichment and control is provided by 12 "flux trap" type rods with fuel-assembly followers. The fuel assemblies and control rods are hexagonal in cross section.

Table XI-1 CHARACTERISTICS OF ADVANCED PWR CONCEPT FOR SHIP PROPULSION[2]

Reactor:	
Fuel-element type	UO_2 pellets in free-standing stainless-steel jackets
Pellet diameter	0.514 in.
Jacket dimensions	0.594 in. outside diameter by 0.037 in. thick
Fuel assemblies (stationary)	Hexagonal, containing 61 rods on 0.845-in. triangular pitch
Fuel assemblies (control-rod followers)	Hexagonal, containing 58 rods on 0.783-in. triangular pitch
Number of fuel assemblies	49 stationary, 12 on control rods
Total fuel rods in core	3685
Control rods	12, hexagonal, flux-trap type
Active core length	60 in.
Equivalent core diameter	55 in.
Heat flux, Btu/(hr)(sq ft):	
Average	108,000
Maximum	301,000
Fuel enrichment, wt.% U^{235}:	
Inner zone	3.2
Intermediate zone	3.9
Outer zone	5.5
Average fuel exposure	14,000 Mwd/metric ton of uranium
Reactor-vessel dimensions	6.58 ft in inside diameter by 23.4 ft high
Reactor-vessel design pressure	2500 psig
Plant:	
Steam generator, type	1, shell and vertical U tube
Steam generator, dimensions	6.83-ft maximum outside diameter by 18.6 ft high
Primary circulating pumps	2, each 5800 gal/min, vertical, single-stage, turbine driven with limited leakage seals
Main turbine	Cross compound
Steam conditions	600 psig, 605°F (111°F superheat)
Exhaust pressure	1.5 in. Hg absolute
SHP, normal	27,300
SHP, maximum	30,000
Net efficiency, normal power	28.2%
Containment vessel	Steel, 34 ft in diameter by 50 ft high

The heat balance for the plant is shown in Fig. XI-2, and some of the more important plant characteristics are tabulated in Table XI-1. For a comparison with current design practice, reference may be made to the description of the N.S. *Savannah* plant in Sec. VI of this issue.

In addition to the plant described above, the study considered a similar plant designed for a primary operating pressure of 1300 psi. A

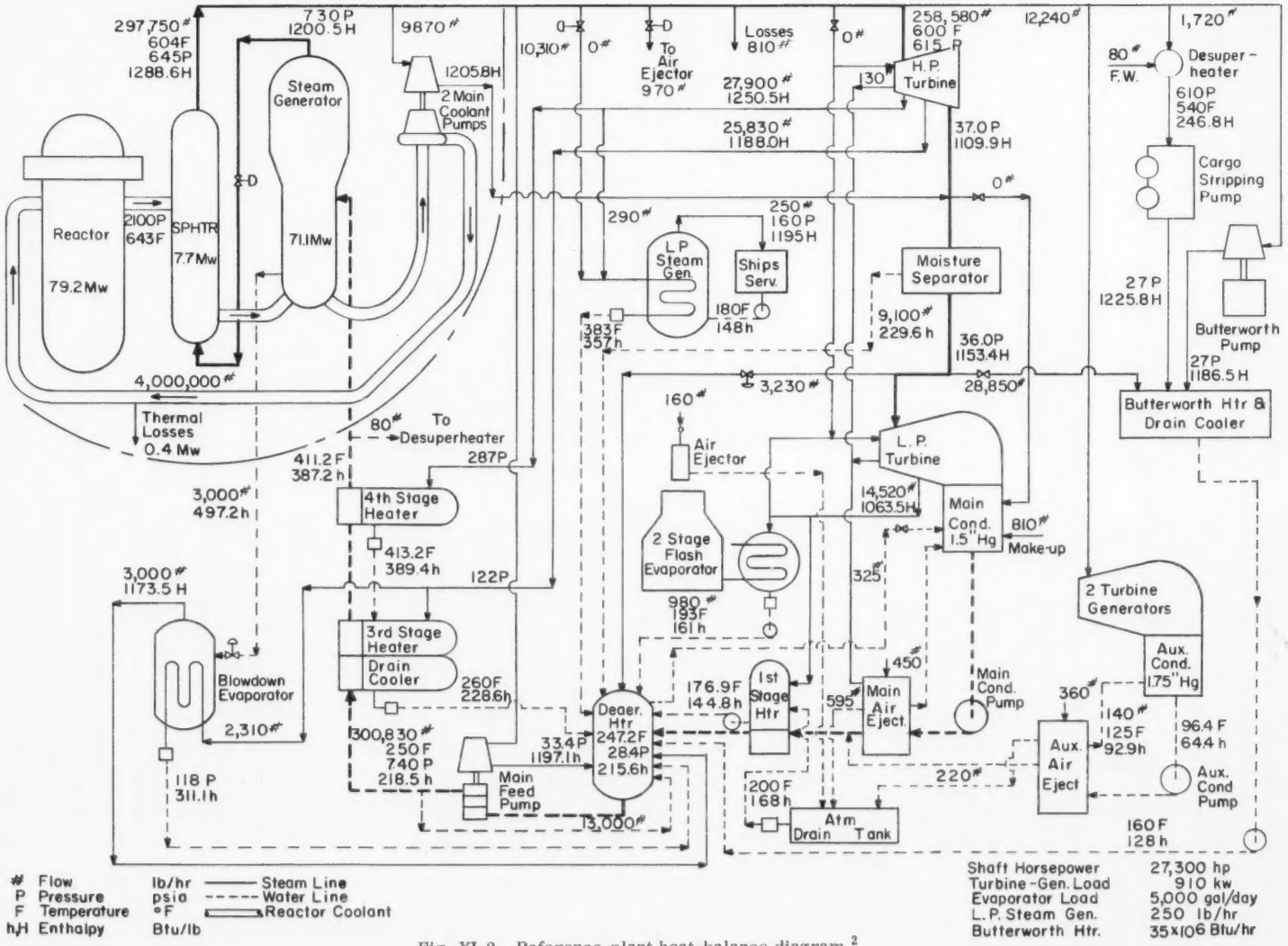

Fig. XI-2 Reference-plant heat-balance diagram.[2]

more advanced approach, where the superheater is built into the reactor vessel itself (in the steam dome), was also examined. An alternate core design, which was of the "spiked" type, was examined.[5]

Considerable attention was given to achieving simplicity of plant control, and a part of the study was directed toward the conceptual development of a design requiring minimum operating attention. The basic design approach is thought to favor this objective because of the reactor system's inherent load-following and self-regulating characteristics, which allow it to absorb most and perhaps all normal maneuvering transients without control-rod motion. After the steam flow is reduced by closing the turbine throttle, for example, the steam pressure at the superheater exit begins to rise. However, at this point a pressure-sensing device actuates a throttling valve between the steam generator and the superheater (Fig. XI-1). Thus at reduced load the steam pressure at the turbine throttle does not rise as is common in pressurized-water-reactor plants, even though the pressure is permitted to rise in the steam generator. The rising pressure in the steam generator and the concurrent rise in boiling temperature reduce the amount of steam produced. The temperature of the primary water returning to the core rises, and the core power falls because of a strong negative temperature coefficient of reactivity. Thus the plant is expected to take advantage of the inherent self-control and load-following characteristics of the pressurized-water reactor without making any special demands on the steam turbine. Reference 3 reports transient calculations that have been made to check the expected dynamic behavior of the plant.

References

1. Combustion Engineering, Inc., Advanced Indirect Cycle Water Reactor Studies for Maritime Applications. Part I. Cost Analysis and Future Development, USAEC Report CEND-150(Pt.I), April 1962.
2. Combustion Engineering, Inc., Advanced Indirect Cycle Water Reactor Studies for Maritime Applications. Part II. Plant Conceptual Studies, USAEC Report CEND-150(Pt.II), March 1962.
3. Combustion Engineering, Inc., Advanced Indirect Cycle Water Reactor Studies for Maritime Applications. Part III. Analog Simulation of Reactor Plant Transients, USAEC Report CEND-150(Pt.III), Oct. 23, 1961.
4. Combustion Engineering, Inc., Advanced Indirect Cycle Water Reactor Studies for Maritime Applications. Part IV. Steam Driven Coolant Pumps, USAEC Report CEND-150(Pt.IV), Oct. 23, 1961.
5. Combustion Engineering, Inc., Advanced Indirect Cycle Water Reactor Studies for Maritime Applications. Part V. Spiked Core Concept, USAEC Report CEND-150(Pt.V), Oct. 23, 1961.
6. Combustion Engineering, Inc., Advanced Indirect Cycle Water Reactor Studies for Maritime Applications. Part VI. Natural Circulation Capabilities, USAEC Report CEND-150(Pt.VI), Nov. 21, 1961.
7. Combustion Engineering, Inc., and George G. Sharp, Inc., Nuclear Powered Tanker, Design and Economic Analysis, Pressurized Water Reactor, USAEC Report CEND-62, January 1960.

NUCLEAR SCIENCE ABSTRACTS

The U. S. Atomic Energy Commission, Division of Technical Information, publishes *Nuclear Science Abstracts (NSA)*, a semimonthly journal containing abstracts of the literature of nuclear science and engineering.

NSA covers (1) research reports of the U. S. Atomic Energy Commission and its contractors; (2) research reports of government agencies, universities, and industrial research organizations on a world-wide basis; and (3) translations, patents, books, and articles appearing in technical and scientific journals.

Complete indexes covering subject, author, source, and report number are included in each issue. These are cumulated quarterly, semiannually, and annually providing a detailed and convenient key to the literature.

Availability of *NSA*

SALE *NSA* is available on subscription from the Superintendent of Documents, U. S. Government Printing Office, Washington 25, D. C., at $22.00 per year for the semimonthly abstract issues and $15.00 per year for the four cumulated-index issues. Subscriptions are postpaid within the United States, Canada, Mexico, and all Central and South American countries, except Argentina, Brazil, British and French Guiana, Surinam, and British Honduras. Subscribers in these Central and South American countries, and in all other countries throughout the world, should remit $27.50 per year for subscriptions to semimonthly abstract issues and $17.50 per year for the four cumulated-index issues.

EXCHANGE *NSA* is also available on an exchange basis to universities, research institutions, industrial firms, and publishers of scientific information. Inquiries should be directed to the Division of Technical Information Extension, U. S. Atomic Energy Commission, P. O. Box 62, Oak Ridge, Tennessee.

TECHNICAL PROGRESS REVIEWS may be purchased from Superintendent of Documents, U. S. Government Printing Office, Washington 25, D. C. for $2.00 per year for each subscription or for $0.55 per issue. The use of the coupon below will facilitate the handling of your order.

POSTAGE AND REMITTANCE: Postpaid within the United States, Canada, Mexico, and all Central and South American countries except as hereinafter noted. Add $0.50 per year, or $0.15 per single issue, for postage to all other countries, including Argentina, Brazil, British and French Guiana, Surinam, and British Honduras. Payment should be by check, money order, or document coupons, and MUST accompany order. Remittances from foreign countries should be made by international money order, or draft on an American bank, payable to the Superintendent of Documents, or by UNESCO book coupons.

order form

SUPERINTENDENT OF DOCUMENTS
U. S. GOVERNMENT PRINTING OFFICE
WASHINGTON 25, D. C.

Enclosed:
document coupons ☐ check ☐ money order ☐

Charge to Superintendent of Documents No. _____

Please send a one-year subscription to

☐ REACTOR MATERIALS
☐ POWER REACTOR TECHNOLOGY
☐ NUCLEAR SAFETY
☐ REACTOR FUEL PROCESSING

(Each subscription $2.00 a year; $0.55 per issue.)

SUPERINTENDENT OF DOCUMENTS
U. S. GOVERNMENT PRINTING OFFICE
WASHINGTON 25, D. C.

(Print clearly)

Name _____

Street _____

City _____ Zone ____ State _____